Dynamics of photoinduced switching processes

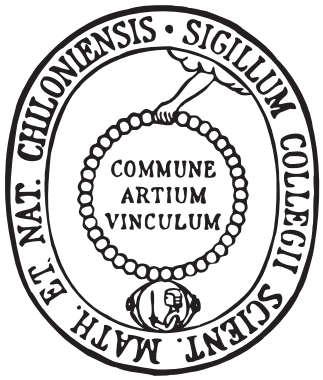

Dissertation

in fulfillment of the requirements
for the degree

Dr. rer. nat.

of the Faculty of Mathematics and Natural Sciences
at Kiel University

submitted by

Jan Boyke Schönborn

Kiel, 26.10.2012

First referee:	Prof. Dr. B. Hartke
Second referee:	Prof. Dr. F. Temps
Date of the oral examination:	12.12.2012
Approved for publication:	12.12.2012
Signed:	Prof. Dr. W. J. Duschl, Dean

Abstract

The field of molecular photo-isomerisable switches has drawn major interest recently. Molecules which can efficiently and reversibly be transformed from one form to another by light are promising for use in molecular electronics, data-storage or as motors in molecular machines.

The topic of this thesis are two important classes of molecular switches: Firstly electrocyclic ring-closure/-opening switches, which are represented by 1,3,5-hexatriene/2,4-cyclohexadiene, furylfulgides and a newly developed class of dilactames, and secondly E/Z-isomerisable switches based on azobenzene or a closely related compound, represented by a diazocine, azobenzene oligomeres coupled by a amino group and an azopyridin functionalised nickel porphyrin.

Due to the complexity of the photo-isomerisation processes, a variety of different multi- and single-determinant static *ab-initio* methods and semiempirical direct dynamics are used to investigate the systems at hand.

A two-dimensional quantum-dynamical study is presented on an *ab-initio* potential energy surface with thus far unachieved agreement with experiment. It is used to challenge 2,4-cyclohexadiene as a model system for other electrocyclic switches, implying the need for high-dimensional dynamics studies for the description of the high-energy isomerisation processes.

The applicability of the semiempirical MR-CI-OM3 method to more complicated electrocyclic switches is proven by a comparison to accurate *ab-initio* and experimental data. Using direct dynamics simulations with this method, the reasons for the differences between the ring-closure reactions of E-isopropyl- and E-methyl-furylfulgide are unravelled. Additionally, static simulations are used to study unusual electronic wave function changes in the isomerisation of Z-methyl-furylfulgide to the E-form and to understand the broad and structured absorption band of cyclic furylfulgides at about 450 nm, which is found to be linked to the excited-state nuclear wave function. Concluding the presented studies of electrocyclic switches, a new class of switches is designed from scratch and studied by static and dynamic means.

The studies of azobenzene-based systems presented here are accurate *ab-initio* calculations that support theoretical and experimental studies of diazocine dynamics done by collaborators at Kiel University, the assessment of the applicability of the MRCI-OM2 model to 4-aminoazobenzene and bis[4-(phenylazo)phenyl]amine, a detailed CC2 study of the electronic states of the EEE-tris[4-(phenylazo)phenyl]amine and the two aforementioned systems, and a multiconfigurational study of the electronic states that might facilitate the photo-isomerisation of an azopyridin moiety in a nickel porphyrin complex that leads to a spin state change from singlet to triplet.

Kurzfassung

Die Untersuchung molekularer photoisomerisierbarer Schalter ist seit einiger Zeit von großem Interesse. Effizient und reversibel durch Licht von einer in eine andere Form überführbare Moleküle versprechen Anwendungen auf molekularer Ebene in Elektronik, Datenspeichern und Maschinen.

Thema dieser Arbeit sind zwei wichtige Klassen molekularer Schalter, zum einen elektrozyklische Ringschluss/-öffnungs Schalter, vertreten durch 1,3,5-Hexatrien/-2,4-Cyclohexadien, Furylfulgide und eine neu entwickelte Klasse von Lactamen, und zum anderen E/Z-isomerisierbare Schalter, die auf Azobenzol oder einer verwandten Verbindung basieren, vertreten durch ein Diazozin, über eine Aminogruppe verbundene Azobenzololigomere und ein azopyridinfunktionalisiertes Nickelporphyrin.

Die komplexen Photoisomerisierungprozesse der Moleküle werden mit einer Vielzahl verschiedener Multi- und Eindeterminanten-*ab-initio*-Methoden und semiempirischen dynamischen Methoden untersucht.

Durch eine zweidimensionale Quantendynamiksimulation der Ringöffnungsreaktion von 2,4-Cyclohexadien auf einer *ab-initio*-Potentialenergiefläche, die zuvor unerreichte Übereinstimmung mit Experimenten zeigt, wird die Anwendbarkeit dieses Systems als Modell für andere elektrozyklische Schalter in Frage gestellt. Die Untersuchungen legen die Nutzung hochdimensionaler dynamischer Simulationen zum Verständnis der Isomerisierungsprozesse nahe.

Durch einen Vergleich mit *ab-initio*- und experimentellen Daten wird nachgewiesen, dass die semiempirische Methode MRCI-OM3 auf elektrozyklische Schalter angewendet werden kann. Mittels Simulationen der Kerndynamik unter Verwendung dieser Methode werden die Gründe für die Unterschiede der Ringschlussreaktionen von E-Isopropyl- und E-Methylfurylfulgid identifiziert. Mit Hilfe von statischen Untersuchungen werden überdies die ungewöhnlichen Veränderungen der elektronischen Wellenfunktion von Z-Methylfurylfulgid im Verlauf der Z/E-Isomerisierung und die Bandenform des ersten elektronischen Übergangs der zyklischen Furylfulgide untersucht. Zum Abschluss der Untersuchungen von elektrozyklischen Schaltern werden die gesammelten Erkenntnisse genutzt, um ein neues Grundgerüst für Schalter zu entwickeln und zu untersuchen.

In den Untersuchungen von azobenzolverwandten Systemen werden *ab-initio* Simulationen zu einem Diazozin präsentiert, die genutzt werden, um Dynamiksimulationen und Experimente von Kooperationspartnern zu unterstützen. Die Anwendbarkeit eines MR-CI-OM2-Modells auf 4-Aminoazobenzol und Bis[4-(phenylazo)-phenyl]amin wird durch den Vergleich mit Experimenten und CC2-Simulationen untersucht und ein geeigneter Ansatz für die Simulation der Photoisomerisierung identifiziert. Nach Erweiterung der CC2-Simulationen auf EEE-Tris[4-(phenylazo)-phenyl]amin werden die elektronisch angeregten Zustände der Oligomere detailliert

analysiert. Im letzten Projekt der Arbeit werden die elektronischen Zustände identifiziert, die eine E/Z-isomerisierung und damit eine Spinzustandsänderung in einem azopyridinfunktionalisierten Nickelporphyrin ermöglichen können.

Contents

1 Introduction

With the development of quantum mechanics in the first half of the 20^{th} century chemistry became accessible to fundamental mathematical theory. For the first time in the existence of chemistry, its most basic chemical feature, the chemical bond, could be described mathematically based on simple physical axioms. This was true at least for the most simple molecule, the dihydrogen cation. Soon it became obvious that although quantum mechanics was an extraordinarily powerful tool, its applicability in chemistry was limited by the complexity of the equations that had to be solved to make predictions for chemically relevant problems. Only the computers and together with them increasingly efficient models and algorithms, becoming more and more powerful, closed the gap between computability and chemical relevance, by making iterative, approximate solutions of unsolvable equations accessible.

The central, analytically unsolvable (at least in most cases), quantum-mechanical equation in chemistry is the molecular Schrödinger equation. The first step to approximately solve this equation is to separate the equation into an electronic and a nuclear part, which is the formally exact Born-Oppenheimer (BO) separation, i. e. the quasi-separate treatment of the nuclei and the electrons. Although this separation by itself does not much for the solvability, as it includes an analytically unsolvable infinite number of coupled electronic states, it significantly decreases the complexity of the problem by splitting it in two and allows for the development of different approximate strategies of solution for the nuclei and electrons separate from each other. Based on the BO separation, methods of various levels of accuracy and computational cost have been developed. The common approach is to first solve the electronic Schrödinger equation for one or a few electronic states, parametrically dependent on the nuclear coordinates, and then to integrate equations of motion for the nuclei.

The part of theoretical chemistry treating the electronic problem, commonly referred to as quantum chemistry, by now is extremely well developed. A variety of commercially available programs today allow laymen to evaluate the wave function of systems from a few atoms to a few hundred atoms. Although broadly used today,

specialised fields in quantum chemistry are still experts' terrain. An important example of these fields are so-called multiconfigurational cases and situations in which two ore more electronic states are to be treated equally well. Multiconfigurational situations are encountered whenever a state cannot be described qualitatively with only one Slater determinant, which corresponds to an arrangement of electrons in one-electron wave functions, a configuration. Traditional quantum chemistry focuses on one configuration and is thus unable to properly treat such cases. For the same reason it fails in the second type of situations. The intention to describe two electronic states equally well causes the need to describe more than one configuration on equal footing, which is impossible in standard quantum chemistry. Both of these situations are usually encountered in the description of photo-de-excitation. Since the electronic de-excitation occurs in regions were at least two electronic states are very close, the accurate relative order of states needs an equally good description of all involved electronic states. In these regions the electronic states are also often comprised of more than one equally important configurations. Thus the study of electronic de-excitation is still a complex field of study in quantum-chemical simulations.

When talking about simulations of the nuclei in theoretical chemistry, in most cases this means the simulation of the dynamics. In contrast to the electronic problem the treatment of nuclei is, for the most part, still a field of experts. Two basic approaches are present in nuclear dynamics. The most fundamental one is to solve the nuclear Schrödinger equation resulting from the Born-Oppenheimer seperation on one or more electronic surfaces. The incorporation of multiple electronic surfaces is, in principle, straightforward in this ansatz as long as electronic energies and the couplings of the treated surfaces are known. The major disadvantage of the quantum treatment of the nuclei is that the number of degrees of freedom that can be treated is rather limited. The advantage of quantum dynamics is that it most closely corresponds to reality. In the space spanned by the coordinates and the electronic states it is basically exact.

Although atomic nuclei are strictly quantum particles, they are heavy enough to allow for the application of classical mechanics to them and for still coming up with reasonably good to very good results for their dynamics. The advantage in the use of classical equations of motion to treat nuclear dynamics is that there is no need to represent the nuclear wavefunction and thus the number of electronic structure calculations is massively reduced. In the classical picture the number of degrees of freedom that can explicitly be treated is therefore much larger than in quantum dynamics. By the development of so-called surface-hopping classical dynamics the most important disadvantage for the application to photochemistry was resolved, opening up this field to the study within this approach.

Studies of ultrafast reactions triggered by the absorption of light by a molecule have become a major field of interest in physical and theoretical chemistry within the

last few decades, culminating in the awarding of 1999's Nobel Prize in chemistry to Ahmed H. Zewail. Investigations of processes occuring on the pico- and femtosecond timescale via sophisticated experimental setups allow scientists to catch chemistry red-handed, and thus open the fundamental processes of chemistry up to studies. To understand the processes observed, a close collaboration of experimental and theoretical scientists is necessary. From the theoreticians' point of view the studies of ultrafast processes take the field of interest to exactly where they want it, in the sense that shorter time scales are easier to simulate than longer ones. Disadvantageously the processes involved in ultrafast photochemistry create new problems already hinted at in the previous three paragraphs. To study ultrafast chemistry theoretically, sophisticated —usually multireferential— electronic structure theory is needed. The methods have to be very accurate and thus time consuming for some applications, for others they only need to be qualitatively correct but then quick to be calculated. Never are these black box methods although they are implemented in various comercially available programs. Static simulations of characteristic points on the electronic states are but one, concededly important, tool for understanding photochemistry. To see the full picture, additional simulations of the dynamic processes are inevitable, as will be demonstrated in this thesis multiple times.

The thesis at hand is devoted to the study of a special kind of ultrafast photochemical processes, photo-switching. Molecular photo-switches are molecules that can be transformed from one form to another by incident light. The reaction has to be effective, reversible and selective for the molecule to qualify as a photo-switch. The thesis is organised as follows. The chapter 2 will give an overview over the most important theoretical basics of the processes under study and the methods applied. Chapters 3 to 6 present the studies performed, beginning with a quantum-dynamical study of the ring-opening reaction of 2,4-cyclohexadiene, an important basic system representing electrocyclic ring-opening/-closure switches, for a long time regarded to be a model-system for more complex photo-switches, in chapter 3. Furylfulgides, representing a class of these more complex switches, are studied in chapter 4 by a variety of static *ab-initio* and semiempirical dynamic models. The studies of electrocyclic switches are concluded in chapter 5, in which a design process coming up with a new class of electrocyclic switches is presented. Chapter 6 is devoted to studies of azobenzene-related E/Z-isomerisable molecules. In this chapter, dynamic and/or static investigations into very different switches are presented, from the sterically constrained diazozine to an azopyridin-functionalised nickel porphyrin. A summary of the studies is given in chapter 7.

2 Theoretical Background

2.1 Basic processes in photochemistry

Photochemical processes happen in two or more electronic states. The electronic relaxation can happen either radiatively via fluorescence and phosphorescence (between states of same or different spin, respectively) or non-radiatively via quenching by the surroundings or via highly interacting regions of the electronic states. In-between electronic processes, relaxation processes bound to one electronic state can occur, for example conformational changes, vibrational energy redistribution or even bond formation and breakage.

The Jablonski diagram in figure 2.1 and the schematic potential energy surfaces depicted in figure 2.2 will be used to visualise the explanation of the processes in the following to sections 2.1.1 and 2.1.2.

2.1.1 Slow processes

The radiative de-excitation and quenching by the surroundings mentioned first in section 2.1 for a long time dominated the models in photochemistry. Theoretical treatment of electronic structure for a long time focused on diatomic molecules and the non-crossing rule [3] derived from that, which states an impossibility of same-spin electronic state-crossing. In these models, which are illustrated on the right hand side of figure 2.2, the fastest electronic de-excitation processes are in the time range of nanoseconds and slower. This leaves the electronically excited molecules ample time for reactions in the excited states, for example 2+2-cycloadditions and other thermally forbidden reactions.

2.1.2 Ultrafast photochemistry

Driven by developments in generation of ultrashort laser pulses by the end of the 20^{th} century, various examples of photo-reactions could be studied that put up serious problems for the models illustrated in section 2.1.1. Important examples of

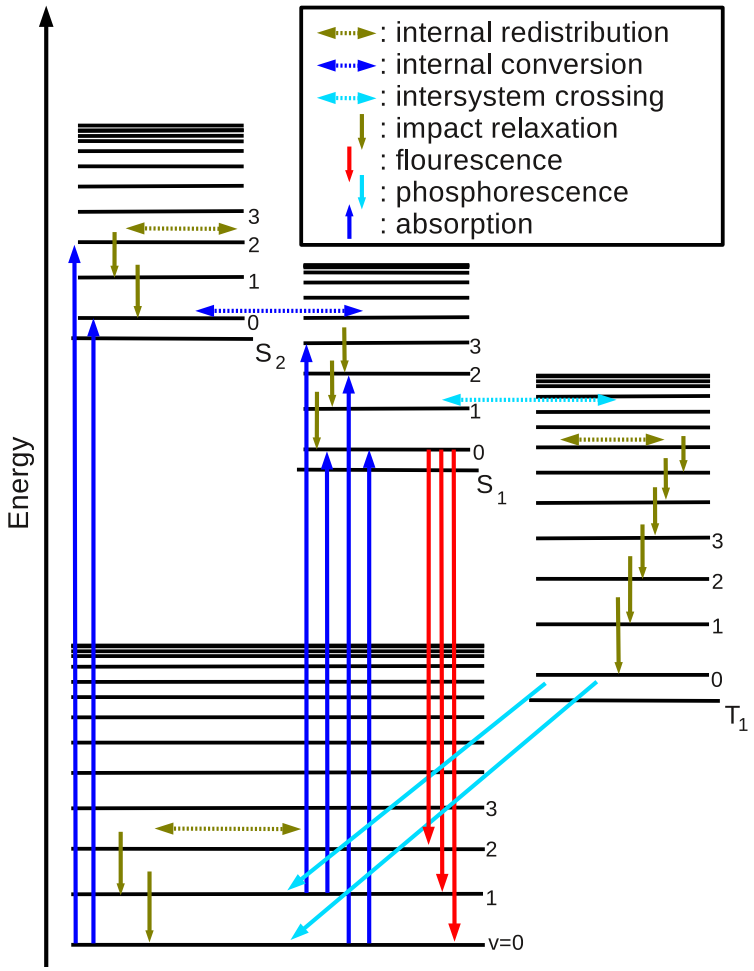

Figure 2.1: Jablonski diagram depicting important photochemical and -physical processes. Processes within one electronic state are given in brown, those involving two states of the same spin in dark blue (absorption and internal conversion) or red (emission) and those involving two states of different spin in light blue.

Figure adapted and expanded from [1].

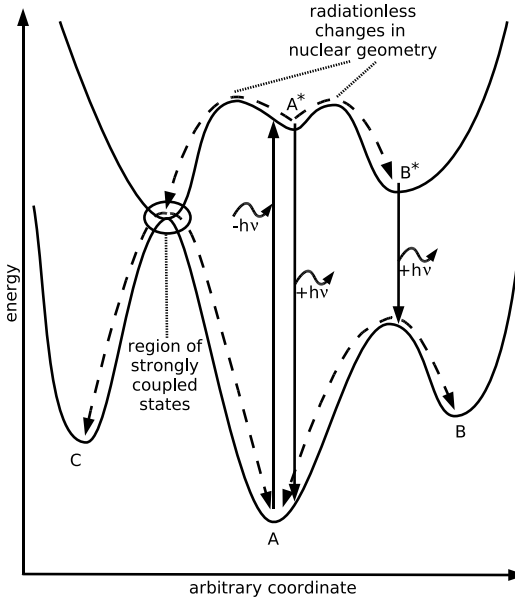

Figure 2.2: Sketch depicting important photochemical and -physical processes.

Figure adapted from [2].

these processes include the photo-relaxation of DNA as a chemical protective process that reduces radiation damage to the genetic material and the photo-isomerisation of retinal in various protein surroundings for various biological purposes, eyesight being only one example. These reactions happen on time scales of pico- or even femtoseconds. Since the time scales relevant for radiative de-excitation (governed by the Einstein factor A_{21}) and quenching by surroundings (collisions with other molecules) were well known and could be ruled out from driving these reactions, new explanations needed to be found. The answer is that in molecules with more than one internal degree of freedom electronic surfaces of same spin can intersect in a subspace two dimensions smaller than the internal coordinate space of the molecule. In these intersection regions called intersection seams, molecules can effectively and quickly cross from one electronic state to the other and therefore are able to convert the electronic excitation energy to vibrational energy completely without any emission of radiation or the need of a collision partner. The vibrational energy can then spread over the internal degrees of freedom of the molecule via internal vibrational redistribution and dissipate to the surroundings by collisions (brown arrows in figure 2.1) after the reaction is already over.

Reactions of this kind have distinct advantages over the classical photo-reactions treated in section 2.1.1. The short lifetimes in the electronically excited states and the overall short reaction time from reactant to the final molecule, being a reaction

product or just the reformed reactant, leaves few options for unwanted side reactions with additional reaction partners. Moreover, the conditions leading to crossings of electronic states are rather special, which further reduces the variety of possible intramolecular side reactions. On the other hand, these special conditions leading to surface crossings make it rather difficult to influence the outcome of reactions, for example making it hard to vary the details and yields or even come up with completely new paths to form intended products.

For various reasons, ultrafast photochemical processes are of relevance to modern scientific investigations. Not only are they common in nature and fulfill important tasks there in visual receptors or as protective processes in DNA, but also in artificial systems. The reactions, if chosen properly, happen very specifically with high yields and the reactants are addressable selectively via irradiation with lasers. A special kind of photochemical reactants are molecules in which not only one reaction can be triggered selectively by irradiation, but also its back reaction is feasible via thermal or even better radiative excitation. These molecules are called photochemical switches. If the photo-reaction will give rise to significant changes in molecular properties or motion, these switches have the potential to be used as building units such as motors in machines or single memory units in storage devices. This thesis will deal with such molecules. Azobenzenes, furylfulgides, fulgimides, spiropyranes and diarylethenes are popular examples.

2.2 Born-Oppenheimer separation and approximation

The fundamental equation in chemistry is the Schrödinger equation given in equation 2.1.

$$\hat{H}\Psi = i\hbar\frac{\partial}{\partial t}\Psi, \tag{2.1}$$

with:

$\hat{H}$	: Hamiltonoperator
Ψ	: Wave function
$\hbar$	: Planck constant/2π
t	: Time
i	: Imaginary unit

After conversion to atomic units, the Hamilton operator in the Schrödinger equation can be expressed by equation 2.2.

$$\begin{aligned}\hat{H} &= -\sum_{A=1}^{M}\frac{1}{2M_A}\nabla_A^2 - \sum_{i=1}^{N}\frac{1}{2}\nabla_i^2 \\ &\quad + \sum_{i=1}^{N}\sum_{j>i}^{N}\frac{1}{r_{ij}} - \sum_{i=1}^{N}\sum_{A=1}^{M}\frac{Z_A}{r_{iA}} + \sum_{A=1}^{M}\sum_{B>A}^{M}\frac{Z_A Z_B}{R_{AB}},\end{aligned} \tag{2.2}$$

with:

M	:	Number of nuclei
A, B	:	Nuclei
M_A	:	Mass of nucleus A
Z_A	:	Charge of nucleus A
N	:	Number of electrons
i, j	:	Electrons
r_{ij}	:	Distance of electrons i and j
r_{iA}	:	Distance of electron i from nuclei A
R_{AB}	:	Distance of nuclei A and B.

The Schrödinger equation can be transformed to the time-independent molecular Schrödinger equation 2.3, by elimination of the time-dependence (which can be re-introduced later on). Via equation 2.2 it accounts for an arbitrary system of electrons and nuclei and therefore forms the basis for the understanding of the complete non-relativistic chemistry.

$$\hat{H}\phi(R,r) = -\frac{1}{2m}\nabla^2\phi(R,r) + V(R,r)\phi(R,r) = E(R,r)\phi(R,r), \tag{2.3}$$

with:

$E(R,r)$: Eigenenergy
R : Spatial coordinates of the nuclei
r : Spatial coordinates of the electrons.

The Hamilton operator of the most general chemical system (equation 2.2) contains terms arising from nuclei only, the kinetic energy and the Coulombic repulsion (first and last), from electrons only, of the same type as for the nuclei, (second and third) and a mixed term accounting for the Coulombic attraction of the electrons and nuclei (fourth). Via the adiabatic separation ansatz (Born-Oppenheimer separation),

equation 2.3 can be split in a nuclear part given in equation 2.4 and an electronic part given in equation 2.5.

$$(\hat{T}_N + E_{el,m}(R))\chi^{(m,k)}(R) + \sum_n (2\hat{T}'_{mn}(R) + \hat{T}''_{mn}(R))\chi^{(n,k)}(R) = E_{tot,k}\chi^{(m,k)} \tag{2.4}$$

with:

$\chi(R)$	: Nuclear wave function
$\hat{T}_N$	: Nuclear kinetic energy operator
$E_{el,m}$	: Electronic energy
$E_{nuc,k}$	: Total energy
$\hat{T}'_{mn}$, $\hat{T}''_{mn}$	: Non-adiabatic coupling terms.

$$\hat{H}_{el}\psi(R,r) = E_{el}(R)\psi(R,r) \tag{2.5}$$

with:

$\psi(R,r)$	: Electronic wave function
$\hat{H}_{el}$	: Electronic Hamilton operator
E_{el}	: Electronic energy.

While equation 2.5 is only parametrically dependent on the nuclear coordinates (R) and can therefore be solved without any knowledge of the nuclear wave function (χ), the exact nuclear Schrödinger equation 2.4 is dependent on an infinite number of coupled electronic eigenstates via the coupling terms in the sum. Exact solutions for either of the equations are unobtainable for any but the most simple cases. In numeric solutions an infinite number of electronic states is neither achievable nor could it be handled. So in addition to the Born-Oppenheimer separation the Born-Oppenheimer approximation, which consists of neglecting the coupling terms in equation 2.4, is applied. This leads to a separation of the electronic surfaces, with the nuclei propagating on one isolated electronic surface.

In cases were electronic surfaces come near each other and interact (see section 2.1.2), the Born-Oppenheimer approximation is not fully applicable anymore. Nonetheless, the coupling is usually not large for many electronic states over the course of one reaction, so the way to circumvent this problem is to explicitly treat and couple the few relevant electronic states, while the other couplings are still neglected in the spirit of the Born-Oppenheimer approximation.

2.3 Finite basis representation

As first step to iteratively solve the electronic Schrödinger equation as derived in section 2.2, a basis expansion ansatz is made for the wave function. Since an infinite basis is unfeasible in a real computation, the basis size is limited to a finite number of basis functions. This ansatz is represented by equation 2.6.

$$\Phi_i(\vec{r}) \approx \sum_{j=1}^{k} c_{ij}\theta_j(r) \tag{2.6}$$

with:

$\Phi_i(\vec{r})$: any electronic wave function depending on the electron coordinates $\vec{r}$
c_{ij} : expansion coefficient for wave function i and basis function j
$\theta_j(\vec{r})$: basis function
k : total number of basis functions.

2.3.1 Types of basis functions

The finiteness of the basis set causes the basis expansion of the wave function to be approximate. To retain the needed amount of accuracy the choice of type and number of basis functions is essential. There are basically two different kinds of basis functions commonly in use. These are either contracted Gaussian functions or plane waves. Both of these have distinct positive and negative features that are more or less suitable for different problems.

Integration of plane wave functions can be done exceedingly fast. Since, this is one of the most time-consuming steps in the methods explained in the following sections, this is a major advantage. Plane waves are intrinsically periodic, therefore they are especially useful in calculations for periodic systems. An expansion in plane wave basis functions can mathematically be shown to converge for functions that qualify as quantum-mechanical wave functions. In the case that there is no knowledge about the final form of the wave function the basis should be suitable for describing unknown features, and plane waves are. However, for this a lot of functions are needed. If there is knowledge about the final wave function before the calculation, the basis functions can be adapted to reflect this. This massively reduces the amount of basis functions —and therefore time— needed for results of similar accuracy, at least partially cancelling the advantage of faster integration for plane wave functions.

The reduction in the number of basis functions based on prior knowledge is the reason behind the use of contracted Gaussians as basis. Using the prior knowledge of the orbitals of hydrogen and the fact that imbedding in a molecule is basically a perturbation of these orbitals, the basic form of the electronic wave function can

be guessed to be a linear combination of atomic orbitals (LCAO). Basis functions consisting of a fixed linear combination (contraction) of Gaussians are placed around the atoms to resemble atomic orbitals. Of course this type of basis lacks the generality of the plane wave basis functions but the amount of basis functions needed can be reduced by orders of magnitude. The use of Gaussians instead of functions more closely resembling the hydrogen orbitals (e.g. Slater functions) is a concession to time needs. Although the integration of Gaussians is slower than for plane waves, it is still much faster and easier than for Slater functions, which are often used in semiempirical methods, for there are far less integrations (see section 2.4.4).

2.4 Methods to solve the electronic Schrödinger equation

2.4.1 The Hartree-Fock method

The Hartree-Fock method is the most important basic approximation for solving the electronic Schrödinger equation. The fundamental idea is to treat the many-electron system by treating the electrons one by one, interacting with the average field generated by all other electrons. This leads to a constrained optimisation problem that can be transformed into a set of pseudo-eigenvalue equations (see equation 2.7) depending on the Fock operator ($\hat{f}$, defined in equation 2.8).

$$\hat{f}\psi_j = \epsilon_j \psi_j \tag{2.7}$$

$$\hat{f} = \hat{h} + \sum_{i}^{n} (\hat{J}_i - \hat{K}_i) \tag{2.8}$$

with:

n	: number of electrons
ψ_j	: spatial orbital j
$\hat{h}_j$	: potential energy operator for electron j with the nuclei
$\hat{J}_i$	: Coulomb operator, electrostatic repulsion resulting from electron i fully delocalised in its orbital
$\hat{K}_i$	: Exchange operator, arising from antisymmetry condition

The Fock operator is an effective one-electron operator, depending on the solutions for all electrons by $\hat{J}$ and $\hat{K}$. This problem is solvable by an iterative process that, in case it does not oscillate, converges to a self consistent field (SCF) of canonical Hartree-Fock orbitals. The resulting orbitals are arranged in an anti-symmetrically

constructed wave function taking the form of a Slater determinant given in equation 2.9.

$$\Psi(r_1,\omega_1,...,r_n,\omega_n) = \frac{1}{\sqrt{n!}} \begin{vmatrix} \chi_1(r_1,\omega_1) & \chi_2(r_1,\omega_1) & \dots & \chi_n(r_1,\omega_1) \\ \chi_1(r_2,\omega_2) & \chi_2(r_2,\omega_2) & \dots & \chi_n(r_2,\omega_2) \\ \vdots & \vdots & \ddots & \vdots \\ \chi_1(r_n,\omega_n) & \chi_2(r_n,\omega_n) & \dots & \chi_n(r_n,\omega_n) \end{vmatrix}, \quad (2.9)$$

with:

r_i	: spatial coordinates of electron i
ω_i	: spin coordinate of electron i
$\chi_j(r_i,\omega_i) = \psi_j(r_i)\sigma_j(\omega_i)$	: spin orbital j
$\sigma_j(\omega_i)$	: spin wave function j

The Slater determinant shown allows for as many different spatial orbitals as there are electrons in the system. This means that it does not imply sets of two electrons with two different spin wave functions sharing the same space (i.e. orbital). A wave function of this kind is called unrestricted wave function (and the method unrestricted Hartree-Fock, UHF). In most even-numbered-electrons systems the electrons are usually treated in pairs of an α- and a β-spin occupying one spatial orbital. This method simplifies the calculation and is sufficient for the description of the electronic ground state of most closed-shell systems. The ansatz in this case is called restricted Hartree-Fock (RHF). An intermediate case is the restricted open-shell Hartree-Fock (ROHF) ansatz, where all possible pairs of α- and β-spin electrons are formed and treated as sharing a common spatial orbital while a variable number of unpaired electrons are treated separately. The restricted open-shell ansatz is important for the treatment of systems with unpaired electrons in the ground state like radicals or many transition metal complexes, while the unrestricted wave function is especially suitable for systems with all spins paired that can separate partially, for example in the homolytic dissociation. A fact of especially historical importance is that the HF wave function ansatz is variational. This means the energy of a HF wave function is an upper limit for the true energy of the treated system. Details on the Hartree-Fock method and the three different models can be found in the literature [4–6].

2.4.2 Correlated methods

If converged to the global minimum, the Hartree-Fock wave function is the optimal one-determinant (i. e. one-electron) wave function within a given basis. Nonetheless, by only including the interaction of an electron with the others fully delocalised in their orbitals via the Fock operator, it lacks explicit electron-electron interaction. The resulting error in energy is called correlation energy ($E_{corr,basis}$), which is, by equation 2.10, defined as the difference between the exact many-electron en-

ergy ($E_{exact,basis}$) in a given basis and the Hartree-Fock energy in the same basis ($E_{HF,basis}$).

$$E_{corr,basis} = E_{exact,basis} - E_{HF,basis} \tag{2.10}$$

Since Hartree-Fock orbitals are eigenfunctions of a Hermitian operator, they are orthogonal and thus linearly independent from each other. Adding the fact that an amount of orbitals equal to the number of electrons (say n) is used in the wave function (this is the UHF case), it exists in a n-dimensional Hilbert space spanned by the orbitals. For any kind of accuracy, more than n linearly independent basis functions, and with that more resulting orbitals, are needed in the HF procedure (say m). That means that the basis has the potential to expand the wave function in a m-dimensional space of which $m - n$ dimensions are not used in the HF ansatz. The central idea of the Hartree-Fock based correlated methods is to recapture flexibility of the basis that is lost in the $m - n$ virtual orbitals by incorporation of further determinants to the wave function ansatz, thus turning the ansatz into a multielectron wave function, in contrast to the effective one-electron wave function in HF. These methods are laid out in the following sections 2.4.2.1 to 2.4.2.4. In multiconfigurational SCF (section 2.4.2.5) and higher correlated methods based on that (sections 2.4.2.6 and 2.4.2.7), the starting wave function is already more flexible but the basic idea stays the same. All these methods are called explicitly correlated.

As long as the Hartree-Fock wave function is at least a reasonable approximation for the real function as outlined in section 2.4.1, the result can be enhanced by use of various methods of which configuration interaction (section 2.4.2.1), many-body perturbation theory (section 2.4.2.3) and coupled-cluster theory (section 2.4.2.4) will be explained in the following sections. Since they start with one optimised Slater determinant as wave function and enhance the result by adding unoptimized other Slater determinants created via a given scheme from the HF determinant, these methods are called single-reference methods.

In cases when one single Slater determinant cannot capture even the basic features of the wave function, the Hartree Fock wave function should not be used as starting point for a correlation treatment, except for the case of full configuration interaction (see section 2.4.2.1), since the single-reference correlation schemes do not work as well as usual in these cases. This is often true for two electronic states close to each other but also in other situations already outlined in section 2.4.1 and further detailed in section 2.4.2.5. If such a situation is encountered, the initial wave function has to be a linear combination of more than one (usually many) Slater determinants, for all of which the contributing orbitals are optimised. The various determinants (which can be viewed as different electron configurations) are treated equally with none being special in any way. For this reason these methods are called multiconfiguration methods. The most important multiconfigurational methods are

explained in section 2.4.2.5 and the ways to further enhance the results by additional correlation treatment are further detailed in sections 2.4.2.6 and 2.4.2.7.

Since a multiconfiguration wave function will give an energy closer to the exact many-electron energy than the Hartree-Fock wave function, it captures some correlation energy. The correlation energy captured by multiconfigurational methods is founded in qualitative differences between the HF and the real wave function. If there is such a difference, the multiconfigurational treatment is essential for the description. The major part of correlation energy is nevertheless to be gathered in the details of the shape of the wave function. For treating these, SCF-like multiconfigurational methods are inefficient and need contributions by multireference (using a multideterminant wave function ansatz as starting point) methods, related to the ones to be explained in sections 2.4.2.1, 2.4.2.3 and 2.4.2.4, for quantitative agreement. It is said that multiconfiguration methods mainly capture the so-called static while other methods mainly treat dynamic correlation.

In situations where static correlation is important, there is no practical way to avoid a multiconfigurational treatment to obtain qualitatively reliable results, which then can be enhanced via an additional dynamic correlation treatment for quantitative results, if computationally feasible.

The distinction between dynamic and static correlation is in no way clear and in fact even nonexistent. An ever more extensive complete-active-space-self-consistent-field (see section 2.4.2.5) calculation converges to the same result as a full-configuration-interaction calculation. The —concededly weak— differentiation is that static correlation energy is the part of correlation energy that comes from qualitative changes in the wave function, while dynamic correlation stems from quantitative errors. Nevertheless, the distinction helps to choose the proper methods for the problem given.

2.4.2.1 Configuration interaction

As the most straightforward of the methods for correlation treatment, configuration interaction (CI) takes a direct path towards recovering the unused flexibility of the basis. By replacing orbitals in the HF slater determinant by unused, so-called virtual orbitals, new determinants can be created. The resulting determinants are called excited (excited because descriptively spoken this corresponds to exciting one electron from one occupied orbital to a virtual orbital). They can be ordered by the number of substitutions into singly, doubly, and so on, excited determinants or shorter singles, doubles and so on. By this nomenclature a hierarchical order for CI is formed.

The wave function ansatz of CI is a linear combination of the HF determinant and all excited determinants up to a preselected order as given in equation 2.11. Often

the excited determinants are used in the form of spin adapted linear combinations, then called configuration state functions (CSFs). As HF, the CI ansatz is variational.

$$\Psi_{CI} = c_{HF}\Psi_{HF} + \sum_{j}^{O}(\sum_{i} c_{i,j}\Phi_{i,j}) \tag{2.11}$$

with:

Ψ_{CI}	: CI wave function
Ψ_{HF}	: HF determinant
c_{HF}	: expansion coefficient for the HF determinant
O	: order of the CI expansion
i	: index of an excited determinant of a given order
$c_{i,j}$	: CI coefficient for the determinant i of order j
$\Phi_{i,j}$	: excited determinant i of order j.

Evidenced by Brillouin's theorem, the cross terms of singles with the HF determinant in the CI matrix vanish, and thus do not directly contribute to the energy of the CI wave function. Therefore the lowest order of CI treatment commonly used in ground-state simulations is CI-[singles,doubles] (CISD). If the CI expansion is carried out to the maximum possible order, which is the number of electrons in the system, the ansatz is called Full-CI (FCI). The FCI wave function is the exact wave function in the space spanned by the basis functions and therefore recovers all correlation energy. A cut-off CI ansatz has two features that lead to little use of these methods nowadays: The correlation energy recovered is neither size-extensive nor size-consistent (for details see [4–6]). Size-extensivity and size-consistency are essential for many applications of electronic structure theory, for example the calculation of association energies, dissociation reactions and many more. Therefore, the usefulness of the CI ansatz is massively reduced.

2.4.2.2 Graphical unitary group approach to configuration interaction

The graphical unitary group approach [7] (GUGA) can be used as an efficient way to evaluate matrix elements of the CI Hamiltonian matrix between different CSFs. The strength of GUGA lies in the fact that in GUGA-CI the generation of the Hamiltonian matrix is facilitated by a graph based on Gel'fand states [8, 9] that allows for only creating non-zero elements. Thus there are no elements constructed that otherwise need to be eliminated again. This is especially useful for sparse matrices which the CI Hamiltonian matrix is.

GUGA is implemented in the MR-CI code used in the MNDO [10] employed in major parts of this thesis. Details of the specific implementation and more general

details on GUGA are given in [11] on which the preceding qualitative explanations are based.

2.4.2.3 Møller-Plesset second-order perturbation theory

Perturbation theory is a well established method in physics developed to incorporate many-body effects into solutions established for simpler problems. This is based on the assumption that the treated model-system is already close to the real one and only needs a small perturbation by the thus far untreated aspects. The first application was the expansion of the exact two-body-problem-based planetary orbits to incorporate the effects of additional planets.

In quantum mechanics, perturbation theory is used to account for many-electron effects. Via the scheme developed by Møller and Plesset (MP) perturbation of a HF wave function is possible. In fact, Møller's and Plesset's definition of the unperturbed Hamiltonian (a sum over Fock operators (see eq. 2.8)) makes the HF wave function the zeroeth-order wave function and the HF energy the first-order energy, so the perturbation of first order is already incorporated in HF. The MP ansatz is, thus far, the only perturbation-theory-based ansatz to result in a size-extensive method, which is why it is used, although the perturbation is not small in it.

For small and medium-sized molecules the computational expense of the second-order MP treatment (MP2) is comparable to HF, usually gathers about 80 % of the correlation energy [5] and is, as mentioned before, size-consistent and -extensive. For these reasons MP2 is the most popular choice when *ab-initio* treatment of ground states is wanted for non-small systems.

The drawbacks of the MP theory is that it is not variational—which is not that important— and that the perturbation series does not converge. The latter aspect, being very bad in principle, is not serious since higher-order MP treatments quickly increase in computational expense to a point where more accurate methods are available at lower expense, and the second order is still accurate no matter whether the higher-order treatments converge or diverge.

2.4.2.4 Coupled-cluster methods

Coupled-cluster (CC) theory is a correlation treatment that can be viewed as being similar to CI. The major difference is that the expansion not only contains the excited determinants but also products of them. This attribute is achieved by expressing the excitation operator as an exponent of Euler's number as presented in equations 2.12 and 2.13.

$$e^{\hat{T}} = 1 + \hat{T}_1 + (\hat{T}_2 + \frac{1}{2}\hat{T}_1^2) + ... \tag{2.12}$$

$$\Psi_{CC} = e^{\hat{T}} \Psi_{HF} \tag{2.13}$$

while:

$$\hat{T}_1 \Psi_{HF} = \sum_{i}^{occ} \sum_{a}^{vir} (t_{i,a} \Phi_{i,a}) \tag{2.14}$$

$$\hat{T}_2 \Psi_{HF} = \sum_{i<j}^{occ} \sum_{a<b}^{vir} (t_{ij,ab} \Phi_{ij,ab}) \tag{2.15}$$

and so on

with:

Ψ_{CC}	: CC wave function
Ψ_{HF}	: HF determinant
$\hat{T}_n$	: excitation operator
Φ	: excited determinant
t	: amplitude of a given determinant, corresponds to CI coefficient

The action of this operator is expressed as a Taylor expansion of the exponential term. When all possible excitations are taken into account, the ansatz is equivalent to the FCI wave function. Special features of CC come into play when the expansion is cut off. If the expansion is cut off, products of the excited determinants, which can straightforwardly be deduced from equation 2.12, contained in the wave function will become important. Via these products, the CC ansatz achieves to gather some of the effects of excitations higher than the cut-off and, more importantly, it becomes size-extensive and -consistent. The downside is that CC is not variational and very expensive in computational cost. The first point is not that important because in chemistry usually relative energies of two different systems are of interest which are non-variational no matter whether the energies themselves are. The second point, on the other hand, often renders CC unusable for treating higher excitations in non-small chemical systems. A very useful feature of CC, significantly enhancing its versatility, is that truncated CC expansions can be enhanced by a perturbative procedure to approach the next order of the CC expansion in an approximate manner. The order treated perturbatively is denoted in parentheses (e. g. CCSD(T)).

A rather recent development in coupled cluster methods are the approximate CCn methods (n=2,3,...). In these methods, the highest order amplitudes (doubles in CC2, triples in CC3) are analytically calculated via a perturbative scheme (although similar to methods like CCSD(T) this is not the same). Although the CCn methods are not excited-state methods by default, efficient linear response methods for calculation of excitation energies that have been developed make especially CC2

probably the most widely used *ab-initio* method for the studies of excited states without doubly excited character away from conical intersections.

At this point, a brief introduction into response theory shall be given, for details see [12, 13]. Response methods are indirect methods to study excited states, by expanding them in excitations of the ground-state determinant by introducing virtual orbitals. This is in priniciple similar to usual correlation treatments. The difference lies in the treated states. Response methods deal with excited states, via a mathematical trick that yields information about these, while usual correlated methods treat the electronic ground state.

In principle the setup is simple. The optimised ground state wave function is treated with a time-dependent perturbation and the first-order (in linear response methods) response of the system, which is the polarisability [12], is monitored. The time-dependent answer can be transformed to a spectrum via Fourier transformation. The resulting spectrum shows the excitation energies as poles from which the contributing determinants and therefore wave functions can be derived. Calculation of higher order responses allows for the calculation of various other excited-state properties like transition dipole moments. Response theories are powerful tools for studies of excited states. They are rather quick to calculate (as long as the ground state method is not computationally expensive) and exist for methods of various accuracy, from time-dependent density functional theory (TD-DFT), via CC2 to traditional CC. Response theories tend to fail for excited states that have important contributions from doubly excited determinants and of course where the ground-state description already fails, for example for multireference cases.

2.4.2.5 Multiconfiguration self-consistent-field methods

In section 2.4.2 it was pointed out that HF results can efficiently be enhanced by methods like CC or CI as long as the HF wave function is qualitatively reasonable or if a full CI treatment is feasible. When this is not the case, the fundamental method, i. e. HF, has to be changed or the correlation treatment will converge slowly, in the best case, or not at all, in the worst, if HF converges at all. Fundamentally, HF can not be a reasonable approximation to the wave function of a system when a single determinant is not sufficient to represent the basic layout of this wave function.

Before going into some of the specifics of multireference methods, an example for a system that necessitates a multiconfigurational treatment will be given (adapted from [5]).

The basic example of multireference cases are structures that can be expressed via at least two chemically reasonable, non-equivalent mesomeric structures. The ozone molecule is one of these, since it can be expressed via the three resonance structures depicted in figure 2.3, two of which are equivalent. The reason that leads

to the necessity of the multiconfigurational treatment is that there is one that is not equivalent to the others, the diradical.

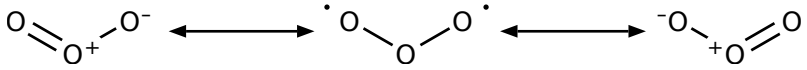

Figure 2.3: Mesomeric resonance structures of ozone.

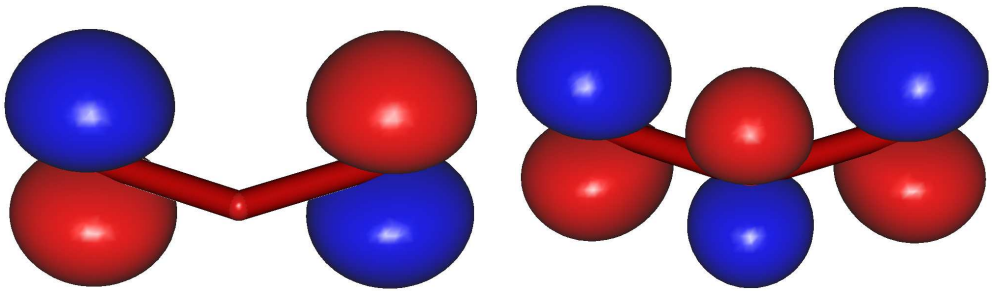

(a) occupancy:1.57 **(b)** occupancy:0.43

Figure 2.4: Final CASSCF(2,2)/6-31g(d) orbitals of the electronic ground state of ozone.

For clarification, complete active space SCF(CASSCF)(2,2) and (12,12) calculations (explanations of the terminology will follow later in this section) were done for ozone in the 6-31g(d) basis set [14] using MOLPRO [15]. From the resulting pseudo-natural orbitals (orbitals that diagonalise the electronic density-matrix in the active space) depicted in figures 2.4 and 2.5, the importance of the multireference treatment becomes clear. In both calculations, the π^*-orbital (figure 2.4) shows important contributions to the electronic ground state which can also be deduced from the corresponding CI-vectors given in table 2.1. The weights of the CASSCF(2,2) CI-vectors can straightforwardly be interpreted in agreement with the simplified model shown in figure 2.3. The configuration 20 (the doubly occupied orbital in figure 2.4a, see the caption of table 2.1 for a detailed explanation of this notation), which represents about two thirds of the final wave function, corresponds to the two equivalent zwitter-ionic structures, while the configuration 02 (the doubly occupied orbital in figure 2.4b) with a coefficient about half as large as the one for 20 accounts for the final third, corresponding to the biradical. Inspection of the orbitals (figure 2.5) and configurations (table 2.1) of the CASSCF(12,12) simulation shows that the CASSCF(2,2) simulation overestimates the contribution of the orbital in figure 2.4b to the system. In the CASSCF(12,12) wave function, the corresponding configuration in total only contributes about a fifth to the wave function, which is about one third of the weight of the unexcited determinant. Still no other configuration shows any major contribution. Thus both simulations clearly support the multiconfigurational picture deduced from the mesomeric formulae.

Other examples for multireference cases of this kind are transition states of dissociation reactions or some transition metal complexes.

Table 2.1: CI-vectors listing configurations with absolute CI coefficients of 0.05 and larger for the CASSCF(2,2) and CASSCF(12,12) wave functions of ozone. The configurations are identified by a listing of orbital occupancies, with numbers corresponding to the total number of electrons, and a and b to one electron in one of the two possible spin states. The orbitals in the configurations are in the same ordering as in figures 2.4 and 2.5

CASSCF(2,2)		CASSCF(12,12)	
configuration	coefficient	configuration	coefficient
20	0.89	222222000000	0.90
02	-0.47	222220200000	-0.29
		220222200000	-0.08
		2222abab0000	-0.06
		2222baba0000	-0.06
		222022020000	-0.06
		222202002000	-0.05

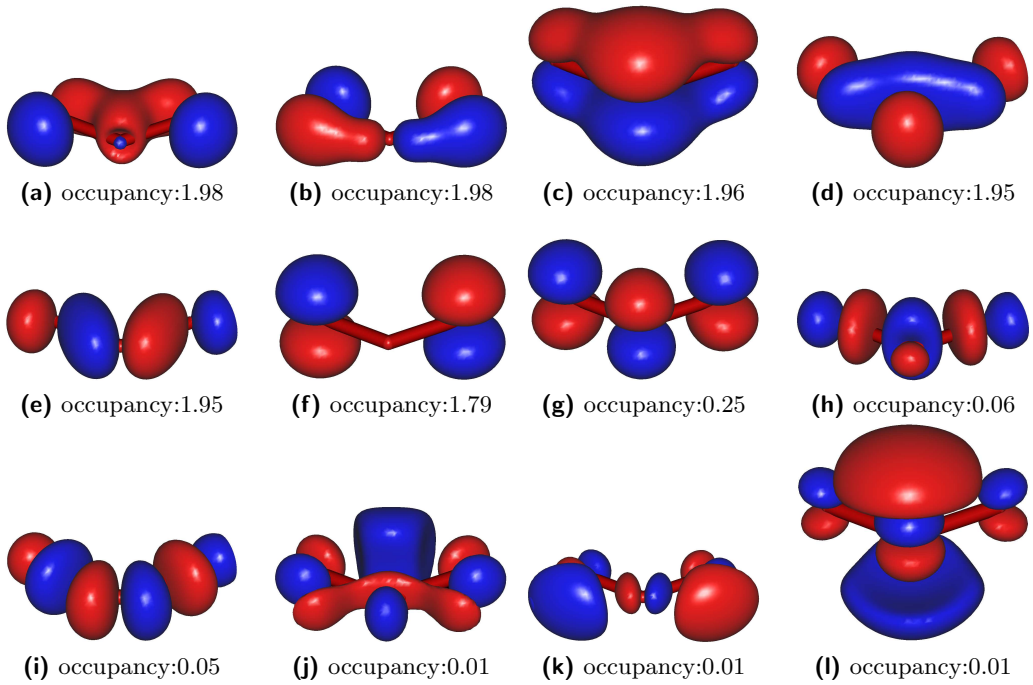

(a) occupancy:1.98 **(b)** occupancy:1.98 **(c)** occupancy:1.96 **(d)** occupancy:1.95

(e) occupancy:1.95 **(f)** occupancy:1.79 **(g)** occupancy:0.25 **(h)** occupancy:0.06

(i) occupancy:0.05 **(j)** occupancy:0.01 **(k)** occupancy:0.01 **(l)** occupancy:0.01

Figure 2.5: Final CASSCF(12,12)/6-31g(d) orbitals of the electronic ground state of ozone.

The type of multireference case most important in this thesis are regions of the potential energy surface where two electronic states of same spin come close to each other (i.e. conical intersections, avoided crossings etc.). In these regions, where the electronic wave function changes significantly over a very small nuclear coordinate space, electronic states that can not sufficiently be approximated by a one-determinant wave function are common. Additionally, a simultaneous unbiased treatment of both electronic states is often needed for smoothly evolving electronic potential energy surfaces in these regions, which is not possible in a single-reference ansatz which is by construction biased towards one state. For this reason, most calculations presented in this thesis are carried out using multiconfigurational methods.

Since the explained problems result from the inability of one-determinant wave functions to represent the basic character of the wave function of the system, the straightforward approach to solve the explained problems is to use a linear combination of determinants as starting approximation to the wave function. The multireference wave function ansatz then gets similar to the CI ansatz (only similar since the exact setup of the determinants is not specified yet). The important difference is that in single-reference CI the calculation of the final wave function is a two-step process, consisting of a HF step to optimise the orbitals followed by the CI step to optimise the CI coefficients, leaving the orbitals untouched. In a multireference calculation the CI coefficients and the orbitals are optimised at the same time in an iterative procedure resulting in the multiconfigurational self-consistent field (MCSCF).

Up to now, nothing was said about the detailed choice of the determinants for the wave function. The most popular method is the CASSCF scheme, already used in the exemplary treatment of ozone. A not completely occupied or empty subset of the atomic orbitals (from any previous calculation of the wave function, they will change during the multiconfigurational calculation) is selected and all determinants that can be created from a FCI treatment of this subset are used in the ansatz. The choice of suitable orbitals for the MCSCF treatment is a problem with no clear path to solve it. There are some rules of thumb, for example taking natural orbitals (orbitals that diagonalise the density matrix) from a previous correlation treatment that are furthest away from double or no occupation (for occupied and virtual orbitals, respectively).

Since the CASSCF scheme contains a full CI expansion within the active space, the total number of orbitals that can be treated is very limited. Additionally, CASSCF is not an efficient method to gather dynamic correlation energy, so the orbitals used in the CASSCF-expansion are usually limited to the ones that are absolutely needed to represent the wave function. The size of the active space in a CASSCF calculation is usually denoted by adding two numbers in parentheses to the method specification, i. e. CASSCF(n,m). In this notation, n gives the number of electrons in the active space and m the number of orbitals. If the space of orbitals needed for a qualitatively correct wave function is too large to be treated in a CASSCF manner, the

restricted active space SCF (RASSCF) method is an option. In RASSCF the active space is separated into three subspaces. The subspaces are depicted schematically in figure 2.6.

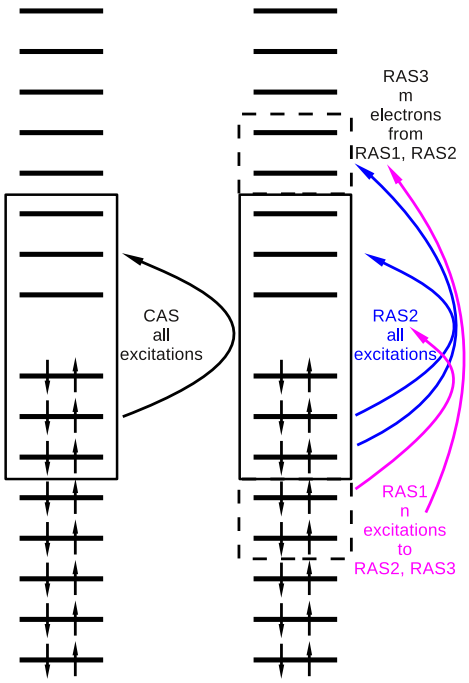

Figure 2.6: Schematic depiction of the differences between RASSCF and CASSCF.

Figure adapted and expanded from [5].

The RAS2 forms the core of the active space. It consists of more orbitals than half the number of electrons (occupied and virtual orbitals in the HF picture). From the RAS2, determinants created by all possible electron distributions are used (this is a CAS in the RAS2). Less important orbitals are collected in the RAS1 and RAS3. The RAS1 consists of occupied orbitals in the HF picture but a set amount (chosen as needed for the system at hand and by computational feasibility) of excitations is allowed from these orbitals to RAS2 and RAS3. RAS3 is the counterpart to RAS1, in the sense that it consists of virtual orbitals in the HF picture. To the RAS3, a set number, not necessarily identical to the excitations from RAS1, of excitations from RAS1 and RAS2 is allowed. All determinants created by this excitation scheme then enter the MCSCF treatment. RASSCF is a useful tool for the handling of very large active spaces in which only low excitation levels are needed. The major problem is that the methods to capture dynamic correlation for multiconfigurational wave functions (see sections 2.4.2.6 and 2.4.2.7) are not commonly implemented or do not even exist for the treatment of RASSCF but only for CASSCF wave functions. For this reason RASSCF is especially popular for systems already prohibitively large for dynamic correlation treatment and even more so as a tool to initially identify

important orbitals for a following CASSCF calculation with dynamic correlation treatment.

An important feature of multiconfigurational methods is that within these models the calculation of the coupling terms in equation 2.4 is possible, due to the possibility to treat the electronic states equally, making them intrinsically suitable for the description of ultrafast photochemical processes.

2.4.2.6 Multireference configuration interaction

Multireference configuration interaction (MR-CI) is basically identical to CI. The difference is that the excitations are created from all the determinants that make up the multiconfigurational wave functions. The HF determinant is usually called reference determinant in classic correlation treatments and the multiconfigurational wave function consists of many evenly treated determinants, hence the method is called multireferential. Truncated MR-CI shares the basic features of truncated CI: it is variational and neither size-extensive nor size-consistent.

An important application of MR-CI is in the field of semiempirical methods (see section 2.4.4). The low flexibility of the minimal basis sets used in semiempirical methods [16–19] leads to the fact that a full-blown MCSCF treatment is usually not necessary to gather static correlation effects. Instead a MR-CI with a very small number of more or less hand-selected reference CSFs is usually applied [20, 21].

Besides multireference perturbation theory there are no other well-established multireferential methods for treating dynamic correlation. For this reason, in spite of the drawbacks, MR-CI is still in widespread use in the field of *ab-initio* quantum chemistry.

2.4.2.7 Multireference perturbation theory

Probably the most frequently used multireference perturbation theory approach, and the only one used in this thesis, is the complete active space second-order perturbation theory presented in [22,23] (CASPT2). For this reason, the following discussion of multireference perturbation theory deals with this approach. Other approaches like the one presented in [24] are similar but will not be treated here. For details on CASPT on a more introductory basis also see [4].

As explained in section 2.4.2.3, the perturbative treatment needs the definition of the zeroeth-order wave function and the zeroeth-order Hamiltonian. The wave function in the multireference case is simply the CASSCF wave function. More difficult than the wave function is the Hamiltonian. Ideally this Hamiltonian converges to the MP Hamiltonian in the single-reference limit and thus to the Fock operator at zeroeth order. Naturally, the CASSCF wave function (Ψ_{CAS}) cannot be expected

to be an eigenfunction of the Fock operator ($\hat{f}$). The action of $\hat{f}$ on Ψ_{CAS} takes the form of a sum of single excitations from Ψ_{CAS} as given in equation 2.16.

$$\hat{f}\Psi_{CAS} = \sum_{ij} f_{pq}\hat{E}_{ij}\Psi_{CAS} \tag{2.16}$$

with:

f_{ji}	: Element ji of the Fock matrix
$\hat{E}_{ij}$	: Single excitation operator.

The zeroeth-order wave function necessarily has to be eigenfunction of the zeroeth-order Hamiltonian. For this reason, the Hamiltonian has to be adapted further. A suitable definition is given in equations 2.17, defining the Hamiltonian, and 2.18 defining a set of orthogonal projectors ($\hat{P}$), with the expectation value of Ψ_{CAS} for $\hat{f}$ as zeroeth-order energy ($E^{(0)}$). The projectors project on the CAS space orthogonal to Ψ_{CAS} ($\hat{P}_K$), and on the spaces arising from excitations of a given order (single and double for $\hat{P}_{SD}$ and so on) which are not part of the CAS space.

$$\hat{H}_0 = E^{(0)} \left|CAS\right\rangle \left\langle CAS\right| + \hat{P}_K\hat{f}\hat{P}_K + \hat{P}_{SD}\hat{f}\hat{P}_{SD} + \hat{P}_{TQ}\hat{f}\hat{P}_{TQ} + ... \tag{2.17}$$

$$1 = \left|CAS\right\rangle \left\langle CAS\right| + \hat{P}_K + \hat{P}_{SD} + \hat{P}_{TQ} + ... \tag{2.18}$$

This operator presented in the articles [22, 23] converges to the MP Hamiltonian in the single-reference case and stays manageable in the multireference case.

A practical problem encountered in CASPT are so-called intruder states [25, 26]. An intruder state occurs when a state created by the perturbative treatment is close in energy to states in the CASSCF wave function. Usually, this manifests itself in a strongly diminished weight of the reference wave function in the final CASPT2 wave function. This often is destructive to the results. The simple solution for intruder state problems is to add to the active space the orbitals involved in the intruder states that are not active in the CASSCF wave function. This is not a sign that the active space is not large enough for a reasonable CASSCF treatment but that the CASPT2 treatment needs a larger active space than a CASSCF study of the underlying system. The problem is that the number of active orbitals is fairly limited due to the full-CI treatment in CASSCF. A well-established way around the inclusion of additional orbitals is the inclusion of a real valued level-shift to the zeroeth-order Hamiltonian. The level-shift lowers the amount of correlation energy gathered by the perturbation. Although part of this can be corrected for, the level-

shift has to be applied carefully and an enlarged active space should always be the first option considered.

2.4.3 Density functional theory

Density functional theory (DFT) is one of the most important frameworks in electronic structure. Since DFT was not used within this thesis in any relevant way, the following treatment of DFT will be very superficial. For more detailed treatments of DFT see the relevant literature [5, 6, 27].

The fundamentals of DFT are the theorems of Hohenberg and Kohn. The first theorem states that it is possible that there is a functional that uniquely determines the potential, the number of electrons and the energy of the system from the electron density (ρ) alone. The second one states that the density is variational, thus the energy calculated from a test density is an upper limit of the true energy. What the theorems do not address the form of the functional at all.

The possibility to use the electron density instead of the actual electrons is intriguing due to a massively reduced dimensionality. In a wave function representation of the system, a dimensionality of four times the number of electrons is needed (three dimensions of space and one of spin per electron), while the density is a function in three dimensions no matter how many electrons there are. Though tried various times over the years, attempts to come up with sufficiently accurate functionals were never successful due to a lack of a accurate kinetic energy functional. In the second important step towards modern DFT, the Slater determinant representation of the electronic wave function was re-introduced in the Kohn-Sham ansatz to calculate the exact kinetic energy of a reference system of non-interacting electrons. This ansatz brings back the problem of dimensionality scaling with the number of electrons but is the only known way to come up with reasonable results for realistic systems. The functional in this ansatz takes the form of a sum of three separate functionals: the kinetic energy functional of the non-interacting electrons ($T(\rho)$), the known classical Coulomb functional ($J(\rho)$) and the unknown exchange-correlation functional ($E_{xc}(\rho)$) that governs everything not treated by the other two.

Various approaches have been suggested for exchange-correlation functionals which can be classified by their route towards constructing the functional. The most simple one, which is of similar accuracy as HF, is the local density approximation (LDA). In LDA, only the density itself contributes to the energy. Usually more accurate than LDA are the generalised gradient approximations (GGA), which use derivatives of the density of first order (GGA) or higher order (meta-GGA). The last family of functionals are the hybrid functionals, which use a weighted amount of exact HF exchange within their exchange part in addition to a GGA ansatz. The hybrid functionals are usually more accurate than LDA and often GGA, while they do neither

surpass nor fall short relative to meta-GGA functionals in a way that a trend could be identified.

Modern DFT methods of (meta-)GGA and hybrid type exhibit a reasonable accuracy while taking comparably small amounts of computer time. This makes DFT one of the most important and widely used methods in modern electronic structure theory. The fact that some inaccuracies appear through the whole "hierarchy" of DFT means that some thought should be spent on when to use which functional. The most important inaccuracy is caused by the wrong long-range behaviour of traditional functionals. This causes serious errors in the description of long-range interactions and thus in the description of hydrogen bonds, adsorption, charge transfer and Rydberg states, to name some examples. The severity of this problem leads to various approaches to fix some or all of these inaccuracies, from addition of semiempirical van der Waals potentials [28] to completely new functionals [29]. In addition to these specific limitations, DFT as a single-determinant theory is limited in the treatment of multireference situations, as lined out for HF-based methods in section 2.4.2.5. Similar to HF, this limitation can be handled to some amount by use of unrestricted or restricted-open Kohn-Sham-determinants.

Through TD-DFT, its response theory, DFT became a very powerful tool for the study of excited states, their properties and their potential energy surfaces, because by TD-DFT the useful compromise between accuracy and computational speed of DFT became available in the realm of excited-state studies.

Although DFT is a rather accurate method when the aforementioned limitations are kept in mind, especially in case of TD-DFT the results have to be treated carefully. The deficiencies of traditional functionals, which were developed with ground states in mind, often become important. Thus the functional used for the problem at hand should be chosen even more carefully. The other important limitation of traditional TD-DFT is the inability to describe states with important contributions from doubly excited determinants [30] (a limitation common to linear response theories). Modern developments in TD-DFT, for example spin-flip TD-DFT [31] (SF-TD-DFT), manage to expand the applicability of TD-DFT to doubly excited states and also allow for the treatment of conical intersections involving the ground state. Still the applicability of SF-TD-DFT is limited, because SF-TD-DFT is comparable to a (2,2) active space with respect to static correlation. Thus only excited states and conical intersections describable in such an active space are in reach of SF-TD-DFT.

2.4.4 Semiempirical methods

In some cases the computational time needed for accurate *ab-initio* or DFT calculations is too long to be affordable. Two basic reasons can be responsible for this: either the system is too large or the system has to be treated very often for different

nuclear geometries. Often though (as is the case in this thesis), the quantum nature of the electrons needs to be retained, thus rendering classical approaches called molecular mechanics useless. Molecular mechanics will not be detailed in this thesis but can be looked up in [5] for example. The need of electronic quantum character means the Schrödinger equation has to be solved. Semiempirical methods are a popular approach in these cases. Before going into some depths for a selected few methods, the basic features will be explained.

The most time-consuming step in a Hartree-Fock cycle is usually the evaluation of integrals over basis functions and operators, especially the two-electron integrals. In semiempirical methods, the computational cost is significantly reduced by various methods that reduce the amount of integral evaluations. The first step in reduction of computational cost is the complete neglect of non-valence electrons. The core electrons are either represented by a reduction of the nuclear charge or by a functional model combining the neglected electrons with the nuclei. Furthermore, the remaining electrons are usually represented by a minimal basis. Of the remaining integrals, many (especially the two-electron integrals) are either neglected or replaced by simple parameter-dependent functions. These atom-specific parameters are adjusted to reproduce a large amount of empirical and accurate *ab-inito* data for various molecules, the training set. Ideally, these parameters are applicable to the atom in every conceivable molecule. In reality, the accuracy of the results is very dependent on the similarity of the simulated molecule to the training set, which naturally is limited in size. Actual semiempirical models usually do not contain parameters for every chemical element, mostly because of the large amount of time and data needed for the adjustment. Thus, the methods are limited to molecules that contain parametrised atoms only. In newer models, the number of parametrised elements is not unlikely to be very small (below ten), because of the short time between establishing the model and today. The asset of semiempirical methods in cases where the model is applicable is that the parametrisation allows for implicitly capturing electron correlation effects in a fraction of the time needed for a HF calculation, because the data in the training set contains electron correlation either via highly accurate *ab-initio* methods or via the experimental data.

Now a short overview about some of the fundamental approximations in semiempirical methods will be given, before going into some details of specific semiempirical methods. More details about the basic approximations can be found in [5, 32–36]. The most basic semiempirical simplification is Zero Differential Overlap (ZDO). ZDO means that all products of basis functions depending on the same electron at different atomic centers are set to zero, which, besides some others, eliminates all two-electron three- and four-center integrals. In its pure form, ZDO is employed in the Neglect of Diatomic Differential Overlap (NDDO) model. Expanding the simplification, Intermediate Neglect of Differential Overlap (INDO) sets two-center two-electron non-Coulomb integrals to zero. This approximation would destroy the

rotational invariance. To avoid that, the dependance of various integrals on the angular momentum quantum number of the involved orbitals has to be eliminated in INDO. In Complete Neglect of Differential Overlap (CNDO), the INDO approximation is expanded by setting two-electron one-center integrals to zero as long as they depend on the overlap of different basis functions.

All the approximations up to now were formally applied to a Hartree-Fock calculation treating valence electrons only, in a minimal basis. Even without any further approximations the results of the calculations would be qualitatively correct at best.

The most popular method to (re-)introduce the accuracy needed for addressing chemically relevant questions is the aforementioned introduction of parameters and parametrised functions for the solutions of the remaining integrals and fitting these parameters to large amounts of data. This was pioneered in the group of Dewar [16].

The most widely used semiempirical methods are the Modified Neglect of Diatomic Overlap (MNDO), the Austin Model 1 (AM1) and the MNDO, Parametric Method Number 3 (MNDO-PM3 or just PM3). They are based on the NDDO approximation using a variety of functions and constants to express the different integrals still to be calculated after applying the NDDO approximations. MNDO and AM1 are essentially identical, with the only difference of AM1 being the functional form of the treatment of the nuclear repulsion, by adding Gaussian-shaped terms. The modifications are needed only because the electrons are not treated exactly, therefore the nuclear repulsion can not be treated exactly either. In PM3, the AM1 model is kept but the optimisation changed from a manual to an automatic one and with that, to a significantly larger training set.

In the PM5 approach a further reduction of the deficiencies of MNDO is tried by introduction of diatomic parameters into the nuclear repulsion part of the model, although this enhances the results, the increase in the number of parameters due to atomic pairs is an important drawback.

A different family of semiempirical methods, although related via MNDO and AM1, are the orthogonalisation models 1 to 3 (OM1 to 3) developed by Thiel and coworkers [19, 37]. Since these methods experience widespread use in this thesis, they will be detailed in their own section 2.4.4.1.

Recently, semiempirical models combined with multireferential CI methods began to play an important role in the studies of the dynamics of ultra-fast photochemical processes [20, 38–41]. The approach presented in [19, 37], which is essential to this thesis, will be and was dealt with in sections 2.4.4.1 and 2.4.2.2. Another approach, developed by Persico and co-workers [21], is the Floating Occupation CI (FOCI) method coupled to AM1. The model was successfully used in various semiclassical direct dynamics studies (see 2.5.2) of azobenzene-related molecules [41–44]. In their simulations, Persico and co-workers used a CAS-CI ansatz, which allowed the electrons to fractionally occupy orbitals in a Gaussian-shaped function along the orbital-energy axis (hence the name), to partially account for higher excitations. An

additional potential parameter was added along the E/Z-isomerisation coordinate and parametrised against accurate *ab-initio* data.

2.4.4.1 OMX

This section will give an overview over the semiempirical models most important to this thesis. A more detailed introduction, derivation and specification of the models is given in [19, 37, 45].

Some of the important deficiencies in modern semiempirical methods can, to a major part, be traced back to a lack of orthogonality in the atomic orbital representation. The orthogonality, which is inherent in the Hartree-Fock approach, effectively reduces the available space the orbital can expand to and by that increases the orbital energy. The NDDO model takes away the intrinsic orthogonality of Hartree-Fock orbitals. Since the energetic effects of the orthogonality are dependent on the nuclear geometry, the potential energy characteristics of the internal degrees of freedom of a molecule, especially dihedral angles, are influenced by the insufficient orthogonality. Within the NDDO model there are two different reasons for neglected orthogonality. One is the collapse of core electrons into core pseudo-potentials, the other one is neglect of the one-electron two-center products. An evaluation of the remaining two-electron integrals within an orthogonalised basis and correcting for the errors caused by neglecting the other two-electron integrals is not feasible without loosing most of the speed-up gained by neglecting the three- and four-center integrals but the actual correction obtainable from these is small and can thus be neglected. This leaves the orthogonalisation effects on the one-electron integrals and the core-valence orthogonality to be treated. The orthogonalisation models (OM) widely applied in this thesis deal with the valence-core and the valence-valence orthogonality by introduction of specially parametrised functions for both the core potential and the integrals. For the core valence interaction, effective-core potentials were introduced, while in the case of the one-electron two-center integrals a truncated, parametrised series expansion is used. Both of these corrections were guided not by empirical data, but by analytic *ab-initio* formulae and numerical *ab-initio* data.

The introduction of the orthogonalisation correction efficiently reduces major deficiencies known from NDDO-based semiempirical methods in the area of conformational properties and long-range interactions, for example in hydrogen bonds or pericyclic reactions.

2.4.5 Exciton coupling as basic approach to coupled multichromophore systems

The exciton model is an old model, developed for the coupling of large systems of excited molecules. The character of the model restricts its use to rather weakly coupled systems but within this limitation allows for the treatment of very large

systems such as the photosynthetic photosystems and complex electronic excitation transfer processes within them. To check the applicability of the exciton model to a multichromophoric azobenzene system is the topic of section 6.6.3. Thus, the model will be discussed in some detail here.

Although historically developed for the description of electronic excitation in extended solids [46], the exciton model was later expanded to the treatment of molecular systems [47, 48]. An exciton is a pair of an electron and an electron hole. The fundamental idea of the molecular exciton approach is that in a multichromophoric system the total wave function of an electronic state, especially excited ones, can be described by a linear combination of single chromophore states with only minor deviations, thus it is in its core a perturbation theory.

Assume an uncoupled system of two identical chromophores **1** and **2**. Since the system is uncoupled, the Hamiltonian of the full system is a sum of the two Hamiltonians of the subsystems $\hat{H}_1$ and $\hat{H}_2$. The ground state wave function of the system then is the product of the wave functions of the subsystems ($|1_{gs}\rangle|2_{gs}\rangle$). The energy of this state is simply twice the ground-state energy of one chromophore ($2 \cdot E_{gs}$). The first excited state is a degenerate state comprised of the ground state of one chromophore and the first excited state of the other, i. e. $|1_{ex}\rangle|2_{gs}\rangle$ and $|1_{gs}\rangle|2_{ex}\rangle$, with an energy of $E_{gs} + E_{ex}$. The transition dipole moment is the transition dipole moment of the subsystems (μ_{mono}) for both states, giving rise to a doubled intensity of the transition due to the degeneracy.

Now assuming a coupling of the chromophores, the Hamiltonian of the system can be expressed via the addition of a coupling term (taking the form of point-dipole point-dipole terms of the multipole expansion [49]), yielding a total Hamiltonian given in equation 2.19. The ground state for the new Hamiltonian is still the product of the wave functions of the subsystems and its energy is given by equation 2.20, with D_{12} being the energy lowering caused by the interaction of the ground states of the subsystems, commonly associated with van-der-Waals interactions, thus called vdW-term from now on.

$$\hat{H}_{ges} = \hat{H}_1 + \hat{H}_2 + \hat{V}_{12} \tag{2.19}$$

$$E_{0,coupled} = E_{gs,1} + E_{gs,2} + \langle 1_{gs}|\langle 2_{gs}|\hat{V}_{12}|2_{gs}\rangle|1_{gs}\rangle = E_{gs,1} + E_{gs,2} + D_{12} \tag{2.20}$$

For the first two excited states of the dimer, a linear combination ansatz of the form given in equation 2.21 is used. Using the notation $H_{ij} = \langle i_{ex}|\langle k_{gs}|\hat{H}_{ges}|j_{ex}\rangle|l_{gs}\rangle$ (i and j indicate the index of the excited chromophore in bra and ket, respecitvely; k and l take the index of the other chromophore, with respect to i and j), the excited-state secular determinant is given by equation 2.22. Solving the eigenvalue problem,

the respective state energies (here given as excitation energies) and vectors can be derived as given by equations 2.23 and 2.24.

$$|12_{ex}\rangle = c_1 \cdot |1_{ex}\rangle|2_{gs}\rangle + c_2 \cdot |1_{gs}\rangle|2_{ex}\rangle \tag{2.21}$$

$$\begin{vmatrix} H_{11} - \lambda & H_{12} \\ H_{21} & H_{22} - \lambda \end{vmatrix} = 0 \tag{2.22}$$

$$\Delta E_{1/2} = \Delta E_{mon} + \Delta D \pm E_{split} \tag{2.23}$$

with:

$$\begin{aligned} H_{11} &= H_{22} \\ H_{12} &= H_{21} \\ \Delta E_{mon} &= E_{ex} - E_{gs} \\ \Delta D &= \langle 1_{ex}|\langle 2_{gs}|\hat{V}_{12}|2_{gs}\rangle|1_{ex}\rangle - \langle 1_{gs}|\langle 2_{gs}|\hat{V}_{12}|2_{gs}\rangle|1_{gs}\rangle \\ E_{split} &= \langle 1_{ex}|\langle 2_{gs}|\hat{V}_{12}|2_{ex}\rangle|1_{gs}\rangle \end{aligned}$$

$$|12_{ex1}\rangle = \frac{1}{\sqrt{2}}(|1_{ex}\rangle|2_{gs}\rangle + |1_{gs}\rangle|2_{ex}\rangle),\ |12_{ex2}\rangle = \frac{1}{\sqrt{2}}(|1_{ex}\rangle|2_{gs}\rangle - |1_{gs}\rangle|2_{ex}\rangle) \tag{2.24}$$

These two resulting state vectors therefore are normalised linear combinations of an electron-hole pair on each monomer, in an additive and a subtractive fashion. In a quasi-classical vector picture, the absolute transition dipole moments for the transition from the dimer S_0 state to the two excited states can be predicted to be $\mu_{dimer} = \mu_{mono} \pm \mu_{mono} \cdot cos(\theta)$, with θ being the angle between the transition dipole moment vectors.

An analogous treatment of a trimeric system yields equation 2.25 for the energies, with corresponding definitions for ΔD and E_{split}, and equation 2.26 for the state vectors. The ground state is as straightforward as for the dimer and thus is not explicitly stated again. The two degenerate states $|123_{ex1}\rangle$ and $|123_{ex2}\rangle$ span a two-dimensional space of a subtractive linear combination of two electron-hole pairs, while state $|123_{ex3}\rangle$ is a fully positive linear combination of three electron-hole pairs. The weights of the excitons in all linear combinations is identical except for the sign. The states $|123_{ex1}\rangle$ and $|123_{ex2}\rangle$ could be orthogonalised but are left in their current state for easier comparison to the studies presented in section 6.6.3. For the same reason, the ordering of the states is done the way it is here. In principle the energetic order depends on the sign of the coupling terms. The ordering used here, is the same as the one encountered in the later studies (section 6.6.3).

$$E_1 = E_2 = \Delta E_{mon} + \Delta D - E_{split},\ E_3 = \Delta E_{mon} + \Delta D + 2E_{split} \tag{2.25}$$

$$
\begin{aligned}
|123_{ex1}\rangle &= \tfrac{1}{\sqrt{2}}(|1_{ex}\rangle|2_{gs}\rangle|3_{gs}\rangle - |1_{gs}\rangle|2_{ex}\rangle|3_{gs}\rangle), \\
|123_{ex2}\rangle &= \tfrac{1}{\sqrt{2}}(|1_{ex}\rangle|2_{gs}\rangle|3_{gs}\rangle - |1_{gs}\rangle|2_{gs}\rangle|3_{ex}\rangle), \\
|123_{ex3}\rangle &= \tfrac{1}{\sqrt{3}}(|1_{ex}\rangle|2_{gs}\rangle|3_{gs}\rangle + |1_{gs}\rangle|2_{ex}\rangle|3_{gs}\rangle + |1_{gs}\rangle|2_{gs}\rangle|3_{ex}\rangle)
\end{aligned} \tag{2.26}
$$

2.5 Treatment of the nuclei

The Born-Oppenheimer separation allows for the separate treatment of the electronic and the nuclear problem. Following more or less complete use of the Born-Oppenheimer approximation (see section 2.2) allows for focusing on one or some electronic states via the methods presented in section 2.4. These results can then be used in the description of the nuclei. In most cases the nuclei are treated specifically to simulate the dynamics of a system. Therefore the section will deal with dynamic systems.

The higher mass of the nuclei compared to the electrons gives rise to an important feature in the treatment of the nuclei, namely the option to not describe them as quantum particles but as classical particles while still retaining many of the features of their dynamics. For this reason the section will be split into two parts, one dealing (very shortly) with the quantum treatment (see [50, 51] for more details) and one with the classical treatment (see [52] for details) of the nuclei.

2.5.1 Wave packet dynamics

The most obvious quantum-mechanical approach for treating the nuclei would be to use the results from electronic structure calculations and with them to solve equation 2.4 within the Born-Oppenheimer approximation, while re-introducing the time-dependency. Various methods exist following this approach. Retaining the quantum nature of the nuclei directly accounts for some effects that can be important for chemical reactions, namely wave function interference, tunneling and, most importantly for the processes dealt with in this thesis, explicit propagation of the nuclei on coupled electronic surfaces.

The most important drawback of quantum-mechanical simulation of nuclear dynamics is the need to represent the wave function in all relevant coordinates. In a classically treated molecule, at a given time one has exactly one value for each coordinate. A quantum-mechanical molecule, on the other hand, is spread within the coordinates. In traditional nuclear quantum dynamics, this leads to the memory needed to store the wave function and the number of potential energy calculations (i. e. solutions of the electronic Schrödinger equation) to scale exponentially with the number of internal degrees of freedom treated in the simulation. Especially the latter puts a serious limitation on the system size that can be treated. Depending on the accuracy of the treatment of the electronic problem, this limit is somewhere between three to nine degrees of freedom. However, newer developments in the field

of multiconfiguration-time-dependent-Hartree [51] (MCTDH) push that limit but do not actually solve the problem of exponential scaling. For the highest-dimensional cases this is achieved by representing the potential in less important degrees of freedom by simple functions, not by explicitly solving the electronic problem.

2.5.2 Classical dynamics

An alternative to the quantum treatment is the classical one. Treating nuclei as classical particles strips them from the ability to tunnel, interfere or spread over different electronic states. While tunneling and interference are quantum effects important only for highly accurate calculations or in special situations, the involvement of multiple electronic states is essential for the description of any ultrafast photo-reaction. Additionally, the classical model introduces the need to simulate an ensemble of molecules, while in the quantum picture only one simulation is needed. The need for an ensemble of molecules is inconvenient (although not as restrictive as the exponential scaling in quantum dynamics) and gives rise to a need for fast energy calculations, ruling out highly accurate methods for all but the smallest molecules. Still classical nuclear dynamics are routinely applied today to systems of sizes from a few atoms to full proteins in solvating water. The latter only for the most simple potential energy models.

The actual propagation is a straightforward numerical integration of Newton's equations of motion via one of various integration schemes. Details can be found in the established literature [52].

To treat more than one electronic state more intricate schemes are needed. There are two established methods for such dynamics (then often called semiclassical). One approach is Ehrenfest dynamics [53], the other is surface hopping via Tully's fewest switching algorithm [54]. The methods treat the coupled surfaces in very different ways. In Ehrenfest dynamics, the surfaces are mixed by adding them after multiplication with a weighting factor, once a trajectory reaches a region of non-negligible coupling. From then on, the trajectory propagates on the average of the two surfaces. In Tully's approach, the surfaces stay unchanged but at every time step there is a chance that a trajectory switches the surface it is propagating on. The probability for this so-called surface hop is determined by the coupling of the states involved and set up in a way that assures state populations for an ensemble of trajectories that is equivalent to the distribution a wave packet would assume in the same region, with the fewest possible surface transitions. Velocities are scaled after a electronic transition so that conservation of energy is assured.

The surface-hopping approach presents a simple and efficient way to simulate electronic de-excitation in the realm of classical nuclear dynamics and thus allows for the full-dimensional simulation of comparably large systems, as long as there are sufficiently fast models to solve the electronic Schrödinger equation.

3

Photo-dynamics of cyclohexadiene

3.1 Project motivation

As explained in section 2.4.2, the extraordinary time requirements of multireference *ab-initio* quantum-chemical methods leads to model systems often being needed for calculations to be feasible. For 1,6-ring-opening/-closure switches like fulgides (see section 4), the most simple model system is cyclohexadiene/hexatriene (CHD/HT). Due to the simplicity of the system, it was subject to both experimental and theoretical studies, already from the mid nineties to the beginning of the 21^{st} century [55–63]. Newer studies still deal with the CHD/HT system itself, but a couple of articles ensued using theoretical data from the model system to treat the more complicated fulgide systems [64, 65]. During the beginning of this thesis, this was still state-of-the-art and only changed due to newly found differences between the model and the modeled systems [66].

Up to the beginning of this project, all theoretical investigations where based on reaction path approaches, i. e., based on minimum energy path calculations between selected points of the PES (mainly stationary points and intersection seam minima). Although this is a well established approach, already in the late eighties it was shown that in some cases this approach does not grasp the intricacies of reactions [67].

The aim of this project was basically threefold: To further deepen the understanding of the CHD/HT system, to check the applicability CHD/HT as model for fulgides, and to try a simulation approach not based on and biased by a selection of special points.

3.2 Photochemical ring-opening of cyclohexadiene: quantum wavepacket dynamics on a global ab initio potential energy surface

Contributions to the paper:

- Basic setup of the project i.e. formulation of essential questions and methodology to answer them
- Simulation of the data points of the surface, i. e. setup of the active space, running the geometry optimisations, extraction of energies, identification of strongly coupled regions
- Major contributions to interpretation of the comparability to the experiment
- Major contributions to writing of the parts of the article corresponding to the aforementioned points and of the common parts (introduction, conclusions etc.)

DOI: 10.1021/jp909362c

3.3 Additional information: Development of the potential energy surface

3.3.1 Comparability to higher correlation effects and a diffuse basis

To proof qualitative accuracy of the CASSCF(6,6)/TZVP [68] treatment as presented in the article, additional three-state multi-state CASPT2(6,6)/TZVP and CASSCF(6,6)/6-311++g(2df,p) [14] calculations were carried out as single-point calculations for various geometries of the relaxed surface scan at different values of ϕ. The CASPT2 calculations were performed using MOLCAS [69] and the CASSCF calculations using MOLPRO [15], respectively. The CASPT2 calculations were performed without a level-shift, which reduces the geometries for which the CASPT2 calculation can successfully be carried out, due to intruder state problems (see chapter 2 for details), but enhances the accuracy at the useful geometries. It was not necessary to set up a suitable level-shift for the whole surface, since the useful points are more than enough for the qualitative comparison. In the CASSCF calculations in the diffuse basis, 45° and 35° were used as values of ϕ. The rather scattered

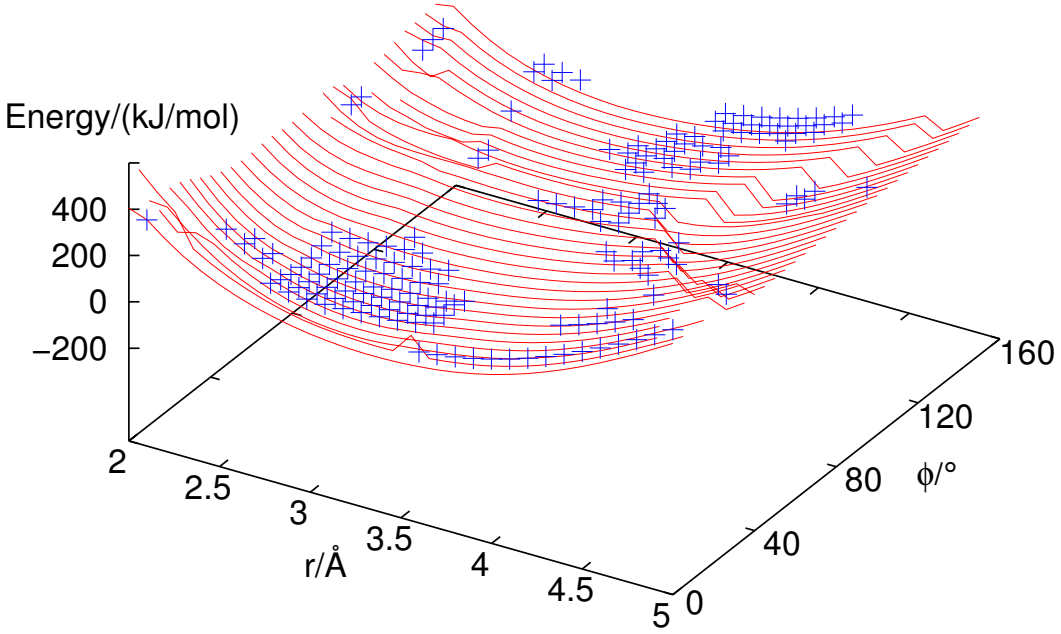

Figure 3.1: S_1 potential energy surface. Depicted are CASSCF/tzvp energies (lines) and CASPT2/tzvp energies (points). Both types of data are relative to the S_1 energy at $r = 3.0$ and $\phi = 35°$ in the given model.

appearance of usable CASPT2 points on the surface (see fig. 3.1) makes a visual comparison of the data as a whole very complicated. To supply feasible graphs for optical comparison, exemplary cuts were taken from the data after shifting the S_1

energy at $r = 3.0$ and $\phi = 35°$ (the minimum on the CASSCF(6,6)/TZVP surface) to zero for both CASSCF and CASPT2 data. The resulting graphs are presented in Fig. 3.2. On first glance, the CASPT2 data look very different from the CASSCF

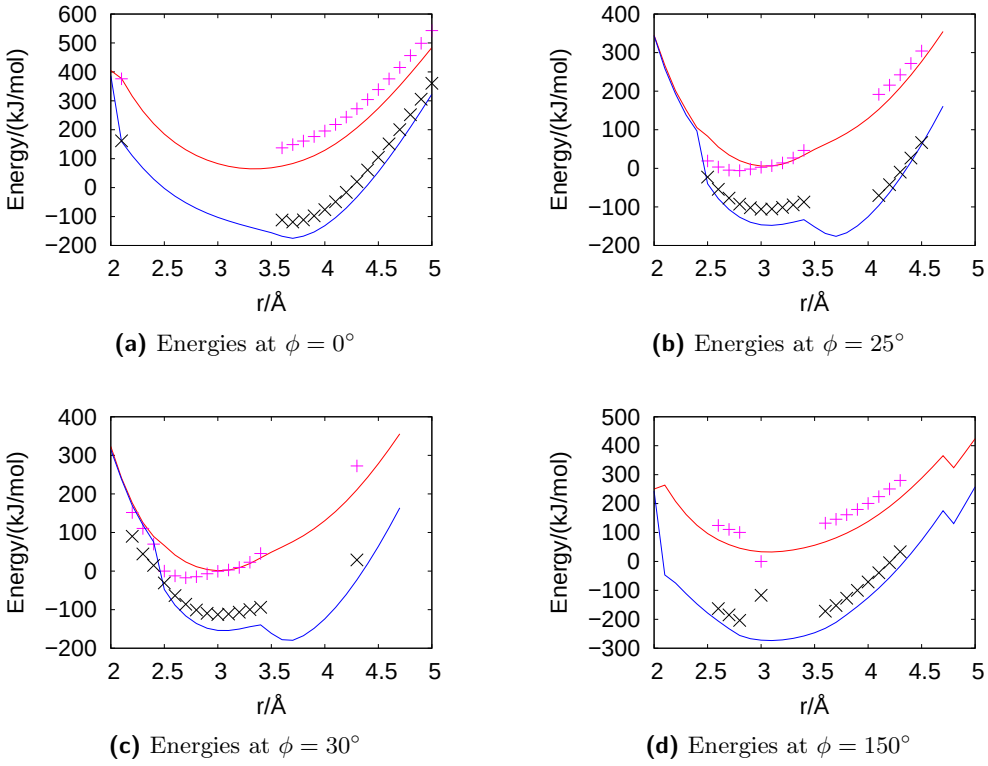

(a) Energies at $\phi = 0°$

(b) Energies at $\phi = 25°$

(c) Energies at $\phi = 30°$

(d) Energies at $\phi = 150°$

Figure 3.2: Exemplary cuts through the comparison of CASSCF (lines) and CASPT2 (points) data as depicted in 3.1. Depicted are the S_1 and S_0 states.

results, especially on the left hand side of figs. 3.2b and 3.2c. A detailed inspection of fig. 3.2c reveals that the CASPT2 energies of the S_1-state show an energetic minimum at about $r = 2.6$ Å, thus shifting the minimum from $r = 3.0$ Å to about 2.6 Å. The points away from the minimum show that the energies for r qualitatively fit in both models, only shifting the characteristic features a bit. This is true for all graphs in fig. 3.2. In total, the shape of the CASPT2 S_1-surface stays similar enough to the CASSCF surface and also shows small energy gaps to the S_0-surface in the same general region. For the data on the effect of diffuse functions, the comparison was straightforward. All energies were calculated relative to the S_1 energy at $r = 3.0$ Å and $\phi = 35°$, which was set to zero in both models. The resulting graphs are depicted in Fig. 3.3. In case of the added diffuse functions the comparison fits nearly quantitatively. The energy gap at the intersection seam (left hand side of both graphs in 3.3) increases by a small amount but leaves the structure of the S_1-surface intact.

In sum, both comparisons show a reasonable qualitative agreement of the relative energies for the first excited state, and both more accurate models show small S_1-S_0 energy differences in the same region of coordinates as in the CASSCF(6,6)/TZVP

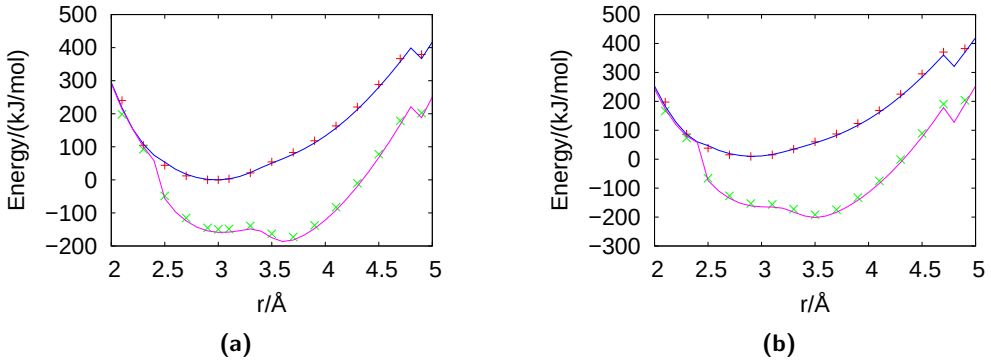

Figure 3.3: Comparison of the potential energy surface shape at $\phi = 35°$ (a) and $\phi = 45°$ (b) for optimised geometries at CASSCF(6,6)/TZVP (lines) and CASSCF(6,9)/6-311++g(2df,p) (points) level. The energies are relative to the energy of the $r = 3.0$ Å and $\phi = 35°$ point for both models.

calculations. This justifies the use of the computationally less expensive model, for the purpose of the presented paper, the predictions of which are purely qualitative in nature.

3.4 Project summary

In this project, a model surface for CHD was set up, with minimal assumptions about special points appearing on the surface. The input was solely the active coordinates and the assumption that the other coordinates (with the exception of the dihedral angle ξ) relax for a given configuration of the active coordinates. In this surface, all distinct features like minima, transition states or intersection seams appear naturally (i. e. as points lowest in energy for a given configuration of active coordinates). This model is very different from the reaction path models in the way that the latter puts a constraint on the reaction, by funneling it into a reaction path. Although surpassing a reaction path ansatz in some regards, the relaxed surface model has distinct disadvantages: Firstly, the model intrinsically focuses on one electronic state with no possibility to consistently treat other states explicitly. Secondly, the relaxation in the case of CHD causes the conical intersection seam to appear at relatively high energies, while the parts of lower energy are not part of the surface. This causes the model to be unsuitable for the description of low-energy processes.

It was possible to show that dynamics on the less biased relaxed surface yields results complementary and in certain respects superior to reaction-path-based surfaces. In regard of the depopulation frequency of the S_1-state the simulations on the relaxed surface clearly surpass the reaction-path approach in comparisons with the experiment. The simulations allow for mechanistic interpretations: The de-excitation process of CHD/HT is likely to be dominated by high-energy regions of

the intersection seam. These parts are not part of minimum-energy-path-based interpretations used by the time of this project. The two steps in the S_1-population are caused by de-excitation at significantly different geometries.

The new interpretations of the data contributed to the removal of CHD as a model for more complex molecules showing electrocyclic ring-opening reactions.

4

Photo-isomerisation reactions of furylfulgidederivatives

4.1 Project Motivation

Furylfulgides and fulgimides are among the promising candidates for molecular switches [70]. Various studies have been carried out to study the switching behaviour of, and possible applications for, these molecules [71–83]. Since the departure from cyclohexadiene as a model system (see section 3.2 and reference [84, 85] for details), there was a lack of theoretical dynamical data on these systems. In absence of a suitable model system, the full systems have to be used in the simulations. For systems of this size the computational cost of electronic structure and dynamics calculations quickly grows, especially with no previous knowledge of important molecular coordinates. Semiempirical electronic structure methods and semiclassical full-dimensional nuclear dynamics offer an intriguing solution to this problem (see sections 2.4.4 and 2.4.4 for more information).

The aim of this project was to gain insights in the intricate processes happening during the electrocyclic ring-closure/-opening reactions of (mostly) furylfulgides via various approaches. The major part of the project was to prove the applicability of Thiel's OM methods [19, 20, 37, 40] combined with a MR-CI treatment [11] to furylfulgides. The semiempirical method was coupled to Tully's surface hopping semiclassical dynamics framework [38, 54] within the MNDO [10] program. With proven applicability, these simulations are the first full-dimensional theoretical study of the dynamics of furylfulgides. The simulations offered important new insights into the details of the photo-isomerisation processes of these molecules, especially in close cooperation with experimentalists. In experiments, strong changes in the photochemical behaviour upon seemingly minor substitutions were observed. The theoretical study allowed for an unbiased analysis of possible reasons for these effects. In minor parts of the project, static *ab-initio* studies were used to further deepen the understanding of the isomerisation processes observed in fulgides.

4.2 Photochemical dynamics of E-iPr-furylfulgide

Contributions to the paper:

- Setup of the semiempirical model
- Setup and execution of the *ab-initio* simulations
- Accuracy check of the semiempirical model (optimisations and single point simulations)
- Simulation and evaluation of the dynamics
- Interpretation of the dynamical and static data
- Major contributions to writing the article

DOI: 10.1039/c2cp41817g

4.3 Electronic supplementary information for: Photochemical dynamics of E-iPr-furylfulgide

4.4 Additional information: Photochemical dynamics of E-methylfurylfulgide

To further deepen the understanding of the de-excitation processes in furylfulgides, another derivative of this class of molecules was studied. The most suitable candidate for this was E-methylfurylfulgide (figure. 4.1), suggested and already studied experimentally by Siewertsen *et al.* [75, 77]. Compared to E-isopropylfurylfulgide the only change is that instead of the isopropyl group connected to atom **C3** there is a methyl group. This very small modification was a likely substitution to leave the electronic structure of the furylfulgide system intact. Still, by size and more importantly mass, the substitution was expected to shift the balance between the electrocyclic and the central ethylenic de-excitation pathways, as noted in the outlook of the publication given in section 4.2.

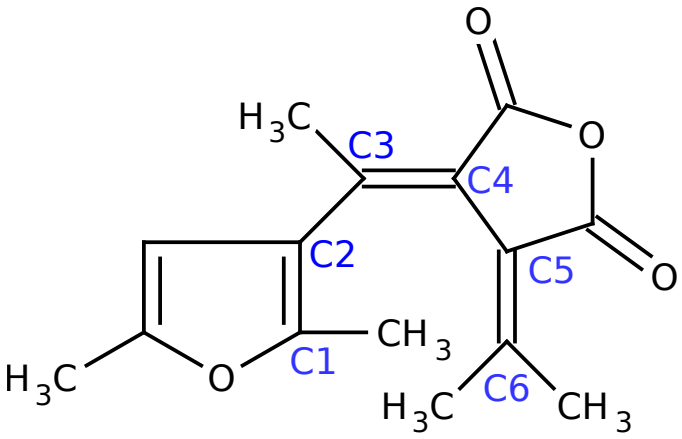

Figure 4.1: α-isomer of E-methylfurylfulgide. The difference to E-isopropylfurylfulgide is the methyl group connected to atom **C3**, replacing the isopropyl group.

4.4.1 Static spectra of E-methylfurylfulgide

The setup of the semiempirical treatment was identical to the setup for E-isopropylfurylfulgide presented in article 4.2. E-methylfurylfulgide has the same number of conjugated double bonds as E-isopropylfurylfulgide, so an identical multireference treatment can be expected to be of similar accuracy. Thus no additional *ab-initio* accuracy checks were carried out.

Starting point for the comparison was the static spectrum of E-methylfurylfulgide. A static spectrum was derived from 150 fs long sampling trajectories of E-methylfurylfulgide, 69 for the α- and 20 for the β-isomer, using a ratio of 7α:3β for the conformer distribution taken from literature [78]. A Gaussian-shaped resolution

function of 20 nm full-width-at-half-maximum (FWHM) was used for convolution of the raw data, analogous to the static spectrum for E-isopropylfurylfulgide. The resulting spectrum is shown in red in figure 4.2, in comparison to the experimental spectrum (in pink) taken from Siewertsen *et al.* [78]. A red-shift of the simulated spectrum by 2900 cm^{-1} results in the spectrum depicted in blue. The agreement with

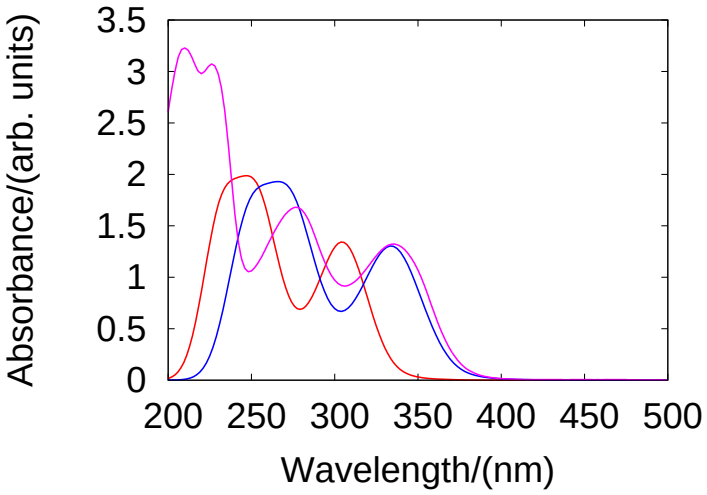

Figure 4.2: Experimental (pink) [78] and simulated spectrum (red) of E-methylfurylfulgide. The blue spectrum is the result of a red-shift of 2900 cm^{-1} applied to the simulated spectrum.

the experimental spectra is similar for E-methylfurylfulgide and E-isopropylfurylfulgide. The blue-shift in comparison the experimental data is virtually identical and the first band fits very well in both cases. The lack of high-energy signals is due to the missing excited states above S_5, in the same fashion as for E-isopropylfurylfulgide (see sec. 4.2). A major difference appears in the highest-energy part of the spectra. Here the simulated E-isopropylfurylfulgide spectrum is in better agreement with the experiment. For easier understanding of the underlying features, state resolved spectra of the E-methylfurylfulgide are given in figure 4.3. The direct comparison shows that the distortion of the second band towards the high-energy regime is caused by $S_5 \leftarrow S_0$ and $S_4 \leftarrow S_0$ excitations in the α-isomer. The contributions from the β-isomer contribute with only a small spectral intensity furthest to the blue in figure 4.2. Three possible reasons for the disagreement with the experiment might be deduced from this. The $S_5 \leftarrow S_0$ and $S_4 \leftarrow S_0$ excitations of the α-isomer are either too intense, or too high in energy or too low in energy compared to the other transitions. None of these can be ruled out but the third one seems to be most likely. If the transitions were too high in energy the real bands would red-shift towards the $S_3 \leftarrow S_0$ transition, thereby symmetrising the second band and increasing its intensity. The second band is already too high in intensity relative to the first one, so this discrepancy would increase. On the other hand, a shift of the two highest transitions to higher energies would reduce the intensity of the

second band and, after a split of the bands, increase the symmetry of the second one. A reduced intensity of the transition would also lead to the needed increase in symmetry but it would need to be drastic. This would imply a huge difference in the accuracy of the description for the α- and the β-isomer, since the transition intensities for $S_5 \leftarrow S_0$ and $S_4 \leftarrow S_0$ would then be rather accurate for the β-isomer while being completely off-scale for the α-isomer. Shifting the transitions to higher energies would be possible in both isomers, and with that it would still be possible to assume a similar accuracy for both isomers.

These considerations support the third explanation. Still none of them is ruled out, and even all of them might be true.

No matter what the reason for the discrepancies is, they are happening among the topmost of the simulated states, which is not surprising. In a basis representation the description of highly excited states is expected to be worse than the description of lower-excited ones, in every method, semiempirical or not. While the highly excited states have an impact on the detailed shape of the spectra, both static and transient, they do not affect the underlying dynamics happening on the S_1 and S_0 state. Following the last argument, excited-state dynamics for E-methylfurylfulgide

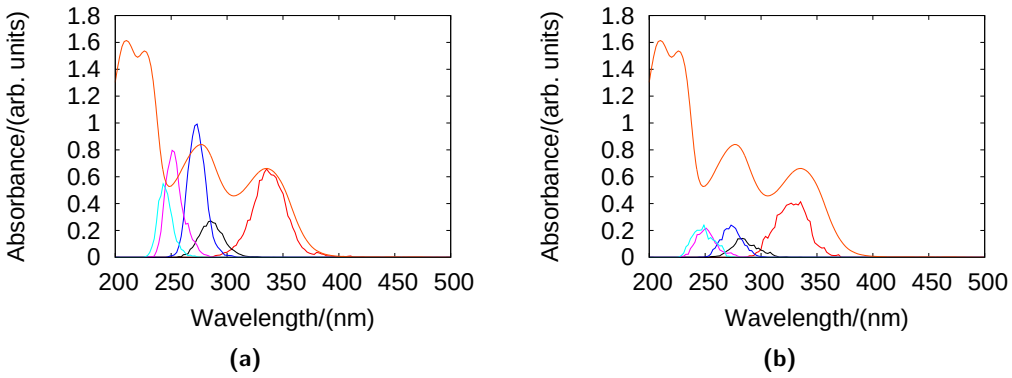

Figure 4.3: Target-state-resolved simulated static spectra for the α-isomer (a) and β-isomer (b) of E-methylfurylfulgide. The excitations are resolved by their final state: S_1: red, S_2: black, S_3: dark blue, S_4: pink, S_5: light blue. The relative heights of the spectra of the two isomers reflect the abundance in the isomeric mixture (7α:3β). The experimental spectrum (orange) is given for easier comparison.

were studied.

4.4.2 Transient spectra of E-methylfurylfulgide

To evaluate the differences in the photo-isomerisation dynamics of E-methylfurylfulgide and E-isopropylfurylfulgide, dynamical data on the former was needed. After verifying the applicability of the semiempirical model via the comparison of simulated and measured static spectra (see section 4.4.1), photo-dynamics simulations were performed for E-methylfurylfulgide in the same fashion as previously for E-

isopropylfurylfulgide but with only 10000 time steps in each trajectory. The α-isomer was covered by 107 trajectories while 35 were calculated for the less important β-isomer. Both these numbers do not represent a statistically sufficient sample but are expected to already show the important features of a statistical ensemble qualitatively. Transient spectra were calculated from the trajectories using a relative weight

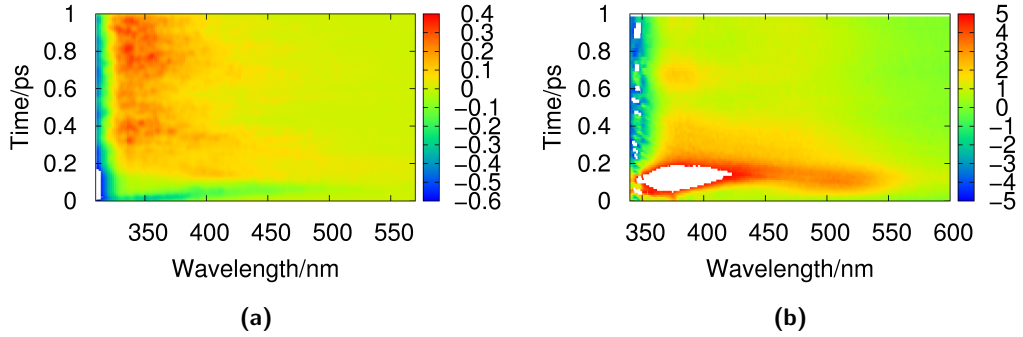

Figure 4.4: Simulated (a) and experimental (b) transient spectra of E-methylfurylfulgide. The change in optical density is colour-coded in arbitrary units.

of 7α:3β and a Gaussian-shaped resolution function of 30 fs FWHM (see section 4.2 for technical details on the calculation of the spectra). The resulting spectrum is depicted in figure 4.4a. For comparison, figure 4.4b plots the corresponding experimental spectral data recorded in n-hexane, taken from [78].

At first glance, the differences between the experimental and the simulated spectrum are worse than for E-isopropylfurylfulgide, although of similar type (see section 4.2). Four main differences can easily be identified and explained: First, the red-shifting negative signal at times below 140 fs. This is due to the lack of excited states beyond S_5, as already explained in the article 4.2. The second is that no cyclic product band forms, while, as third difference, the E to Z isomerisation is overrepresented in the simulation. As the first one, the second and third difference have already been encountered for the E-isopropylfurylfulgide, although this shows product formation. Nonetheless, for E-isopropylfurylfulgide the simulated quantum yield for cyclisation is much lower than the experimental one. The same is true for E-methylfurylfulgide, the experimental quantum yield of which is only 23 % [78] compared to 57 % [78] for E-isopropylfurylfulgide. Simultaneously the experimental E to Z isomerisation quantum yield is hugely greater in E-methylfurylfulgide with 14 % than for E-isopropylfurylfulgide with no experimentally observable isomerisation. Analysing the trajectories reveals that of the 107 trajectories for the α-isomer only 5 show cyclisation. Taking into account the weights of the two isomers, this leaves a quantum yield of about 3 %. At the same time, the theoretical E to Z isomerisation quantum yield is overestimated to be 47 % (42 % for the α- and 60 % for the β-isomer). Both these quantum-yield-related features are present in the simulations of E-isopropylfurylfulgide to a lesser extent and have been attributed to the

lack of solvent in the simulation (see section 4.2 for details). A more detailed discussion of this topic will be picked up by the end of section 4.4.3. The fourth and most pronounced difference is the overestimation of the oscillating feature in the simulated spectrum, which is absent in the simulations of E-isopropylfurylfulgide. This is very likely due to two reasons: One is the overestimation of the E to Z isomerisation rate and with that more spectral intensity at wavelengths between the absorption of the reactant and the desired cyclic product and as second reason the lack of solvent. The absence of solvent means that there is no cooling of the internal energy of the molecules after the reaction and therefore no dampening of the oscillation, which would otherwise be very efficient for the large scale motion that is the result of the E to Z isomerisation. This difference is a feature important for the ground state after the reaction has already occurred, thus the interpretation of the photo-de-excitation data does not depend on this. To visualise this, the spectra were cut after 500 fs and replotted in figure 4.5. As will be detailed in section 4.4.3, 500 fs is long after the molecules have left the first excited state and have reached the final structures at least once.

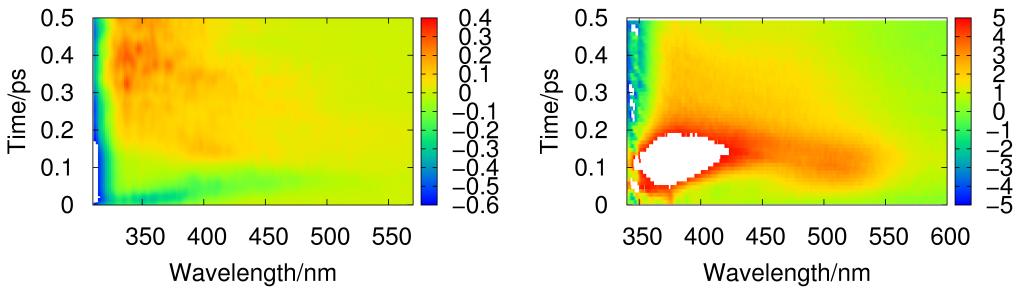

Figure 4.5: Simulated (a) and experimental (b) transient spectra of E-methylfurylfulgide up to times of 0.5 ps. The change in optical density is colour-coded in arbitrary units

The comparison of the two spectra given in figure 4.5 shows very good agreement, when the two excited state absorption features at 375 nm and 520 nm are neglected for the reasons explained in section 4.2, the shape fits extraordinarily well. This is especially true for the step-like structure around 500 nm and 250 fs.

Interesting facts about the β-isomer become visible when the spectra for both isomers are printed out separately. The resulting transient spectra are depicted in figure 4.6. The spectrum of the β-isomer only shows a few very pronounced features. The stimulated emission is very intense at first but then dies out quickly and the hot ground-state absorption sets in much later than for the α-isomer, for the majority of the trajectories not before about 250 fs. While the de-excitation of the β-isomer is some ten femtoseconds slower, this cannot be the only reason for the appearance of the spectrum. If the slower reaction speed were the reason, the spectrum would just

be shifted, but the spectrum lacks the hot ground-state-absorption coming into the depicted range from the red side of the spectrum. In the α-isomer, this stems from electronically de-excited molecules leaving the conical intersection region towards the ground state minima. Thus the lack of this signal in the spectrum of the β-isomer indicates insufficient transition dipole moment in the regions far away from the ground state minima to cause the discussed blue-shifting spectral feature.

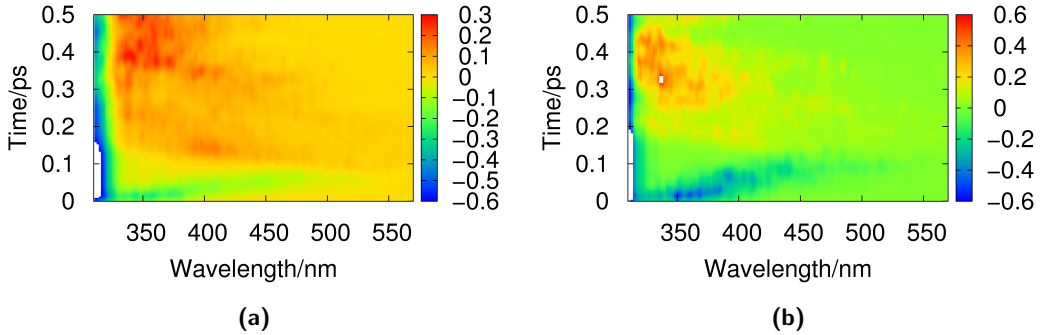

Figure 4.6: Simulated transient spectra for the α-isomer (a) and β-isomer (b) of E-methylfurylfulgide up to times of 0.5 ps. The change in optical density is colour-coded in arbitrary units.

4.4.3 Photo-isomerisation dynamics of E-methylfurylfulgide

In the following only the trajectories of the α-isomer will be dealt with, since they are the ones showing all of the paths, while the β-isomer is only able to show the central and the terminal ethylenic de-excitation path, with the latter being extraordinary unlikely (an explanation follows in this section).

The analysis of the de-excitation process of the trajectories reveals the same paths already identified for E-isopropylfurylfulgide, with strongly changed relative likeliness of happening, though. For a visualisation of these, the occurrence of state transitions from S_1 to S_0 was plotted with respect to the coordinates characterising the parts of the conical intersection seam connected to the de-excitation pathways (cf. section 4.2). The resulting maps are depicted in figure 4.7. The intersection seam minima have not been optimised for E-methylfurylfulgide. As shown in section 4.2, this is by no means a necessity for understanding the basic dynamical processes.

All maps clearly show a clustering of state transitions around the central ethylenic crossing seam (second path in section 4.2). This is in sharp contrast to the boomerang-shaped pictures encountered in E-isopropylfurylfulgide. A close inspection of the maps shows hints of a boomerang shape, especially in figures 4.7b and 4.7c, but clearly the central ethylenic path dominates the reaction.

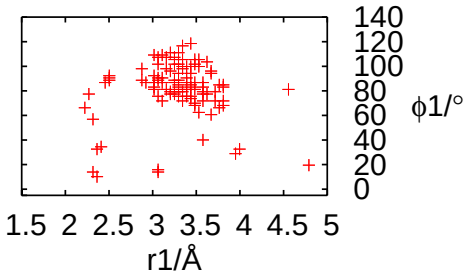

(a) Transitions plotted against $r1$ and $\phi1$.

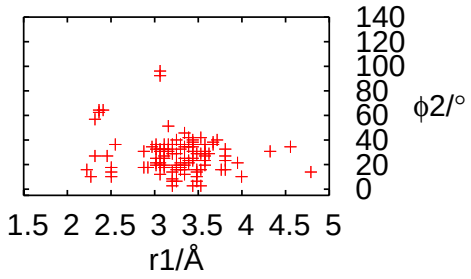

(b) Transitions plotted against $r1$ and $\phi2$.

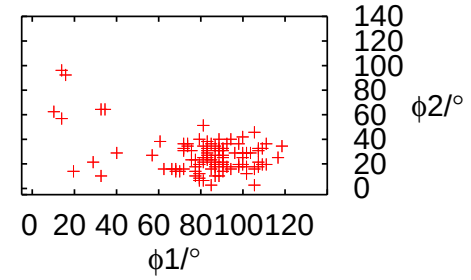

(c) Transitions plotted against $\phi1$ and $\phi2$.

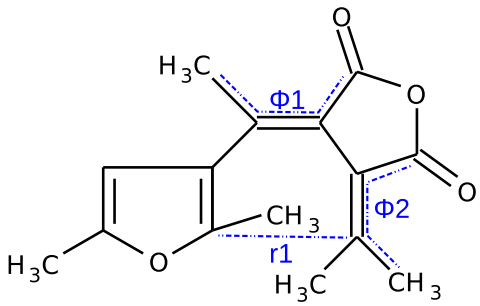

(d) Degrees of freedom of E-methylfurylfulgide relevant to the identification of the three possible de-excitation pathways.

Figure 4.7: Location of $S_0 \leftarrow S_1$ transitions in de-excitation-paths-identifying internal coordinates (4.7a to 4.7c). The coordinates are given in 4.7d.

By connecting identification criteria with the three pathways, a given trajectory can be assigned to a specific path. Following the arguments from section 4.2, this method is intrinsically ambiguous but very well able to give a qualitative impression of the abundance of the respective pathway. A total of 92 trajectories can be attributed to the dominant central ethylenic path (the path being identified by S_1 to S_0 state transitions within $75° \leq \phi1 \leq 105°$), while 14 trajectories tread the zwitterionic path (criterion: $1.2\text{Å} \leq r1 \leq 2.55\text{Å}$) and only one trajectory takes the terminal ethylenic path (criterion: $80° \leq \phi2 \leq 100°$).

To understand the underlying processes, the time development of the three reaction-path-determining coordinates was averaged over all α-isomer trajectories for both E-isopropyl- and E-methylfurylfulgide. The resulting graphs are depicted in figure 4.8. Figure 4.8c shows the development along $\phi2$ towards the terminal ethylenic conical intersection. The most visible distinction in this figure is the second increase in the blue curve. It is not mostly caused by development along the terminal ethylenic reaction path, which is a minority pathway, but by the beginning formation of cyclic product. Support for this can be found in figure 4.8a. There the blue curve starts a steep descent at about 120 fs towards the zwitterionic intersection seam (at around 2.2 Å in $r1$ for E-isopropylfurylfulgide) that happens at the same time as the second increase in figure 4.8c happens. Comparing the $r1$ development of both molecules, E-isopropylfurylfulgide apparently has a head start towards the

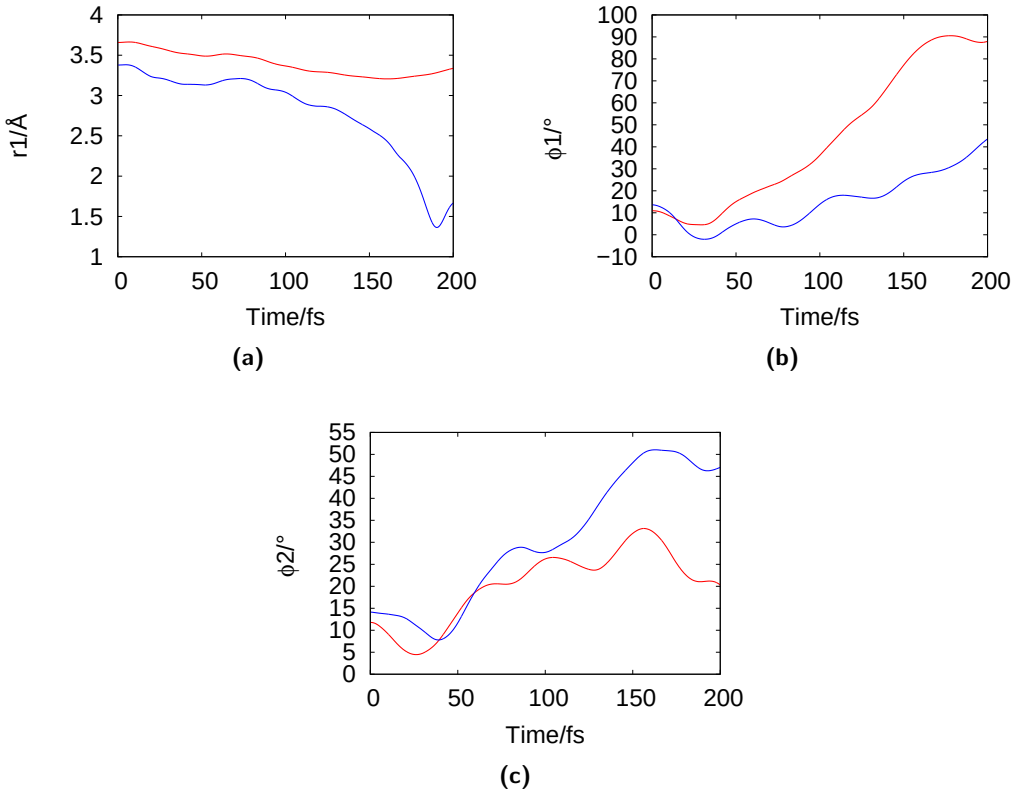

Figure 4.8: Average value of the reaction-path characteristic coordinates ($r1$: a, $\phi1$: b and $\phi1$: c) during the first 250 fs of the photo-de-excitation of E-methylfurylfulgide (red) and E-isopropylfurylfulgide (blue).

zwitterionic intersection seam. A preorientation effect was already put forth as a hypothesis by Siewertsen *et al.* [78] and is evident here. From the head start on, the coordinate develops basically parallel until about 125 fs, where the average value of $r1$ in E-isopropylfurylfulgide drops due to the starting formation of the cyclic product in about one third of the trajectories while the E-methylfurylfulgide value levels around 3.5 Å. Thus something has to have happened to stop the E-methylfurylfulgide from approaching the intersection seam. A straightforward explanation for that can be found by inspecting figure 4.8b. It becomes very clear from the figure that methylfurylfulgide approaches the intersection seam faster along $\phi 1$ than the isopropylfurylfulgide does, as evident in the strongly different slopes of the curves.

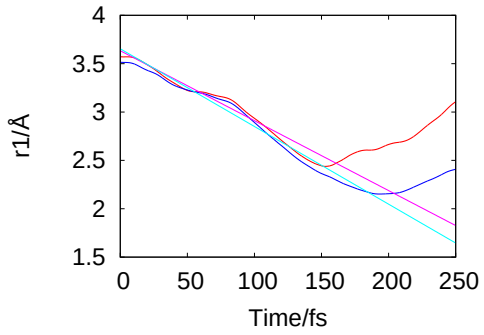

(a) Average value of $r1$ taken over trajectories attributed to the zwitterionic pathway only.

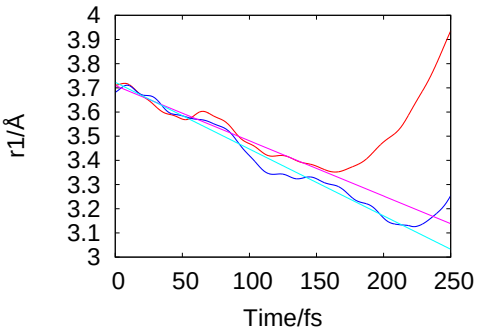

(b) Average value of $r1$ taken over trajectories attributed to the central ethylenic pathway only.

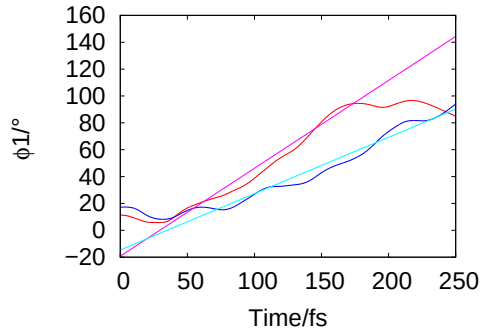

(c) Average value of $\phi 1$ taken over trajectories attributed to the central ethylenic pathway only.

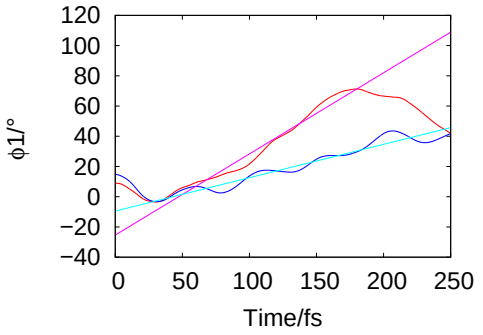

(d) Average value of $\phi 1$ taken over trajectories attributed to the zwitterionic pathway only.

Figure 4.9: Average value of the reaction-path characteristic coordinates ($r1$: 4.9a and 4.9b $\phi 1$: 4.9c and 4.9d) during the first 250 fs of the photo-de-excitation of E-methylfurylfulgide (red) and E-isopropylfurylfulgide (blue) and corresponding linear regressions (pink and light-blue respectively).

Figure 4.9 depicts a more detailed inspection of trajectories attributed to one of the two majority paths encountered in the studied molecules, the zwitterionic and the central ethylenic path. From the figures 4.9a and 4.9b it becomes obvious that trajectories assigned identical with respect to the zwitterionic path originate from very similar values of $r1$. The same is not true for figs 4.9c and 4.9d and the central

ethylenic path. However, figure 4.9d shows another very striking feature. Even when finally attributed to the zwitterionic pathway, the trajectories of methylfurylfulgide make more progress along the central ethylenic path than comparable trajectories for isopropylfurylfulgide. An additional important feature is observable in all figures in figure 4.9, namely that the methylfurylfulgide reaches the turning point of the progression along a coordinate at least 50 fs earlier than the isopropylfurylfulgide does. To give numbers to this speed-up, the more linear parts of the graphs in figure 4.9 were fit by linear regression. The results of this are given in figure 4.9 and tab. 4.1. From these fits it can be deduced that while the progression along $r1$ is of virtually identical speed, the progression along $\phi 1$ happens more than 1.5 times faster for the methyl-substituted furylfulgide than for the isopropyl-substituted one. The preceding findings allow for important conclusions. The introduction

Table 4.1: Parameters for the linear regressions of the more linear parts in figure 4.9, assuming the functional form $f(x) = a * x + b$.

Coordinate, path, substituent	first time for regression	last time for regression	$(a \pm \Delta a)$ /(Å/fs)	$(b \pm \Delta b)$ /(Å)
$r1$, zwitterionic, methyl	20 fs	130 fs	$-7.23 * 10^{-3}$ $\pm 4.68 * 10^{-5}$	3.63 $\pm 3.82 * 10^{-3}$
$r1$, zwitterionic, isopropyl	20 fs	140 fs	$-8.03 * 10^{-3}$ $\pm 4.81 * 10^{-5}$	3.65 $\pm 1.36 * 10^{-4}$
$r1$, central ethlenic, methyl	13 fs	150 fs	$-2.28 * 10^{-3}$ $\pm 1.55 * 10^{-5}$	3.71 $\pm 1.40 * 10^{-3}$
$r1$, central ethlenic, isopropyl	20 fs	200 fs	$-2.76 * 10^{-3}$ $\pm 1.17 * 10^{-5}$	3.72 $\pm 1.43 * 10^{-3}$
$\phi 1$, zwitterionic, methyl	35 fs	165 fs	$-5.37 * 10^{-1}$ $\pm 2.81 * 10^{-3}$	25.37 $\pm 3.00 * 10^{-1}$
$\phi 1$, zwitterionic, isopropyl	40 fs	190 fs	$-2.21 * 10^{-1}$ $\pm 1.50 * 10^{-3}$	-9.51 $\pm 1.84 * 10^{-1}$
$\phi 1$, central ethlenic, methyl	40 fs	165 fs	$-6.54 * 10^{-1}$ $\pm 3.70 * 10^{-3}$	-19.26 $\pm 4.02 * 10^{-1}$
$\phi 1$, central ethlenic, isopropyl	40 fs	260 fs	$-4.19 * 10^{-1}$ $\pm 1.54 * 10^{-3}$	-14.63 $\pm 2.51 * 10^{-1}$

of the methyl group instead of the isopropyl group greatly increases the speed of progression along the central ethylenic path, while it leaves the zwitterionic path unchanged. This reduces the cyclisation quantum yield in two ways. The obvious one is that the central ethylenic direction becomes dominant in the trajectories, leading to most of them reaching the intersection seam in regions attributable to the corresponding conical intersection. The other, more subtle effect is that due to the competition with the faster central ethylenic de-excitation, the trajectories attributable to the zwitterionic path are trajectories that have a rather early surface transition on their way towards the cyclic product. As explained in sec. 4.2, the point on the $r1$ coordinate, where the state transition occurs, plays an important

role in the effectiveness of the zwitterionic de-excitation with respect to cyclisation. This second effect should be visible in a reduced effectiveness of the zwitterionic path in E-methylfurylfulgide with respect to final product formation.

In total these processes lead to a theoretical quantum yield of about 40 % (about 7 % for E-isopropylfurylfulgide) for the E to Z isoimerisation of the α-isomer, while only 5 % of the trajectories show cyclisation (about 30 % for E-isopropylfurylfulgide). The isomerisation along the terminal ethylenic pathway seems to be negligible based on the trajectories simulated so far. Thus the simulated quantum yield for the E to Z isomerisation is about twice as large as the measured one [78], and the one for cyclisation about three times smaller. These numbers might seem grave but are in line with similar findings for E-isopropylfurylfulgide and can easily be reasoned by taking into account the different conditions in the simulated and the measured system. While the experiments where carried out in a solution of n-hexane, the theoretically studied system was in a vacuum (except for a heat bath for the initial sampling). Although the solvent is not expected to electronically influence the system, it surely puts sterical constraints to work. These sterical effects most likely will disfavour large-scale motions of the excited molecules, with the central ethylenic de-excitation and especially the following E to Z isomerisation being the largest-scale motions encounterd in the simulation. This might of course also distort the exact amount of effect the methyl-substituent has compared to isopropyl, but is not expected to change the fundamental nature of it.

Other possible sources for disagreement were thoroughly discussed in the electronic supplementary information for the article on E-isopropylfurylfulgide in section 4.3.

Future studies of ring-closure reactions of different furylfulgides will possibly deepen the understanding of the effects laid out in sections 4.2, 4.3 and 4.4, by enhancing the statistics, addition of solvent, and most importantly studies of the effects of other substituents.

4.5 Importance of a low-lying $n\pi^*$-state in the isomerisation reaction of Z-methylfurylfulgide.

Contributions to the paper:

- Identification of the central question
- Setup and execution of the simulations
- Interpretation of the data
- Major contributions to writing the article

revised article submitted to J. Photochem. Photobiol. A on Jan., 30, 2013

4.6 Electronic supplementary information for: Importance of a low-lying $n\pi^*$-state in the isomerisation reaction of Z-methylfurylfulgide.

4.7 Additional information: Importance of a low-lying $n\pi^*$-state in the isomerisation reaction of Z-methylfurylfulgide.

In the following section, a more detailed analysis of the effects of the addition of n-orbitals to the active space of Z-methylfurylfulgide is presented. The details given here were deemed too special for the article presented in section 4.5 and would have stretched it to an unsuitable length.

The conclusion of the article points out that the change of character in the wave functions of the calculated electronic states should manifest itself in changes of observable properties. Although the access to observable data is somewhat limited in the presented simulations, one readily accessible observable is the evolution of the transition dipole moments of the treated states during the CASSCF(10,9)/6-31g(d,p) [14] quadratic steepest descent paths. Before a detailed inspection of the transition dipole moments, a look at the energies along the paths is suitable. The energies are depicted in figure 4.10. The figure 4.10a shows that the energy of the

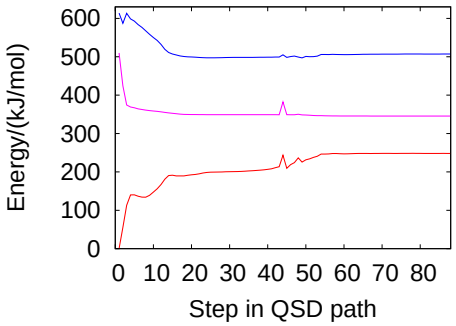

(a) n-orbital-space QSD-path.

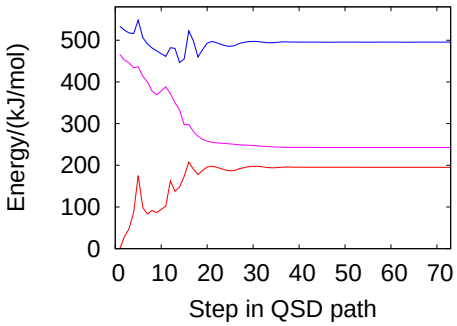

(b) π-only-orbital-space QSD-path.

Figure 4.10: CASSCF(10,9)/6-31g(d,p) state energies along the QSD paths. S_0: red, S_1: pink, S_2: blue.

S_1 state smoothly decreases with an exception in one step, with the major progress during the first four steps, when the n- and π-orbitals separate. The S_2 state energy shows similar behaviour, while the S_0-energy increases but shows a similar structure within the increase. On the other hand, the energy along the π-only path (figure 4.10b) shows a less monotonic behaviour, especially in the beginning, with the S_0- and S_2-states behaving even worse. This alone might very well be taken as a sign of the lesser suitability of the π-orbital-only wave function.

Still, an inspection of the transition dipole moments is reasonable, firstly to see whether the unsmooth behaviour also shows in the dipole-moments and secondly to

check for effects of the n-π-orbital separation on an easily observable property, as predicted in the article (section 4.5). Figure 4.11 depicts the evolution of the x-,y- and z-polarised squared dipole moments of Z-methylfurylfulgide along the QSD-paths. Figures 4.11d to 4.11f show the evolution for the π-orbital-only path. From these it becomes clear that while the energy-development shows some rattling, the transition dipole moments, especially the z-component, behave even more erratically over the QSD-paths. This is very likely to be unphysical and does not support the applicability of the π-orbital-only wave function model. On the other hand, the squared transition dipole moments for the n-orbital-containing wave function model, depicted in the figures 4.11a to 4.11c, vary rather smoothly with the exception of a few kinks. This is to be expected for smoothly varying wave functions. In figure 4.11a, a steep decrease of the squared transition dipole moment (neglecting the initial kink) can clearly be observed during the first few steps, when the separation of the n- and π-orbitals happens. The following changes to an almost zero transition dipole moment happen over many more steps and, as pointed out in section 4.5, happen over a much larger coordinate space and are of much smaller scale. For figure 4.11c, the picture is similar although more complex. In line with Figure 4.11a, during the first about five steps the transition dipole moments decrease. Afterwards a new feature appears with rising values over the first part of the localisation of the π-orbitals (approximately the steps 5 to 15, see the S_0-state energy in figure 4.10a for comparison). On the second and last phase of the localisation of the π-orbitals the transition dipole moments decrease again. The last figure dealing with the n-orbital space QSD path (4.11c) shows a rather continuous increase of transition dipole moments during the first two phases mentioned for the previous figure. The exception here is the steep increase within the first three steps of the path. Most problematic with the development of the transition dipole moments of the $S_2 \leftarrow S_0$-transition (see figure 4.11b) is that their evolution is happening during a process on the S_1-state therefore these changes are very difficult to observe, if at all. The changes in figures 4.11a and 4.11c, on the other hand, are observable straightforwardly in experiments by spectroscopic methods, thus offering an observable trace of the character of the electronic wave function. A problem might be the very short time in which they will happen presumably. As pointed out in section 4.5, the initial localisation happens over a very small region in coordinate space with steep gradients (easily to be seen from the S_1-state energy in figure 4.10a) and will therefore be likely to happen quickly.

4.8 Understanding the structure of the static spectrum of C-furylfulgides.

The cyclic form of furylfulgides is essential for their switching cycle. Therefore a detailed understanding of the electronic properties of this form is indispensable.

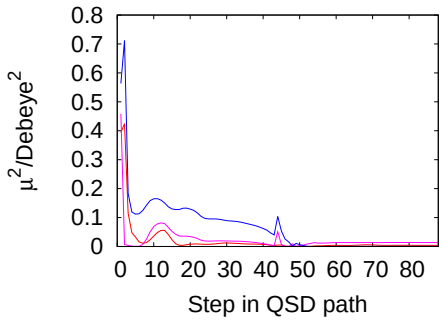

(a) Squared transition dipole moments between S_1 and S_0 along the *n*-orbital-space QSD-path. x- and y-component enlarged by 20.

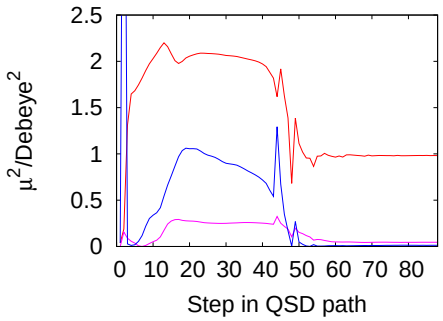

(b) Squared transition dipol -moments between S_2 and S_0 along the *n*-orbital-space QSD-path.

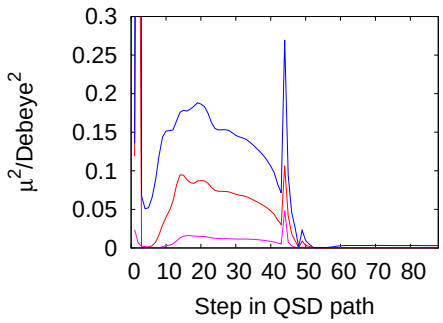

(c) Squared transition dipole moments between S_2 and S_1 along the *n*-orbital-space QSD-path.

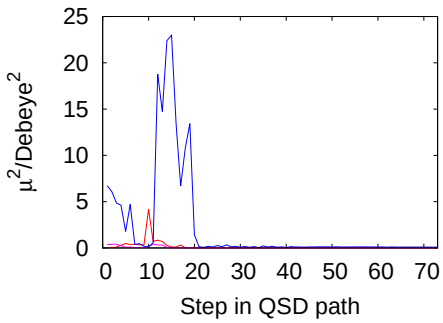

(d) Squared transition dipole moments between S_1 and S_0 along the π-only-orbital-space QSD-path.

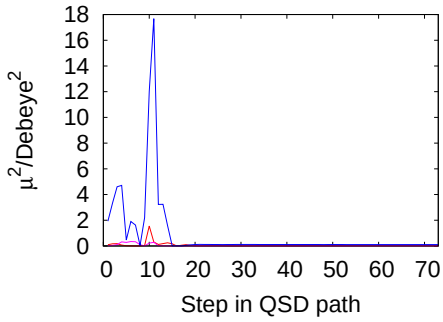

(e) Squared transition dipole moments between S_2 and S_0 along the π-only-orbital-space QSD-path.

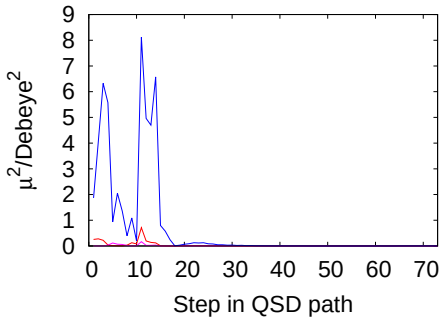

(f) Squared transition dipole moments between S_2 and S_1 along the π-only-orbital-space QSD-path.

Figure 4.11: Squares of CASSCF(10,9)/6-31g(d,p) transition dipole moments along the QSD paths. x-component: red, y-component: pink, z-component: blue

Siewertsen *et al.* [78] published the static UV/Vis-spectra of various furylfulgides. All of these molecules show a more or less pronounced shoulder in the first excitation band. Up to now, the structure of this first band has not been addressed in any study. The following sections will cover possible explanations for the structure and discuss their likeliness. Possibilities are: First, the existence of another electronically excited state energetically close to the first one (the energy difference would have to be around 30 kJ/mol); second, the distribution of the probed ground state ensemble a second minimum on the ground state for example might split the band into two bands arising from two different isomers; third, and last, the details of the excited-state potential energy surface might give rise to the detailed band structure. In any case, the most likely explanation should hold for all furylfulgides presented by Siewertsen *et al.* [78].

4.8.1 Electronic states at the cyclic Franck-Condon point

Thus far no theoretical or experimental study of the ring opening reaction of furylfulgides suggested the involvement of a second excited state. Futher investigations were carried out to verify this. In the simulations presented in sections 4.2, 4.3 and 4.4.2, no additional electronic state appears in the energetic proximity of the S_1 state in the geometrical vicinity of the cyclic product. For further evidence beyond the semiempirical data, CC2 calculations were carried out using TURBOMOLE [86] at the MP2 optimised geometry of the cyclic structure of isopropylfurylfulgide presented in section 4.3. The first four electronically excited states were simulated in the def2-SVP [87] and def2-TZVPP [88] basis sets. The results show no signs of a second excited state close to the S_1-state with a similarly large transition dipole moment. The S_2-state is about 1 eV higher in energy than the S_1-state and has significantly smaller oscillator strength ($1.71 \cdot 10^{-1}$ compared to $2.82 \cdot 10^{-3}$) for the transitions to the respective state from the electronic ground state. On the other hand, the energy difference to the $S_1 \leftarrow S_0$ transition and the relative intensity fits well with the intepretation of the $S_2 \leftarrow S_0$-band being part of the second observable band in the experimental spectrum.

Based on the data presented here and in literature, the involvement of a second excited state in the first spectral band of the furylfulgides can be taken to be very unlikely and thus, the first possible explanation for the band-shape is ruled out.

4.8.2 Effects of ground state sampling on the spectral structure

To sample the ground state at the Franck-Condon point, semiempirical direct dynamics coupled to a heat bath were carried out as presented in section 4.2. The orbitals used were orbitals retrieved from a reactive trajectory of E-isopropylfurylfulgide, the active space of which was tracked over the course of the reaction. A total of 50 trajectories was simulated, propagated for 200 fs (2000 time steps) each.

A static spectrum was extracted in the usual fashion, shifted by 2450 cm^{-1} and convoluted with a Gaussian-shaped resolution function 30 nm wide. The resulting spectrum is depicted in figure 4.12.

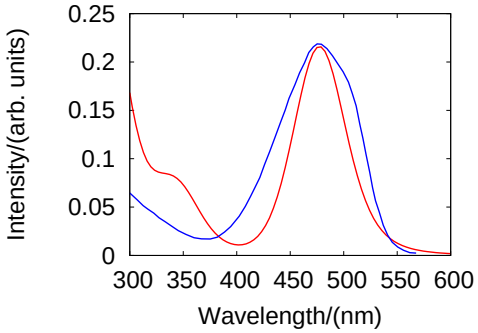

Figure 4.12: Simulated (red) and experimental(blue) UV/Vis-spectrum of cyclic isopropylfurylfulgide. The simulated spectrum was shifted by 2450 nm and convoluted with a 30 nm-wide Gaussian.

In contrast to the experimental spectrum, the simulated one shows no distinct structure in the first band. Additionally, the band corresponding to the $S_1 \leftarrow S_0$ transition is very sharp, compared to the broad experimental band. Widening of the resolution function until the width of the two spectra agrees would in principle be possible but would lead to an unphysically bad resolution, since not all bands in the spectrum are that wide. In agreement with the CC2 simulations presented in section 4.8.1, the first excited state is the only electronic state in the region of the first spectral band for the semiempirical simulation, which supports the simulations. At first glance, the lack of a structured band might be attributed to the rather short equilibration time of 200 fs. The argument does not hold because the cyclic fulgides are very stiff molecules, therefore needing only short times for the sampling of their degrees of freedom. Although some of the fulgides have slowly equilibrating substituents, the reason for the structured band must be present in all of the fulgides studied in [78]. Therefore the 200 fs equlibration time are enough to sample the ground state distribution.

In conclusion, the simulated static spectra offer no explanation for the band structure. This can either be attributed to the semiempirical method not being accurate enough, or the effect being a direct consequence of the excited-state wave function.

The first explanation is unlikely due to the large magnitude of the observed spectral effect and the overall good agreement of the semiempirical and *ab-initio* data (see sections 4.2 and 4.4 and also established literature [19, 20, 37, 40, 85]).

The second possible reason becomes clear upon analysis of the process that generates the spectra. On the ground state, an ensemble of molecular structures corresponding to a temperature of 300 K is calculated. For all of these structures the squares of the transition dipole moments together with the excitation wavelengths are used to set up the spectrum. This scheme incorporates the electronic wave

functions of both states via their energy and the transition dipole moment and the ground state nuclear wave function classically via the sampling of the ground state. In the quantum picture, also the excited state nuclear wave function (of which there is no information in the direct MD simulation) contributes to the spectral shape via the Franck-Condon factor. So the influence on the spectral shape carried by the nuclear wave function of the final state of the excitation cannot be addressed in the calculation of the spectrum. The following section will address this part.

4.8.3 Influence of the nuclear wave function of the excited state on the static spectrum

The last possible explanation for the band structure is intrinsic to the involved excited state and the quantum nature of the nuclei. From various studies of fulgides it is known that the helical S_1-state minimum and the S_1-S_0 conical intersection are in close vicinity to each other and the Franck-Condon point. They are separated by a small barrier on the S_1 surface (see for example [85]). This means the S_1 state energy surface will display a double-well structure in some coordinate. The basic idea is that a single-well ground state nuclear wave function in combination with a double-well wave function on the excited state will lead to Franck-Condon factors that give rise to a band-shape observed in the experimental spectra. The identification of a suitable coordinate in a real molecule is not an easy task. A promising coordinate is the intrinsic reaction coordinate from the ground state ring-opening transition state (see Yoshioka *et al.* [89]) to the cyclic minimum. The simulation of this path is highly demanding computationally due to a need of a multireference electronic wave function and of the Hessian. The multireference Hessian is analytically not available in the programs in the Hartke group. That means that the Hessian has to be calculated numerically and needs multiple re-evaluations during the transition state identification and the reaction path following.

To check the fundamental prediction without a Hessian, a one-dimensional model system was set up. A Morse potential was used as ground-state potential. The excited-state potential was approximated by another Morse potential with an added Gaussian to generate the double-well structure. The details of the used potentials are given in equations 4.1, 4.2 and table 4.2. All parameters were converted to atomic units if they were not already in atomic units before the simulation.

$$V_{morse} = D_e(1 - e^{-\beta\cdot(q-q_e)})^2 \tag{4.1}$$

$$V_{morse} = D_e(1 - e^{-\beta\cdot(q-q_e)})^2 + A\cdot(e^{-0.5\cdot((q-q_{eg})/\sigma)^2}) \tag{4.2}$$

The parameters are on similar scales as encountered in real situations. 348kJ/mol

Table 4.2: Parameters for the model potentials used in the proof-of-principle calculation of the Franck-Condon factors for cyclic furylfulgide models. All parameters were converted to atomic units before calculation of the potentials.

parameter	ground state potential	excited state potential
D_e	348kJ/mol	348kJ/mol
q_e	-0.3 Å	0.0 Å
β	2.0 Å	1.0 Å
A		0.01 atomic energy units
q_{eg}		0.05 Å
σ		0.1 Bohr

is on the order of a C-C single bond dissociation enthalpy. The parameter β for the ground state leads to an energy difference of about 1300 cm^{-1} for the low-lying vibrational states when combined with a reduced mass of 4.1005 atomic mass units, both in agreement with a harmonic vibrational analysis of C-isopropylfurylfugide carried out using the Gaussian09 program [90] on MP2/cc-pVDZ [91] level for the C-C stretch vibration facilitating the ring opening. The parameters for the Gaussian lead to a barrier height of about 20 kJ/mol on the excited state, which is in qualitative agreement with the 5 kcal/mol reported in [85]. The resulting potentials are given in figure 4.13.

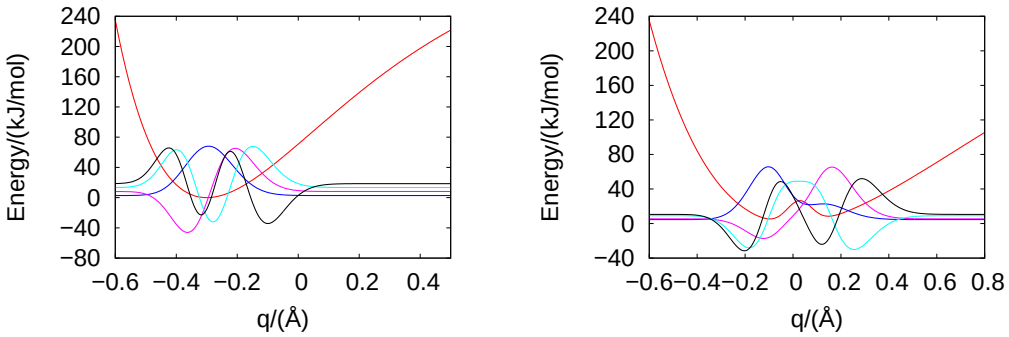

(a) Ground state model potential

(b) S_1 state model potential

Figure 4.13: Model potentials for the simulation of the cyclic-furylfulgide model Franck-Condon factors. The four lowest vibrational states for each potential are depicted. The functions were shifted to their eigenenergy and scaled for reasons of depiction.

The vibrational eigenfunctions and energies were numerically calculated in a sine basis using 250 basis functions. The program used was adapted from a program written during the theoretical chemistry practical course and is available from the author on inquiry. Using the eigenfunctions, the scalar products of the vibrational ground state with the first 30 eigenstates of the excited state potential were calculated and squared to get the relative transition intensities. The spectrum was shifted to the same spectral region as the $S_1 \leftarrow S_0$-band, while the relative energies within

the band are dictated by the relative energies of the eigenstates, and convoluted with a resolution function of 30 nm. The resulting spectrum is depicted in figure 4.14.

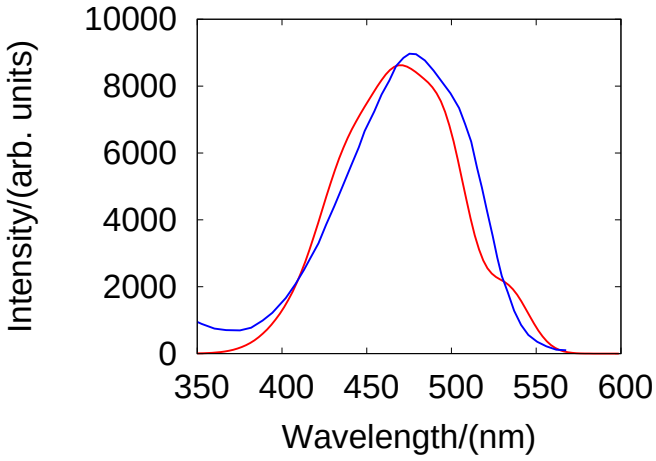

Figure 4.14: First excitation band of the experimental spectrum (blue) of cyclic isopropylfurylfulgide. Overlaid in red is the simulated spectral shape based on the Franck-Condon factors calculated using the potentials in equations 4.1 and 4.2 and the parameters given in table 4.2.

The simulated spectrum clearly shows the characteristic shoulder visible in the experiments and also fits well with the width of the experiment. A detailed agreement is not expected taking into account the very simple model used. Clearly electronic properties, like the detailed energy landscape and transition dipole moments, of the states will play a role in the details of the band structure, especially that close to a conical intersection. Also, the use of Franck-Condon factors, which are derived from the Born-Oppenheimer separation, is only qualitatively correct here for sure.

For confirmation that the depicted spectrum is not an unusual accident, more parameter sets were tried, changing the relative positions of the minima, the barrier height and the reduced mass. The resulting squares of the Franck-Condon factors of the lowest 25 vibrational eigenstates of the double-well potential with the ground-state of the Morse potential are given in figure 4.15. All spectra were convoluted with the same Gaussian-shaped resolution function of 30 nm width.

Figures 4.15a to 4.15c clearly show traces of the shoulder on the long wavelength side of the spectrum with a more or less pronounced step from the $v_1 \leftarrow v_0$ transition. For the row from figure 4.15d to 4.15f the picture is less simple, nonetheless the bands still show a shoulder or a separate maximum on the red side of the band, but also show more or less pronounced shoulders on the blue side. The data undoubtedly proves that the basic structure of the spectra is quite resistant to variation of the conditions in certain ranges, in the sense that broad bands with a pronounced structure are omnipresent. Thus it can be considered as proven that the special features of the potential energy surface of the fulgides can give rise to the observed structure of the spectra of the cyclic furylfulgides.

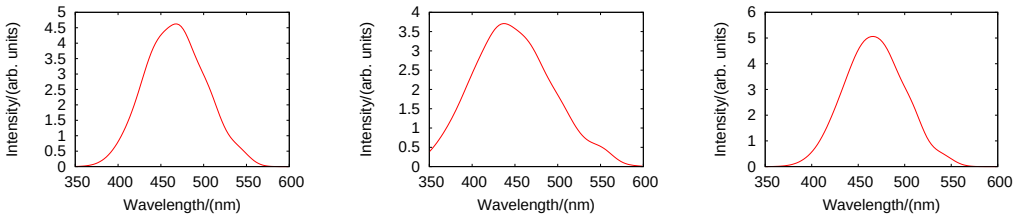

(a) $A = 0.005$ atomic energy units → barrier height → 10kJ/mol.

(b) $q_{e,double-well} = 0.1$, $q_{eg} = 0.15$ → shift of double-well potential away from the Morse potential.

(c) Reduced mass set to 6.1005 amu.

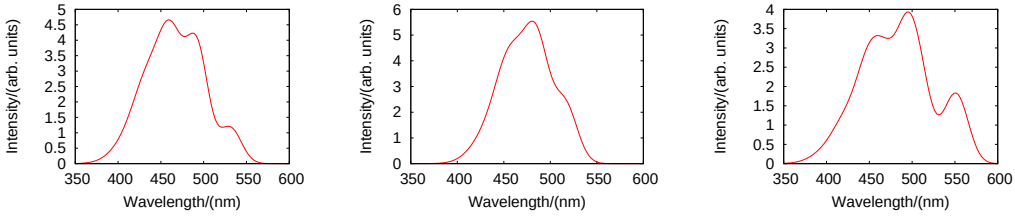

(d) A=0.015 atomic energy units → barrier height ≈ 35kJ/mol.

(e) $q_{e,double-well} = -0.5$, $q_{eg} = 0.0$ → shift of double-well potential towards the Morse potential.

(f) Reduced mass set to 2.1005 amu.

Figure 4.15: Spectral absorption bands simulated for varied potential parameters. The unlisted parameters are unchanged from the ones in table 4.2 and from the previous simulation.

Comparison to the results given in sections 4.8.1 and 4.8.2 shows that only the data presented in this section can sufficiently describe the spectral shape of the first UV/Vis-band in the cyclic furylfulgides. At the same time the fact that the presented mechanism is crucially dependent on accounting for the excited state vibrational wave function gives a simple answer why it has not been discussed thus far. A full proof of the processes would need a very detailed quantum-mechanical treatment of both the electrons and the nuclei. The presented study avoids an explicit calculation of the excited-state surface and only feeds some features into a very simplified model, thus presenting a hypothesis that explains the band structure very well, but will have to be tested in future work. Currently the author is working on the aforementioned reaction path simulation but was not able to finish them in time for this thesis.

4.9 Project summary

In the course of the project it was possible to collect various thus far unknown insights into the properties of furylfulgides. The publication in section 4.2 presents the first full-dimensional study of the photo-isomerisation processes of a furylfulgide. By this it was possible to point out a distinct weakness in reaction-path representations of reactions of E-isopropylfurylfulgide. The large relative energy of the Franck-Condon point compared to the zwitterionic conical intersection on the S_1-

surface (about 2 eV in the semiempirical model) leads to the reaction leaving the reaction path and exploring parts of the potential energy surface beyond. Therefore reaction path interpretations can not completely capture the processes in these photo-reactions.

By validation of the semiempirical MRCI approach for use in electrocyclic ring-closure reactions an important tool could be added to the kit for theoretical studies of similar systems. The small amount of time needed in comparison to *ab-initio* methods leaves the option of detailed dynamics studies to deepen the understanding and also allow for quick evaluation of thus unknown and unsynthesised systems on the computer, ruling out unsuitable candidates before attempts at synthesis have been started.

Using this new tool, a first question regarding furylfulgides could be taken on. Within the full-dimensional approach, it was possible to straightforwardly interpret the very different quantum yields for the photo-cyclisation of E-isopropylfurylfulgide and E-methylfurylfulgide. The different mass of the isopropyl and the methyl substituent has a major kinematic influence on these systems: In E-isopropylfurylfulgide, it leads to the zwitterionic pathway to be favoured, while the central-ethylenic pathway is favoured in the E-methylfurylfulgide. Together with a preorientation of the isopropyl-functionalised furylfulgide this can clearly be held responsible for the enhanced ring-closure quantum yields of E-isopropylfurylfulgide. With the detailed understanding of the influence of this seemingly minor changes in substitution, an important first theoretical step has been made for future collaborations with experimental physical and organic chemists on the way to tailor-made electrocyclic switches with desired properties.

In a detailed *ab-initio* study of the photo-isomerisation path of Z-methylfurylfulgide towards the E-isomer, it was possible to address the importance of a thus unconsidered $n\pi^*$-state in the photo-isomerisation. The intricate ordering and change of character of the excited states leads to the unimportance of the $n\pi^*$-state in the E to Z isomerisation but a very likely contribution of an excitation of that character to the Z to E isomerisation. This major electronic difference between the E to Z and the Z to E isomerisation pathways offer a possible starting point for the interpretation of the complicated data of the Z to E isomerisation gathered by experiments [92].

By detailed investigations of the Franck-Condon region of cyclic furylfulgides it was possible to come up with a convincing explanation for the complicated structure of the first vibronic excitation band of these molecules. The characteristic band shape of cyclic furylfulgides can be traced back to the special geometrical arrangement of the S_0 and S_1 minima and the conical intersection connecting these. The resulting double-well structure very likely causes strongly oscillating Franck-Condon factors, the effects of which can be observed even with the limited resolution caused by the measurement in solution. This is not an unreasonable but still an unusual

observation and thus far the only explanation put forth for the unusually wide and structured band-shape observed.

5

Design of electrocyclic ring-opening/ring-closure molecular switches

5.1 Project motivation

As explained in chapter 4, furylfulgides are a fairly well studied class of systems. Although furylfulgides are far from completely understood, the studies are very far-reaching with respect to synthetic modification of the parent systems [70]. Therefore, it seemed reasonable from the viewpoint of theory to shift some attention from furylfulgides to other systems potentially showing the same electrocyclic reaction but with more unstudied possibilities to influence reactivity of the system by substitution. For similar reasons, the well known diarylethenes [93–95] and fulgimides [96,97] were not used. The approach was to build a completely new design, starting from the basic building unit of such systems: a hexatriene-like system in the open form and a cyclohexadiene-like structure in the closed form. In the design process, substituents were added to reduce the amount of possible de-excitation pathways or at least to bias reactions towards the intended paths, to shift the excitation wavelengths towards the visible and to preorient ground-state minima towards the wanted reactions, most importantly freezing the dihedral angle attributable for the kink in the CHD surface and for the α- and β-isomer in furylfulgides (see chapters 3 and 4).

5.2 Design process

A design of photo-switches from scratch is to some extent a trial and error process and therefore a method for quick evaluation of the possible suitability of a given system is needed. Based on the accuracy checks presented in sections 4.2 and 4.3 and on the generality of the method, the semiempirical method used in these studies seems to be a suitable tool for that.

For this reason the design process really started only when the MNDO program [10] was available in the group and the applicability of the MR-CI-OM3 model was proven. Nevertheless, various systems were investigated before using CASSCF

methods, examples of which are given in figure 5.1. Although none of the depicted systems was pursued further, important conclusions were drawn from those studies. Both the cyclic aldehyde depicted in figure 5.1a and the symetrically bridged hexatriene 5.1b are too stiff. While they were built with this intent, they both did overly well. The symmetric system, fixed at the dihedral angle discussed in chapter 3, came close to the intended effect. The ring size of the bridging rings was enlarged to six carbon atoms, and double bonds were added to shift the absorption towards visible light. An exemplary system is depicted in figure 5.1c. The heterocyclic structure was chosen to avoid the formation of benzene upon cyclisation.

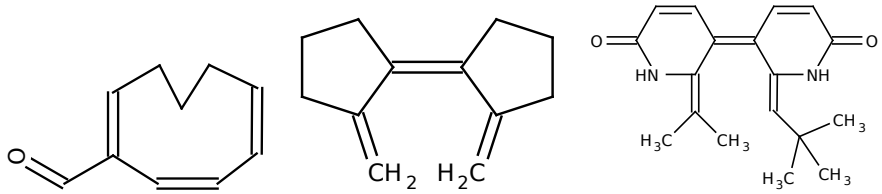

(a) Bridged aldehyde system. **(b)** Cyclopentane-derived hexatriene. **(c)** Dilactone-based electrocyclic switch.

Figure 5.1: Exemplary early models studied during the design process.

At this time of the design process, MNDO became available and its applicability was sufficiently checked for the use on electrocyclic ring-closure/-opening reactions. In following studies using the MR-CI-OM3 model coupled to direct dynamics, the terminal substituents on the hexatriene units were adapted to find a balance between ring-closure and ring-opening reactions for the dilactone system given in figure 5.1c and a corresponding dilactame. The functionalisation of the terminal carbon atoms of the central hexatriene unit is a flexible way to influence this balance, because the size of the substituents sterically pushes apart the carbon atoms forming the new bond, which enhances the likeliness of the ring-opening reaction. The final molecules are given in figure 5.2, the lactame based molecule 5.2a was the first to be studied, while the lactone 5.2b came second, which is part of the reason the lactone was studies less thoroughly.

5.3 Focused study of final electrocyclic switches

After identification of promising molecules, the prospective candidates were extensively studied using a variety of methods. For both molecules, the ground-state minima were optimised using CC2/def2-TZVPP and CASSCF(10,10)/6-31g(d,p) [14,98] wave function models, carried out in TURBOMOLE [86] and MOLPRO [15], respectively. Minimum-energy paths were simulated, starting from the Franck-Condon points of the S_1-state, and S_1-S_0-CoIn were optimised. In addition to the *ab-initio* simulations, a total of 75 photo-de-excitation trajectories for the lactame in both the cyclic and the open form were simulated using semiempirical wave function models analogous to the ones used in sections 4.2, 4.4.1 and 4.4.2. For the lactone being

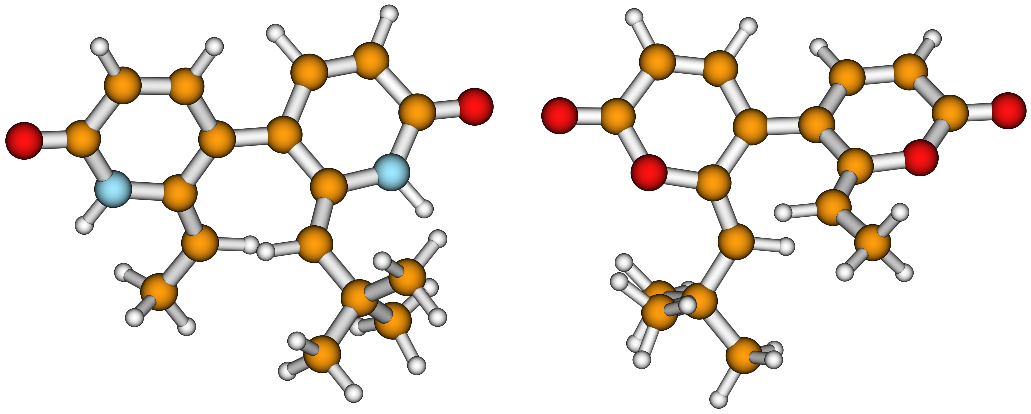

(a) Final dilactame-based electrocyclic switch. **(b)** Final dilactone-based electrocyclic switch.

Figure 5.2: Final suggested structures for new electrocyclic switches.

studied secondly the amount of data is more restricted. The following sections will cover these detailed studies.

5.3.1 Ab-initio studies of final electrocyclic switches

In the region of the Franck-Condon point, single-reference methods are the most efficient way to study the newly suggested switches. CC2/def2-TZVPP [88] optimisations of the ground-state minima and excitation energies for the six lowest excited states of the open and cyclic form were performed for both molecules during an internship by Julian Müller. The results are given in tables 5.1 and 5.2.

Table 5.1: Energies in eV of the studied electrocyclic switches relative to the closed minimum. Excitation energies from the respective Franck-Condon point are given in parentheses if differing.

	molecule			
	lactame		lactone	
	closed	open	closed	open
S_0	0.00	1.85	0.00	1.54
S_1	3.52	4.35(2.49)	3.54	4.32(2.79)
S_2	3.92	5.37(3.52)	3.93	5.39(3.86)
S_3	4.37	5.60(3.75)	4.62	5.63(4.10)
S_4	4.42	5.73(3.87)	4.65	5.80(4.27)
S_5	4.51	5.98(4.13)	4.78	5.87(4.33)
S_6	4.92	5.99(4.14)	5.03	5.96(4.42)

For both molecules, the open structure is significantly higher in energy than the closed one. In contrast to furylfulgides, ring closure leads to a blue-shift of the first electronic transition. Judging from the energies only, the lactame seems unsuitable as a photochromic switch since the excited states of the closed form are not separable from the open states of the open form by photo-excitation. Upon closer inspection of

the oscillator strengths for the transitions to the S_2-state of the closed lactame and to the S_4- and S_3-states of the open lactame, which are similar in energy, the transition to S_2-state is revealed to have a larger oscillator strength than the transitions of the open form. This may not be an ideal situation but leaves an option to predominantly excite the closed form. For the lactone, the picture is simpler: The excitation energy of the first excited state of the closed form falls into a gap of the excition energies of the open form. Additionally, the next closest transition of the open form ($S_2 \leftarrow S_1$) only has about half as much oscillator strength compared to the $S_1 \leftarrow S_0$ transition of the closed form. A more detailed analysis will follow in section 5.3.2.

Table 5.2: Oscillator strengths of the six lowest electronic transitions of the suggested electrocyclic switches.

	molecule			
	lactame		lactone	
final state	closed	open	closed	open
S_1	$2.2 \cdot 10^{-2}$	$7.8 \cdot 10^{-2}$	$7.5 \cdot 10^{-2}$	$1.2 \cdot 10^{-1}$
S_2	$1.2 \cdot 10^{-1}$	$4.4 \cdot 10^{-2}$	$1.1 \cdot 10^{-1}$	$3.1 \cdot 10^{-2}$
S_3	$1.2 \cdot 10^{-4}$	$3.4 \cdot 10^{-2}$	$1.0 \cdot 10^{-3}$	$1.0 \cdot 10^{-1}$
S_4	$4.8 \cdot 10^{-5}$	$1.5 \cdot 10^{-2}$	$2.2 \cdot 10^{-4}$	$9.0 \cdot 10^{-4}$
S_5	$5.8 \cdot 10^{-1}$	$1.2 \cdot 10^{-1}$	$4.5 \cdot 10^{-1}$	$6.8 \cdot 10^{-2}$
S_6	$2.7 \cdot 10^{-2}$	$3.6 \cdot 10^{-1}$	$3.4 \cdot 10^{-2}$	$4.5 \cdot 10^{-1}$

Expanding the *ab-initio* studies, the Franck-Condon points of the lactame were optimised using a CASSCF(10,10)/6-31g(d,p) wave function model averaged over four states, containing only π-orbitals for the open forms and a pair of σ-orbitals in the newly formed bond for the closed forms, in addition to a (8,8)-π space. Single-point calculations were carried out in a multistate (MS)-CASPT2(10,10)/(ANO-L-VTZP (for heavy atoms in the conjugated system) and ANO-L(carbon)/S(hydrogen)-VDZP (for atoms not part of the conjugated systems) [99,100] model to account for effects of dynamic correlation using Molcas [69]. A Cholesky decomposition [101–104] with a cut-off of 10^{-8} was used and four electronic states with a level-shift of 0.25 Hartree were treated. Table 5.3 gives a comparison of the CASPT2 and CC2 energies. A

Table 5.3: CC2 and CASPT2 energies of the studied lactame in eV relative to the closed minimum. Excitation energies from the respective Franck-Condon point are given in parenthesis if differing.

	wave function model					
	CC2		CASPT2//CASSCF		CASPT2//CC2	
	closed	open	closed	open	closed	open
S_0	0.00	1.85	0.00	1.59	0.00	1.66
S_1	3.52	4.35(2.49)	4.02	5.67(4.08)	3.38	5.00(3.33)
S_2	3.92	5.37(3.52)	4.96	6.34(4.76)	4.69	5.58(3.92)
S_3	4.37	5.60(3.75)	5.71	6.62(5.03)	5.37	5.99(4.32)

comparison of the results reveals severe disagreements at first sight. The excited states in the CASPT2 model are significantly higher in energy than in the CC2 model, while the relative energies of the two ground-state minima are in reasonable agreement. Most importantly, the relative energies of the first excited state at the Franck-Condon points do not fully reflect the inversion of the relative energies compared to furylfulgides, which is present in both CC2 and OM3-MRCI simulations, but only imply nearly identical excitation energies. The changed relative excitation energies appear in both CC2 and OM3-MRCI and the trend is also present in the CASPT2 simulations. This lends credibility to the observed feature. The agreement of the CC2 and the OM3-MRCI and the fact that the CASPT2 calculations do not show important doubly excited determinants imply that the more accurate results can be expected from the CC2 simulations, due to the larger basis and the more reliable description of dynamic correlation energy, especially during the geometry optimisation (were a CASSCF wave function model was used in the multireference case), thus leading to a structure that is adapted to the incoorporation of dynamic correlation in contrast to the CASSCF optimised geometry. To check influence of the dynamic correlation on the geometry optimisation, the CASPT2 energies were re-evaluated at the CC2 optimised geometry. This lowers the excitation energies for the system but the discrepancies in relative excitation energies between open and closed form persist.

Due to the multiconfigurational character encountered during the photo-de-excitation, the CASPT2 wave function model is the only *ab-initio* model that can be applied to intermediate structures in the de-excitations and thus was used nevertheless. Minima of the first excited state and a helical conical intersection were optimised for tha dilactame using the CASSCF(10,10)/6-31g(d,p) model previously established, and single-point MS-CASPT2 calculations were performed for these. The resulting energies are given in table 5.4 and the geometries in figure 5.3. On the open side of the reaction, the data is compatible with a reactive de-excitation from the S_1-state. The conical intersection structure is a distorted form of the zwitterionic conical intersections known from other electrocyclic switches [60, 66, 84, 85] and thus likely to facilitate ring closure. On the closed side, the picture is less easily interpreted. The most striking point is that the S_1-minimum is higher in energy than the corresponding Franck-Condon point. The most likely reason for this is that the S_1-minimum structure was optimised neglecting dynamic correlation and thus the rather distorted structure in figure 5.3b is probably not a minimum and not close to one upon incorporation of dynamic correlation.

5.3.2 Semiempirical studies of suggested electrocyclic switches

A total of 75 trajectories was run for both the open ring and the cyclic structures of the lactame, sampling the ground state at 300 K for 150 fs each. Spectra were extracted in the usual fashion and convoluted with a resolution function of 20 nm

Table 5.4: CASPT2 energies of the optimised excited state geometries of the studied lactame in eV relative to the closed minimum. The conical intersection is the same for both sides of the reaction

	side of the reaction					
	open			closed		
	S_0	S_1	S_2	S_0	S_1	S_2
S_0-minimum	1.59	5.67	6.34	0.00	4.02	4.96
S_1-minimum	2.43	4.52	4.92	1.82	4.68	5.88
conical intersection	4.06	4.12	5.92	4.06	4.12	5.92

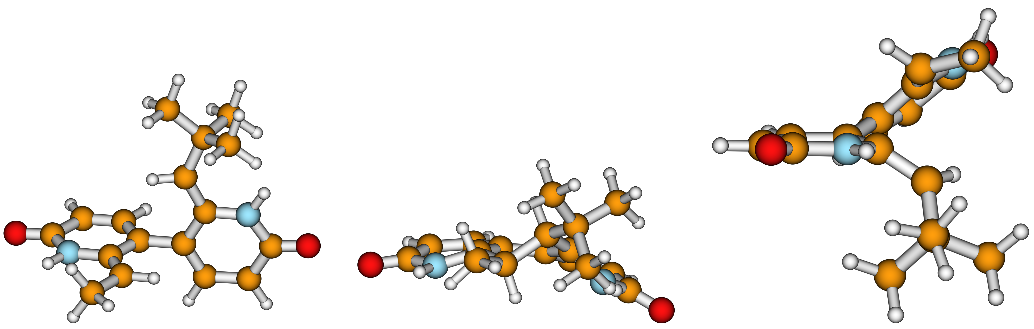

(a) S_1-minimum on the open side of the ring-closure reaction.

(b) S_1-minimum on the closed side of the ring-opening reaction.

(c) S_1-S_0 helical conical intersection.

Figure 5.3: Intermediate structures of the lactame likely to facilitate a ring-opening and -closure.

width. The resulting spectra are given in figure 5.4. Both the open and the closed semiempirical spectra fit well with the CC2 excitation energies for the most part. Although the scaling needed for the spectra to be of comparable intensity is different for the two forms, the agreement is sufficient to affirm further use of the semiempirical model.

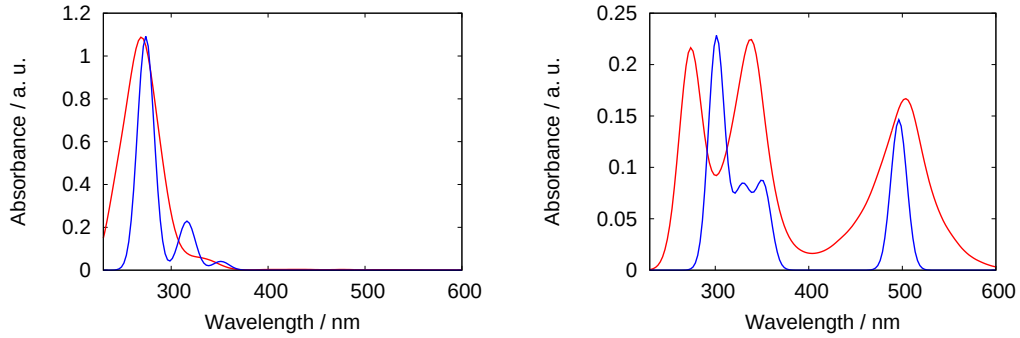

(a) Closed form **(b)** Open form.

Figure 5.4: Spectra of the lactame based switch simulated in the OM3-MRCI model (red), convoluted with a 20 nm wide Gaussian resolution function. CC2 excitations scaled for comparison and convoluted with a 20 nm resolution function are given in blue.

The static spectra of the lactone-based switches were studied in the same fashion as the ones of the lactame-based switch, with 50 Brownian motion trajectories for the simulations of the spectra of the open and the closed form. The resulting spectra are given in figure 5.5, together with the results of the CC2 calculations. Although the fit between *ab-initio* and semiempirical data is less good for the lactone than for the lactame, the agreement between the spectra is still reasonable.

In the spectra of both switches, the spectral bands of closed and open form appear not to be seperated well enough to allow for selective excitation of the isomers. For two reasons, further investigations of the molecules with respect to their switching properties is still useful. The band separation strongly depends on the accuracy of the simulated spectra. As the differences between the simulated data already show, the simulations are not accurate enough to rule out inaccuracies of that size. Therefore, it may very well be possible that the experimental spectra allow for selective excitation. Secondly, even if the experimental spectra do not allow for selective excitation, studies of the basic framework can possibly rule them out as objects of experimental study or make them new possible basic frameworks for other studies to come.

To establish the switching properties of the new frameworks, photo-de-excitation trajectories were simulated starting on the first excited state. The simulations for the lactame resulted in photo-isomerisation quantum yields of 46 % of a total of 63 trajectories for the ring-closure and 14 % of a total of 51 trajectories for the ring-opening reaction. Due to the weak oscillator strength for the $S_1 \leftarrow S_0$ transition in

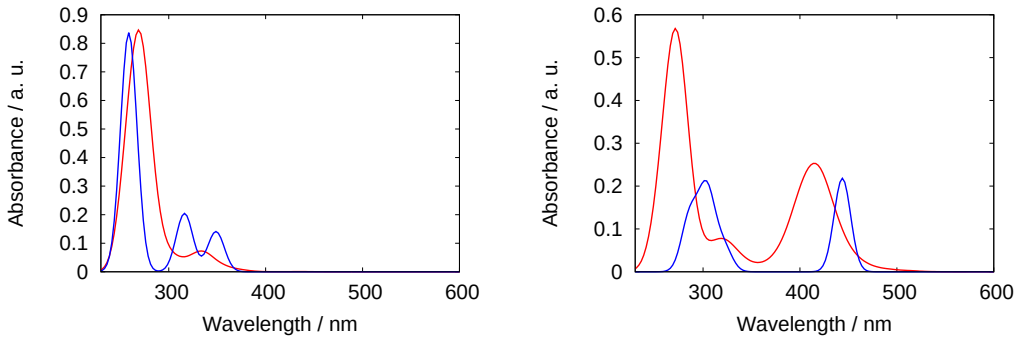

(a) Closed form. **(b)** Open form.

Figure 5.5: Spectra of the lactone based switch simulated in the OM3-MRCI model (red), convoluted with a 20 nm wide Gaussian resolution function. CC2 excitations scaled for comparison and convoluted with a 20 nm resolution function are given in blue.

the closed lactame, the photo-isomerisation trajectories were started on the S_2-state in this case. In addition to the bad ring-opening quantum yield, about a quarter of the trajectories that do not show an opening in the central ring de-excite along a path that results in breaking the amide at the carbonyl carbon, instead of the opening of the central ring. The bond breaking occurs predominantly but not exclusively on the same side of the molecule as the tertiary-butyl substituent. For the lactone, the ring-closure quantum yield is 42 % of 43 trajectories while the ring-opening is completely absent in a total of 40 trajectories started on the S_1-state and 50 started on the S_2-state. Instead, the molecule de-excited exclusively via the pathways involving the possible bond-breakage in the lactone rings. This behaviour renders both the lactame and especially the lactone unsuitable as photochromic switches. Nevertheless further investigations were finished to study the basic framework, which still might be useful with some minor modifications.

Close inspection of figure 5.6, reveals that the methyl and the tertiary-butyl substituents end up in quasi-equatorial positions after ring-closure. Although the structure is comparably rigid, a conformational change to the axial position might be possible. In the simulations, the conformational change is likely to happen after the photo-isomerisation from the open to the closed form of the lactone but also happens in the lactame. The ring-opening from the closed ring with axial ligands leads to an open structure with ligands pointing to the inside of the helical structure, which is the E,E'-isomer compared to the Z,Z'-isomer, which is the parent system. Since different de-excitation dynamics can be expected in these structures, the possible conformers and isomers of both lactame and lactone were studied in the same way as the parent systems.

From 50 Brownian-motion trajectories for each molecule and isomer, static spectra were extracted. Figure 5.7 depicts the resulting spectra together with the corresponding static spectra of the parent systems. The spectra of the open forms

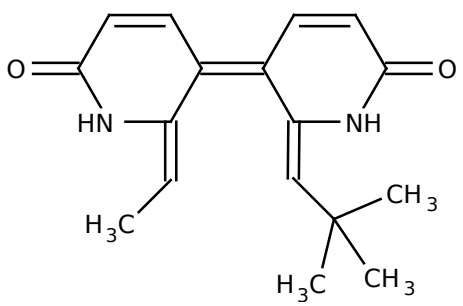

(a) Open form of the lactame based switch.

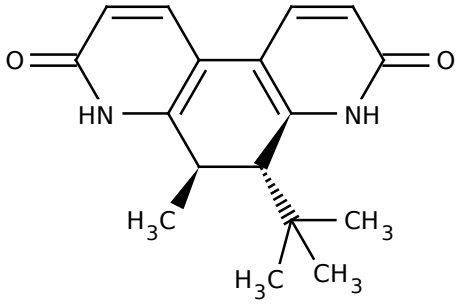

(b) Closed form of the lactame based switch.

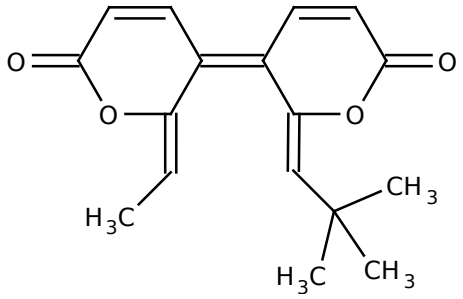

(c) Open form of the lactone based switch.

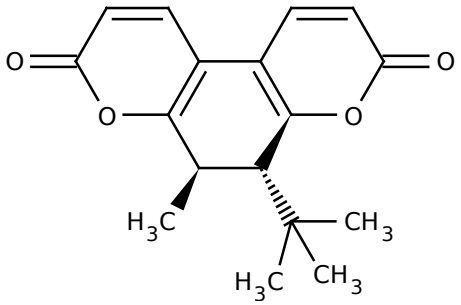

(d) Closed form of the lactone based switch.

Figure 5.6: Structural formulae of the parent isomers of the suggested molecular switches.

(figures 5.7a and 5.7b) change strongly in the isomerised forms, compared to the parent spectra. Although the basic features are retained, the bands shift and broaden significantly. The spectra of the closed forms (figures 5.7c and 5.7d) on the other hand are basically insensitive to the isomerisation. This very different influence is not surprising. The π-system is very rigid in the cyclic form and is not influenced much by the conformational change, thus the spectra do not change. In the open form, the different orientation puts the sterically demanding ligands into the center of the molecule and thus strongly influences the internal geometry of the π-system and with it the electronic spectra.

Following established procedure (see section 4.2), de-excitation dynamics were simulated for the lactame-based molecule, using the final structure from the Brownian-motion trajectories as input structure. Trajectories started at the open lactame structure (figure 5.6a) showed a ring-closure quantum yield of about 71 % in a total of 45 trajectories which is significantly higher than for the structure studied first. The trajectories started from the quasi-axial closed structure show no basic difference compared to the pseudo-equatorial alignment (see figure 5.6b) of substituents with ring-opening quantum yields of about 4 % in a total of 47 trajectories and also exhibit the explained beginning degradation reaction. The de-excitation of the changed lactone-based isomers were not studied for reasons of the overall worse findings of the lactone-based system and no expectation of further insights.

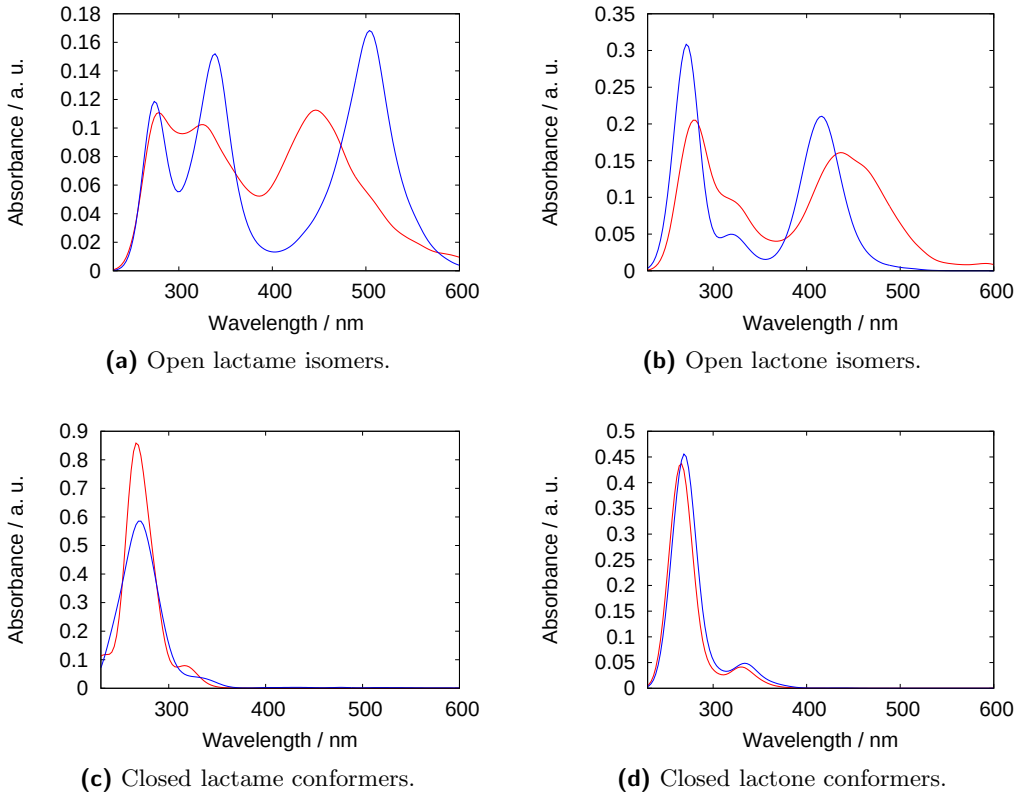

(a) Open lactame isomers.

(b) Open lactone isomers.

(c) Closed lactame conformers.

(d) Closed lactone conformers.

Figure 5.7: Simulated spectra of the E,E'-isomers (red) and Z,Z'-isomers (blue) of the open systems (top row) and quasi-axial (red) and quasi-equatorial (blue) closed conformers (bottom row) of the suggested molecular switches.

5.4 Open questions

Some questions about the suggested molecules stay open for investigation. The most important point is the unwanted de-excitation path in the cyclic form. The most obvious possibility to avoid bond breakage is to strengthen the ring. A possibility would be to change the carbonyl group to a hydroxyl group and a hydrogen, changing the lactone to an acetale and the lactame to an *N,O*-acetale (depicted in figure 5.8), thus destabilising the dissociation products. Although the modification of the rings will influence the absorption bands, the possibility of overlapping excitation wavelengths is still present. The change in the conjugated double-bond system upon cyclisation allows to influence the electronic states of the open and the closed form differently. Possible places for the substitution to influence the excitation wavelengths of the isomers are abundant in the heterocycles (highlighted in red in figure 5.8). The finding that the arrangement of the terminal substituents towards the middle of the molecules greatly increases the ring-closure quantum yield offers a possibility for further enhancement of the system by fixing them in that position. However, this may also negatively affect the quantum yield of a hypothetical molecule that shows reasonable ring-opening efficiency and cause isomerisation at the central double-bond by opening the helical minimum. Definitely, it would increase the difficulty to find suitable wavelengths for selective excitation due to the broadening of the spectra of the open form. If the isomerisation reaction proves to be too disadvantageous, a restriction of the necessary degrees of freedom will be possible by connecting the isomerising substituents to the outer rings, although this would very likely to increase difficulties in synthesis significantly (indicated in blue in figure 5.8).

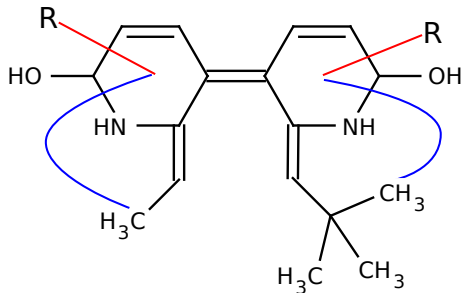

Figure 5.8: Structural changes recommended for further studies of the suggested framework.

5.5 Project summary

Within this project, it was possible to come up with a new framework as suggestion for possible new molecular switches. The suggested molecules were studied statically and dynamically. In both respects they show properties that rule them out as

molecular switches in this exact form but strongly suggest the suitability of the basic framework. Effective photochemical isomerisation towards ring-closure was observed in the relevant isomers of both molecules, with side reactions virtually absent in the simulations of the open structures. The closed forms, on the other hand, exhibit degradation reactions during the de-excitation processes.

Both molecules are predicted show excitation bands far in the visible range in their open forms, while the first spectral bands of the closed ones are predicted in the near UV. The predicted excitation energies are presumably too high, as previously gathered data on the simulation of spectra suggests so. Therefore there is reason to expect suitable wavelengths for excitation.

Multireferential *ab-initio* simulations of excited-state geometries of the lactame-based system have been shown to support the semiempirical simulations in the sense that they predict suitable minima and CoIn points for reactive de-excitation for the open form, while they are inconclusive for the closed form.

Although the designed molecules still show some weaknesses, straightforward modification recommendations are possible that might enhance the properties of the studied molecules within further studies.

6 Excited state properties of Azobenzenederivatives

6.1 Project motivation

Azobenzene and related molecules are a class of systems with very favourable properties for the use as molecular switches in various applications [105–108]. The photoinducible E/Z-isomerisation causes major changes in the absorption spectra, the length and the dipole moment of these molecules. The isomerisation is reversible, degradation is virtually absent and, depending on the system, the reaction is extremely efficient [109,110]. This makes azobenzene-related molecules one of the most studied molecular photo-switches in existence. The abundance of experimental interest [111–119] goes hand in hand with prominent theoretical investigations [120–123]. The large amount of investigations causes the azobenzene-related systems of interest to increase in complexity in many cases. In this chapter, studies of three different azobenzene-related systems will be presented. The first system under study is dihydrodibenzodiazocine, an internally strained azobenzene-related molecule. The internal constraint causes an inverted stability of the isomers (thus the Z-form is more stable), an increased band-splitting in the UV/Vis spectra and significantly enhanced switching properties. In the second part of the chapter, theoretical investigations of a systematically varied oligochromophore system, presented in [124], are given. The investigations consist of the identification of a suitable semiempirical model for upcoming isomerisation dynamics investigations and a systematic *ab-initio* study carried out to help understanding the detailed features observed in static UV/Vis spectra. The last part of the chapter is dedicated to multiconfiguration studies of an azopyridin-functionalised nickel porphyrin, which is the first molecule to show ligand-driven coordination-induced spin-state switching [125]. This type of system is deemed to promise future applications as a contrast agent in the field magnetic resonance imaging, although not in this specific form, as it is unsoluble in water. The investigations are aimed at the goal of understanding the rather low excitation energy needed to induce the E to Z isomerisation, which in turn causes a change in the electronic spin ground state from singlet to triplet.

6.2 Unusual photochemical dynamics of a bridged azobenzene derivative

Contributions to the paper:

- setup and execution of the multireference *ab-initio* accuracy checks for the applied semiempirical scheme

DOI: 10.1063/1.3479397

6.3 Electronic supplementary information: Unusual photochemical dynamics of a bridged azobenzene derivative

6.4 Superior $Z \rightarrow E$ and $E \rightarrow Z$ photoswitching dynamics of dihydrodibenzodiazocine, a bridged azobenzene, by $S_1(n\pi^*)$ excitation at $\lambda = 387$ and 490 nm

Contributions to the paper:

- setup and execution of multireference *ab-initio* calculations

DOI: 10.1039/c0cp01148g

6.5 Electronic supplementary information: Superior $Z \rightarrow E$ and $E \rightarrow Z$ photoswitching dynamics of dihydrodibenzodiazocine, a bridged azobenzene, by $S_1(n\pi^*)$ excitation at $\lambda = 387$ and 490 nm

6.6 Direct molecular dynamics studies of azobenzene-based multichromophore systems.

After dealing with single-chomophore systems, the following section will be committed to presenting first steps in the simulation of multichromophoric systems as depicted in figures 6.1a to 6.1c.

These systems pose a distinct experimental difficulty. The isomeric mixtures obtained upon irradiation are quantifiable experimentally [124] but up to now inseparable and the isomers cannot be excited completely separately. That means that all dynamical studies besides the ones for the most stable EE-isomer 6.1a will show spectra arising from an overlay of processes for all three molecules. This increases the complexity of interpretation on the experimental side, especially since the long-time goal of the project is to deal with the even larger trimeric system 6.1d. Therefore the long-time goal on the theoretical side of the project would be to simulate photo-de-excitation dynamics of the oligomeric systems. Although it was not possible to address this goal in this thesis for resons given in the following paragraphs, significant progress was made.

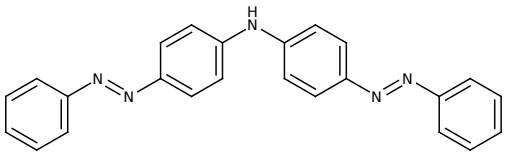

(a) EE-form of bis[4-(phenylazo)phenyl)]amine.

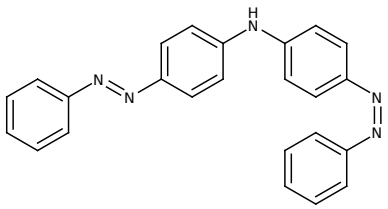

(b) EZ-form of bis[4-(phenylazo)phenyl)]amine.

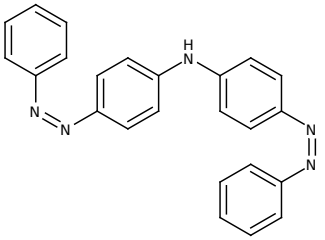

(c) ZZ-form of bis[4-(phenylazo)phenyl)]amine.

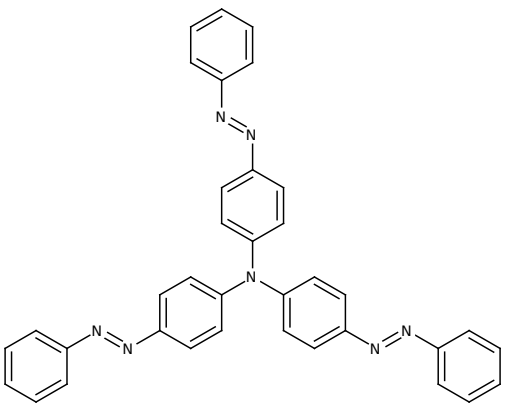

(d) EEE-form of tris[4-(phenylazo)phenyl)]-amine.

Figure 6.1: All possible isomeric forms bis[4-(phenylazo)phenyl)]amine and the EEE-form of tris[4-(phenylazo)phenyl)]amine.

With respect to the theoretical description presented in this thesis, the systems are not at all simpler. The most obvious problem is the increased size that, no matter what method is used, leads to either large increases in computation time or to a reduction in accuracy. For multireference *ab-initio* methods the increase in computation time would be insurmountable. A description of the systems depicted in figure 6.1 on the same level as for the diazozine in sec. 6.1 would imply a (28,24) active space with a basis between double and triple zeta size for 48 atoms and a MS-CASPT2 treatment for the 3 lowest electronic states (the ground state and the two $n\pi^*$-states). In this already prohibitively large scenario any active-orbital contributions from the coupling nitrogen atom are still neglected. For this reason, a multireference *ab-initio* investigation of the excited-state potential energy surfaces of this molecule was impossible.

Secondly, the nitrogen atom between the two azobenzene units formally allows for conjugation, thus completely delocalising the excited states. If a rotation of the azobenzene units is still possible, this will lift the conjugation of the system already during Brownian motion. The uncertain amount of interaction of the two azobenzene parts and the connecting nitrogen atom make a treatment of the system by calculation of the wave functions of low-lying states of isolated azobenzene and formation of the excited states of the full system as linear combinations of these more difficult than it already is for well separated systems.

Instead of the two methods mentioned above (i.e. *ab-initio* calculations of the full system or of the subsystems and then combining them), the demonstrated applicability of Thiel's semiempirical MRCI-OM2 method to azobenzene systems [20, 40] was taken advantage of. The semiempirical framework allows for nuclear dynamics while the complete electronic wave function of the molecule can be treated with no prior assumptions about the interactions of the two chromophores. In the following sections, studies of the comparability of different semiempirical setups will be presented, judging their applicability by a detailed comparison to the experimental static spectra of EE-bis[4-(phenylazo)phenyl)]amine (figure 6.1a) and the photostationary state resulting from continuous irradiation with light of 385 nm.

6.6.1 Computational setup

In a study of the dynamics of free azobenzene, Weingart *et al.* [20] used a (10,10) active space consisting of nine π-orbitals and one nitrogen lone-pair orbital (this is a linear combination of the n-orbitals located at the azo-bridge) with single and double excitations using three reference configurations: the RHF ground state and the single and double excitation from the HOMO to the LUMO. In the case of bis[4-(phenylazo)phenyl)]amine, a similar model would include an active space of 20 electrons in 20 orbital plus a lone pair as contribution from the bridging nitrogen, forming a (22,21) active space. For large-scale studies of the dynamics ensuing upon photo-excitation, this would be computationally too expensive. This is true even

more for the trimeric systems. To find a reasonable compromise, various semiempirical setups where calculated and tested against experimental static spectra.

The largest model contained the seven occupied orbitals highest in energy and the seven virtual orbitals lowest in energy, treating all single and double excitations in this space. The idea behind this choice is to take three occupied orbitals (two π, one n) and three virtual π orbitals for each benzene moiety, one occupied orbital from the bridging nitrogen atom and one virtual orbital from whichever π-system is most suitable at the given time step. Three different sets of reference configurations were used for this orbital set. The first one consisted of the RHF ground state configuration and the single and double excitation from HOMO to LUMO. In the second set, ten of the most important configurations, taken from a previous calculation in the same active space that identified the configurations with largest expansion coefficients in the CI vector for the given isomer, were used. The last set consisted of seven configurations also picked from the most important configurations but this time from all isomers. The electron configurations are given in tables 6.1 to 6.3.

Table 6.1: Reference configurations used for Brownian dynamics of EE- and ZE-bis[4-(phenylazo)phenyl)]amine in a (14,14) active space with double excitations and a 10-reference-functions wave function. The character of the orbitals is indicated for the EE-form. In the ZE-form the same character is present in the active space but the definite characterisation is not possible anymore.

	Orbital number													
	64	65	66	67	68	69	70	71	72	73	74	75	76	77
character	π	π	π	n	n	π	π	π	π	π	π	π	π	π
occupation	2	2	2	2	2	2	2	0	0	0	0	0	0	0
occupation	2	2	2	2	2	2	1	1	0	0	0	0	0	0
occupation	2	2	2	2	2	2	1	0	1	0	0	0	0	0
occupation	2	2	2	2	2	1	2	1	0	0	0	0	0	0
occupation	2	2	2	2	2	1	2	0	1	0	0	0	0	0
occupation	2	2	2	2	1	2	2	1	0	0	0	0	0	0
occupation	2	2	2	1	2	2	2	0	1	0	0	0	0	0
occupation	2	2	2	2	1	2	2	0	1	0	0	0	0	0
occupation	2	2	2	1	2	2	2	1	0	0	0	0	0	0
occupation	2	2	1	2	2	2	2	1	0	0	0	0	0	0

A second active space consisted of the same seven occupied orbitals as before but left the additional virtual orbital out. The resulting active space was of (14,13) size. As before, single and double excitations were accounted for. For one set of calculations the reference wave function was set up from three configurations corresponding to the RHF ground state and the single and double HOMO to LUMO excitation, therefore being analogous to the three-configuration reference wave function for the (14,14) active space. Another set was calculated for a seven-reference wave function consisting of the same reference-configurations as for the (14,14) active space (see table 6.3 for details).

Table 6.2: Reference configurations used for Brownian dynamics of ZZ-bis[4-(phenylazo)phenyl)]amine in a (14,14) active space with double excitations and a 10-reference-functions wave function.

	Orbital number													
	64	65	66	67	68	69	70	71	72	73	74	75	76	77
occupation	2	2	2	2	2	2	2	0	0	0	0	0	0	0
occupation	2	2	2	2	2	2	1	1	0	0	0	0	0	0
occupation	2	2	2	2	2	2	1	0	1	0	0	0	0	0
occupation	2	2	2	2	1	2	2	1	0	0	0	0	0	0
occupation	2	2	2	2	1	2	2	0	1	0	0	0	0	0
occupation	2	2	2	2	2	1	2	1	0	0	0	0	0	0
occupation	2	2	2	1	2	2	2	0	1	0	0	0	0	0
occupation	2	2	2	2	2	1	2	0	1	0	0	0	0	0
occupation	2	2	2	1	2	2	2	1	0	0	0	0	0	0
occupation	1	2	2	2	2	2	2	1	0	0	0	0	0	0

Table 6.3: Reference configurations used for Brownian dynamics of bis[4-(phenylazo)phenyl)]amine in a (14,14) and (14,13) active space with double excitations and a 7-reference-functions wave function. For the (14,13) active space leave out the last column.

	Orbital number													
	64	65	66	67	68	69	70	71	72	73	74	75	76	77
occupation	2	2	2	2	2	2	2	0	0	0	0	0	0	0
occupation	2	2	2	1	2	2	2	1	0	0	0	0	0	0
occupation	2	2	2	2	1	2	2	0	1	0	0	0	0	0
occupation	2	2	2	2	2	2	1	1	0	0	0	0	0	0
occupation	2	2	2	2	2	1	2	0	1	0	0	0	0	0
occupation	2	2	2	2	2	2	1	0	1	0	0	0	0	0
occupation	2	2	2	2	2	1	2	1	0	0	0	0	0	0

For all the presented setups, a set of ten ground state molecular dynamics trajectories of EE-bis[4-(phenylazo)phenyl)]amine were simulated 7500 time steps of 0.1 fs each. The simulation was coupled to a velocity scaling thermostat, acting every 200 time steps and scaling the velocities to be compatible with a Boltzmann distribution at 300 K. For the six lowest singlet states, energies and transition dipole moments were calculated. Not all of the trajectories could be evaluated due to convergence problems in either SCF or CI part of the calculations. Of ten trajectories usually eight to nine ran without an error. A detailed listing would not convey more useful information, and is therefore not done here.

6.6.2 Static spectra of bis[4-(phenylazo)phenyl)]amine

As for the furylfulgides (see sec. 4.2 for details), static UV/Vis-spectra were extracted from the Brownian motion simulations. The agreement of these spectra with the experimental isomerically pure spectrum of EE-bis[4-(phenylazo)phenyl)]amine recorded in n-hexane was used as first criterion to check the suitability of the applied semiempirical model. The resulting spectra are depicted in figures 6.2 to 6.4. The simulated spectra were scaled by a factor to resemble the intensity of the experimental spectrum. The scaling factors are different for each of the wave function models but are kept constant in all the following simulations. The simulated spectra show

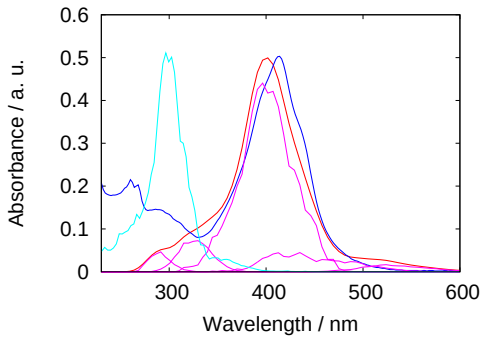

Figure 6.2: Comparison of simulated and experimental (blue) spectra of EE-bis-[4-(phenylazo)phenyl)]amine. The simulated spectra are based on the (14,14) active space model with 10 reference configurations. Depicted in light blue is the unshifted total spectrum from simulation scaled by 0.13. The underlying state-resolved spectra, red-shifted by 8500 cm^{-1} and scaled by 0.12 are given in pink and the full spectrum convoluted with a Gaussian-shaped resolution function of 10 nm FWHM, red-shifted by 8500 cm^{-1} and scaled by 0.40 is depicted in red. Scale factors are given to stress comparability to figure 6.5

reasonable agreement with the experimental one. A quantitative agreement was neither expected for that size a system nor needed. As shown for furylfulgides in chapter 4, qualitatively accurate dynamics simulations offer fruitful insight. The blue-shift in the simulated spectra is in the range of 8200 cm^{-1}, which is not good but not devastating either. Besides the shift, the most obvious discrepancy between

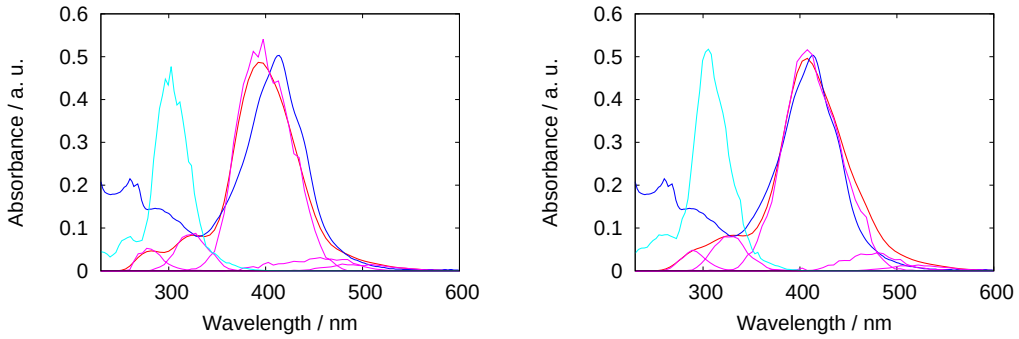

(a) The simulated spectra are based on the (14,14) active space model. Light blue: scaled by 0.12; Pink: red-shifted by 7900 cm^{-1} and scaled by 0.14; Red: red-shifted by 7900 cm^{-1} and scaled by 0.40.

(b) The simulated spectra are based on the (14,13) active space model. Light blue: scaled by 0.14; Pink: red-shifted by 8200 cm^{-1} and scaled by 0.14; Red: red-shifted by 8200 cm^{-1} and scaled by 0.42.

Figure 6.3: Comparison of simulated and experimental (blue) spectra of EE-bis-[4-(phenylazo)phenyl)]amine for the seven configuration model. Depicted in light blue is the unshifted total spectrum from simulation. The underlying spectra, resolved by the final state, are given in pink and the full spectrum convoluted with a Gaussian-shaped resolution function of 10 nm FWHM is depicted in red. Shifts and scale factors are given in the subcaptions to show the comparability to the photostationary state spectra given in figures 6.6.

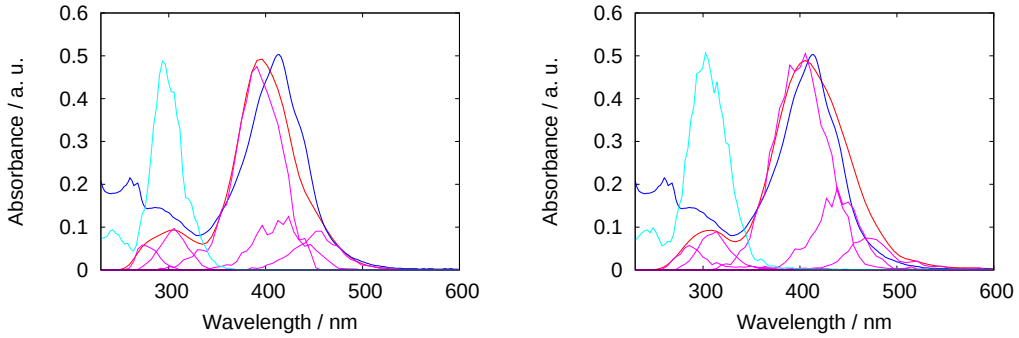

(a) The simulated spectra are based on the (14,14) active space model. Light blue: scaled by 0.13; Pink: red-shifted by 8500 cm^{-1} and scaled by 0.15; Red: red-shifted by 8500 cm^{-1} and scaled by 0.42.

(b) The simulated spectra are based on the (14,13) active space model. Light blue: scaled by 0.17; Pink: red-shifted by 8400 cm^{-1} and scaled by 0.19; Red: red-shifted by 8400 cm^{-1} and scaled by 0.52.

Figure 6.4: Comparison of the simulated and experimental (blue) spectra of EE-bis-[4-(phenylazo)phenyl)]amine for the three configuration model. The underlying spectra, resolved by the final state, are given in pink and the full spectrum convoluted with a Gaussian-shaped resolution function of 10 nm FWHM is depicted in red. Shifts and scale factors are given in the subcaptions to show the comparability to the photostationary state spectra given in figures 6.7.

experimental and simulated spectra are the high-intensity shoulders left and right from the peak of the first band. These shoulders are only weak in the simulated spectra, although the overall asymmetry of the band is quite well reproduced.

The reasons for this difference can be manifold. A rather simple one would be that the energies and/or the relative intensities of the $n\pi^*$-bands (the two rightmost pink bands in all subfigures in figures 6.4 and 6.2) are slightly wrong compared to the intense $\pi\pi^*$-band (the third pink band, dominating the spectra) in the simulated spectra. This can most easily be explained from figure 6.4b. A small rise in the wavelengths of the $n\pi^*$-bands would cause the shoulder to form and also correct for the slightly too quick decay of the simulated spectrum. Differences in the accuracy of description of the states are not unreasonable (see sec. 4.3 for comparison), especially since the states treated are very different in character. If the aforementioned deficiencies in the simulations are not true, the shoulders will be part of the dominating $\pi\pi^*$-excitation-band and do not arise from distinct transitions. This explanation is most obviously derivable from figure 6.2. Here, the relative intensities lead to a band shape that fits exceptionally well with the overall shape of the experimental band but lacks the shoulders on the dominating band. In this case, the reason for the difference might be due to an insufficient representation of the Franck-Condon factors in the simulation. As shown in sec. 4.8.3, the direct molecular dynamics used can never grasp the part of the Franck-Condon factor arising from excited-state nuclear wave function, for it is a classical model with respect to the nuclei. Nonetheless, before this feature should be attributed to that rather complex reason, other possibilities have to be ruled out. The most likely reason may be an insufficient sampling of the ground-state coordinate space. Two points support that. One is the rather small number of trajectories simulated. Although the time information in the trajectories could be neglected since static spectra are simulated and the effective sampling therefore be enhanced, still the total number of trajectories and their length is too small for fully sampling a system of the size of EE-bis[4-(phenylazo)phenyl]amine. The second reason is the concededly weak hint at the red-shifted shoulder in the raw data, which might get more pronounced by a more detailed sampling. Up to now, the data does not allow for a conclusive decision on this topic.

To expand the comparison to the description of the EZ- and ZZ-bis[4-(phenylazo)-phenyl]amine, theoretical static spectra for these molecules were calculated. Although there is no experimental data on the pure isomers, the UV/Vis-spectrum for the photo-stationary state has been measured and the isomeric composition of the photo-stationary state is known. The simulated spectra were weighted with factors corresponding to the isomeric mixture at the photostationary state [124] and could then be compared to the experimental data in the same fashion as the spectrum of the EE-isomer before (the intensities of the experimental spectra are on the same scale). The weight factors used were 0.95(EE):1.00(EZ):0.51(ZZ), which result in

the spectra depicted in figures 6.5 to 6.7 after renormalisation. The most obvious result deducible from these spectra is the complete incapability of the (14,13) active space model with a three-reference-configurations wave function (figure 6.7b) to describe the EZ-system relative to the EE- and the ZZ-isomer. While the ten- and seven-configurations wave function models show excitations with similar intensities for the EE- and EZ-isomers, as can be seen in figure 6.5 and 6.6, the (14,13)-three-configurations-model gives a maximum in spectral intensity for the ZE-isomer that is about two times higher than for the two other isomers. This leads to an over-representation of the spectrum of the EZ-isomer in the weighted spectrum, which is completely incompatible with the structure of the experimental spectrum and significantly increases intensity of the spectrum of the photo-stationary state compared to the spectrum of the EE-isomer. In experiment the effect is opposite: The spectrum of the photo-stationary state has a pronouncedly reduced intensity compared to the EE-isomer [124]. None of the simulations fully describe the necessary decrease in intensity, but the other models at least show some amount of reduction. Since the spectral intensity of the EE-bis[4-(phenylazo)phenyl]amine isomer was scaled to fit the intensity of the isomerically pure sample and this scale factor has been kept for the calculation of the spectra of the photo-stationary state, the reason for the wrong intensity must be that the intensities of the ZE- and the ZZ-isomer are to high relative to that of the EE-isomer.

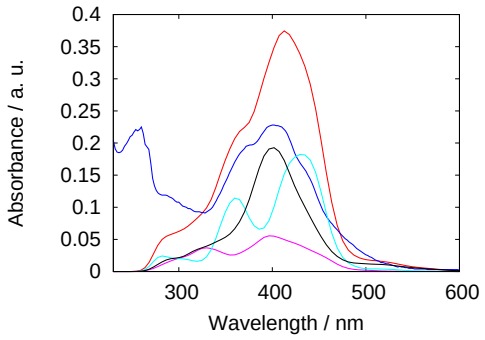

Figure 6.5: Comparison of simulated and experimental (blue) spectra of the photo-stationary state of bis[4-(phenylazo)phenyl]amine. The simulated spectra are derived from the (14,14) active space model with 10 reference configurations. The full simulated spectrum is depicted in red scaled by 0.40 and red-shifted by 8500 cm^{-1} (see also figure 6.2. The spectra of the pure isomers (also red-shifted by 8500 cm^{-1}) scaled by their weight in the photo-stationary state and 0.40 are depicted in EE: black, EZ: light blue and ZZ: pink.

Besides the reduced intensity, the most characteristic feature of the experimental spectrum of the photo-stationary state is the very pronounced two-shoulders structure that is very close to a three-peaks structure. That means that a reasonable description of the system should at least have the potential to show three distinct bands. In the (14,14) active-space model with three references (figure 6.7a), the $n\pi^*$ spectral transitions of the EZ-isomer (light blue) and ZZ-isomer (pink) show a

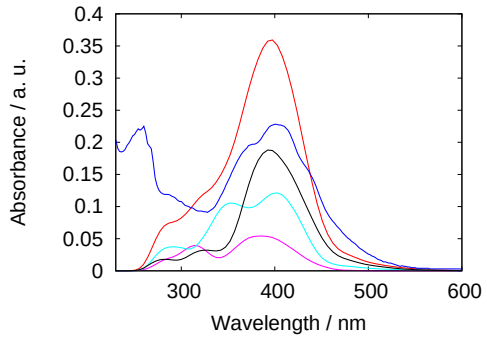

(a) The simulated spectra are derived from the (14,14) active space model. Total spectrum: scaled by 0.40 and red-shifted by 7900 cm^{-1} (also see figure 6.3a); Spectra of the isomers: red-shifted by 7900 cm^{-1}, scaled by their weight in the photo-stationary state and 0.40.

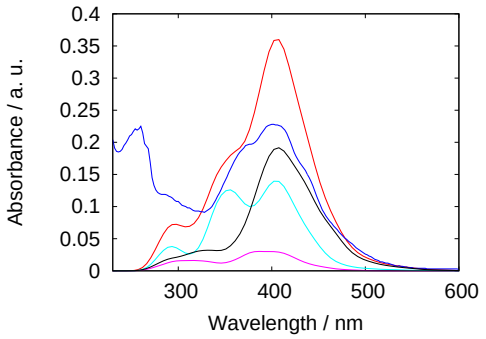

(b) The simulated spectra are derived from the (14,13) active space model. Total spectrum: scaled by 0.42 and red-shifted by 8200 cm^{-1} (also see figure 6.4b); Spectra of the isomers: red-shifted by 8200 cm^{-1}, scaled by their weight in the photo-stationary state and 0.42.

Figure 6.6: Comparison of simulated and experimental (blue) spectra of the photo-stationary state of bis[4-(phenylazo)phenyl]amine for the seven-configurations models. The full simulated spectra are depicted in red. The spectra of the pure isomers are depicted in EE: black, EZ: light blue and ZZ: pink.

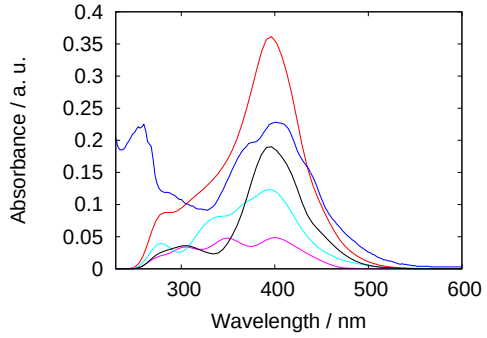

(a) The simulated spectra are derived from the (14,14) active space model. The full simulated spectrum is depicted in red scaled by 0.42 and red-shifted by 8500 cm^{-1} (see also figure 6.4a. The spectra of the pure isomers (also red-shifted by 8500 cm^{-1}) are scaled by their weight in the photo-stationary state and 0.42.

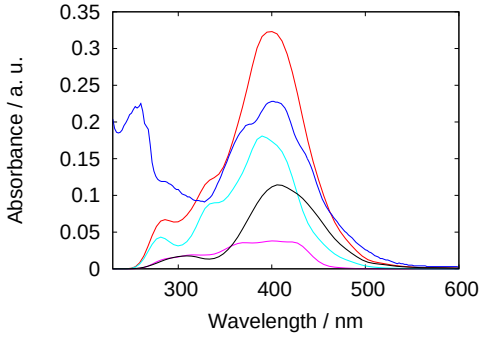

(b) The simulated spectra are derived from the (14,13) active space model. The full simulated spectrum is depicted in red scaled by 0.52 and red-shifted by 8400 cm^{-1} (see also figure 6.4b. The spectra of the pure isomers (also red-shifted by 8400 cm^{-1}) are scaled by their weight in the photo-stationary state and 0.52.

Figure 6.7: Comparison of simulated and experimental (blue) spectra of the photo-stationary state of bis[4-(phenylazo)phenyl]amine for the three-configurations models. Full simulated spectra: red, EE: black, EZ: light blue and ZZ: pink.

very strong blue-shift compared to the EE-spectrum (black). The blue-shift is large enough to move the first spectral maximum below the $\pi\pi^*$-band of the EE-isomer, which is not sufficiently asymmetric by itself. Thus the three-bands structure of the full spectrum is destroyed. When analysed isomer by isomer, the ten- and seven-reference spectra clearly show the three-maxima structure, although for different reasons. In the (14,14) active-space ten-reference model, the excitation maxima of the EZ-isomer enclose the maximum of the EE-isomer (light blue and red in figure 6.5). In this case the shoulders would therefore arise from these peaks in the spectrum of the EZ-isomer. In the (14,14) seven-reference model (figure 6.6a), the asymmetric high-wavelength part of the spectrum of the EE-isomer overlaps with the first peak in the spectrum of the EZ-isomer. This causes a blue-shift of the band maximum of the photo-stationary state to nearly the first maximum of the EZ-spectrum, laying ground for the necessary band shape, although the detailed relative intensities do not sum up to that in the given case.

From the spectra of the pure isomers in the more fitting simulated spectra (especially figure 6.5 and to a lesser extent 6.6), the physically reasonable effects of the isomerisation become obvious. The energies of the spectral transitions shift to shorter wavelengths due to the disturbance of the conjugated system by the Z-configuration in one or both of azobenzene moieties, in the EZ- and the ZZ-isomers respectively. The other effect of the orientation change is an increase in the relative intensity of the $n\pi^*$-transition in the Z-configured azobenzene unit. To some extent, this effect stems from a decreasing intensity of the dominant $\pi\pi^*$-band resulting in a decrease of overall intensity in the spectra of the EZ- and ZZ-isomer. These changes lay ground for the potential three-peak structure in the spectra in figures 6.5 and 6.6.

Based on an evaluation of the data presented in this section, the choice of a semiempirical model for simulations of excited state dynamics of bis[4-(phenylazo)-phenyl]amine can be made. Although being the computationally most expensive model, the (14,14) active space model with ten reference configurations is the most reasonable approach. It shows qualitative agreement with both the isomerically pure EE-spectrum and, to a lesser extent, the spectrum of the photo-stationary state, that is clearly superior to all other models. The description is well enough to justify simulations of photo-dynamics, which will not be part of this thesis, and to allow for some conclusions there.

6.6.3 Comparability of oligomeric chromophores to a single-chromophore system

To gather a deeper understanding of the changes that happen to the chromophoric units due to the coupling, electronic states of the mono-chromophoric parent system 4-amino-azobenzene were studied on the levels of CC2/def2-TZVPP and MRCI-OM2 with two excitations in a (8,8) active space with all reference configurations

needed to yield 80 % reference weight after dynamic correlation treatment, on a structure optimised in the semiempirical model. The excited states of EE-bis[4-(phenylazo)phenyl]amine where studied using the MRCI-OM2 (14,14) active space model presented in the previous section 6.6.2, again using all reference configurations needed to retain a reference weight of 80 %, on a structure optimised in this model, and on CC2/def2-TZVPP level on a B3LYP/6-31+g(d,p) optimised structure supplied by Dipl. Chem. Julia Bahrenburg [124]. This comparison was made to investigate whether the excited states of EE-bis[4-(phenylazo)phenyl]amine can be viewed as states constructed from linear combinations of the excited states of two basically undisturbed 4-amino-E-azobenzene units connected by a central amino-group or might be interpreted within the exciton model laid out in section 2.4.5.

Tables 6.4 and 6.5 list the important excitations for the excited states of these two molecules. The corresponding orbitals are given in figures 6.8 and 6.10 for the CC2 orbitals and in figures 6.9 and 6.11 for the MRCI-OM2 orbitals.

Table 6.4: Weights and character of important excitations (absolute coefficients or amplitudes 0.20 and greater) of the three lowest excited states of EE-bis[4-(phenylazo)phenyl]amine, based on CC2/def2-TZVPP and MRCI-OM2 wave function models. Minus signs in the weights columns indicate negative coefficients or amplitudes.

State	CC2/TZVPP			MRCI-OM2		
	from	to	weight	from	to	weight
S_1	HOMO−8	LUMO	52%(−)	HOMO−2	LUMO	31%(−)
	HOMO−9	LUMO+1	39%	HOMO−3	LUMO+1	23%
				HOMO−2	LUMO+1	21%
				HOMO−3	LUMO	12%(−)
S_2	HOMO−9	LUMO	52%(−)	HOMO−3	LUMO	31%(−)
	HOMO−8	LUMO+1	39%(−)	HOMO−2	LUMO+1	24%
				HOMO−3	LUMO+1	21%(−)
				HOMO−2	LUMO	12%
S_3	HOMO	LUMO	86%	HOMO	LUMO	47%(−)
	HOMO−1	LUMO+1	6%	HOMO−1	LUMO+1	17%
S_4	HOMO	LUMO+1	83%	HOMO	LUMO+1	46%(−)
	HOMO−1	LUMO	7%	HOMO−1	LUMO	24%
S_5	HOMO	LUMO+2	51%	HOMO	LUMO+5	38%(−)
	HOMO−5	LUMO	21%(−)	HOMO	LUMO+4	24%(−)
	HOMO−6	LUMO+1	7%			
	HOMO−1	LUMO+3	5%			

In the following paragraphs, the data will be analysed on the basis of the involved orbitals, regarding the agreement of the used wave function models and the applicability of the exciton model to the case under study.

The data shows that the *n*-orbitals of the dichromophoric system (figures 6.8a, 6.8b for CC2 and 6.9a, 6.9b for MRCI-OM2) can straightforwardly be interpreted

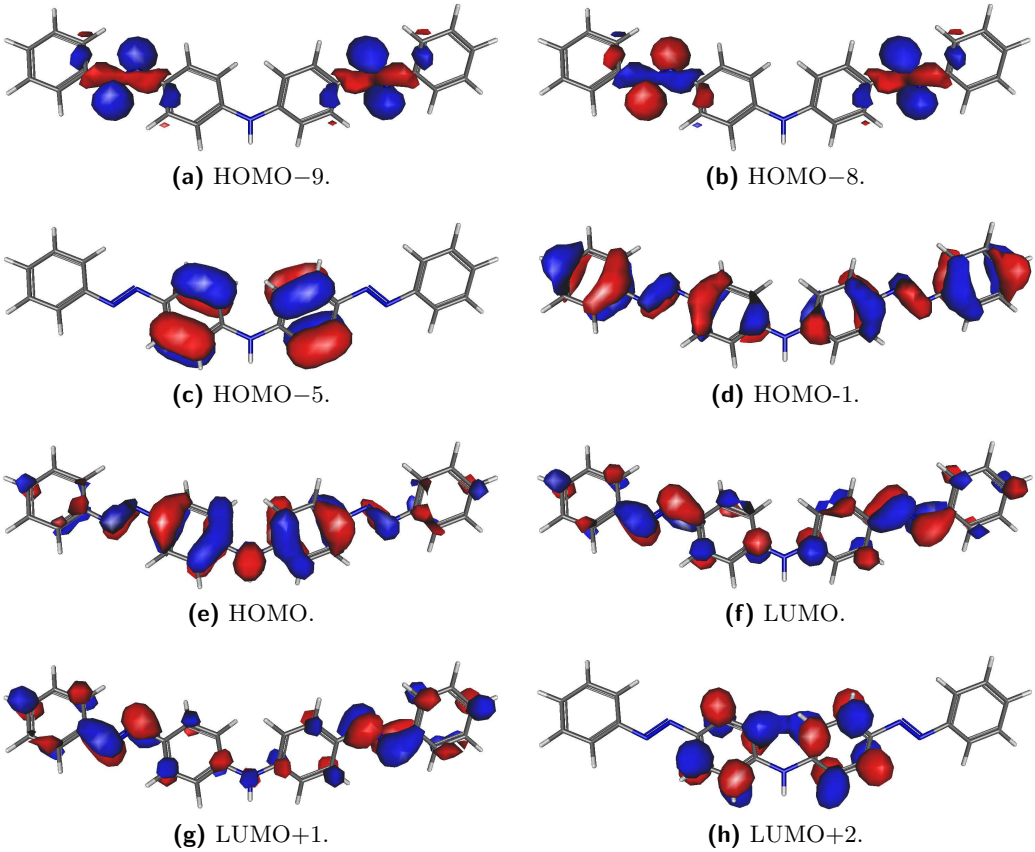

(a) HOMO−9. **(b)** HOMO−8.

(c) HOMO−5. **(d)** HOMO-1.

(e) HOMO. **(f)** LUMO.

(g) LUMO+1. **(h)** LUMO+2.

Figure 6.8: Important orbitals for the five lowest-lying excited states for the CC2/TZVPP simulations of EE-bis[4-(phenylazo)phenyl]amine.

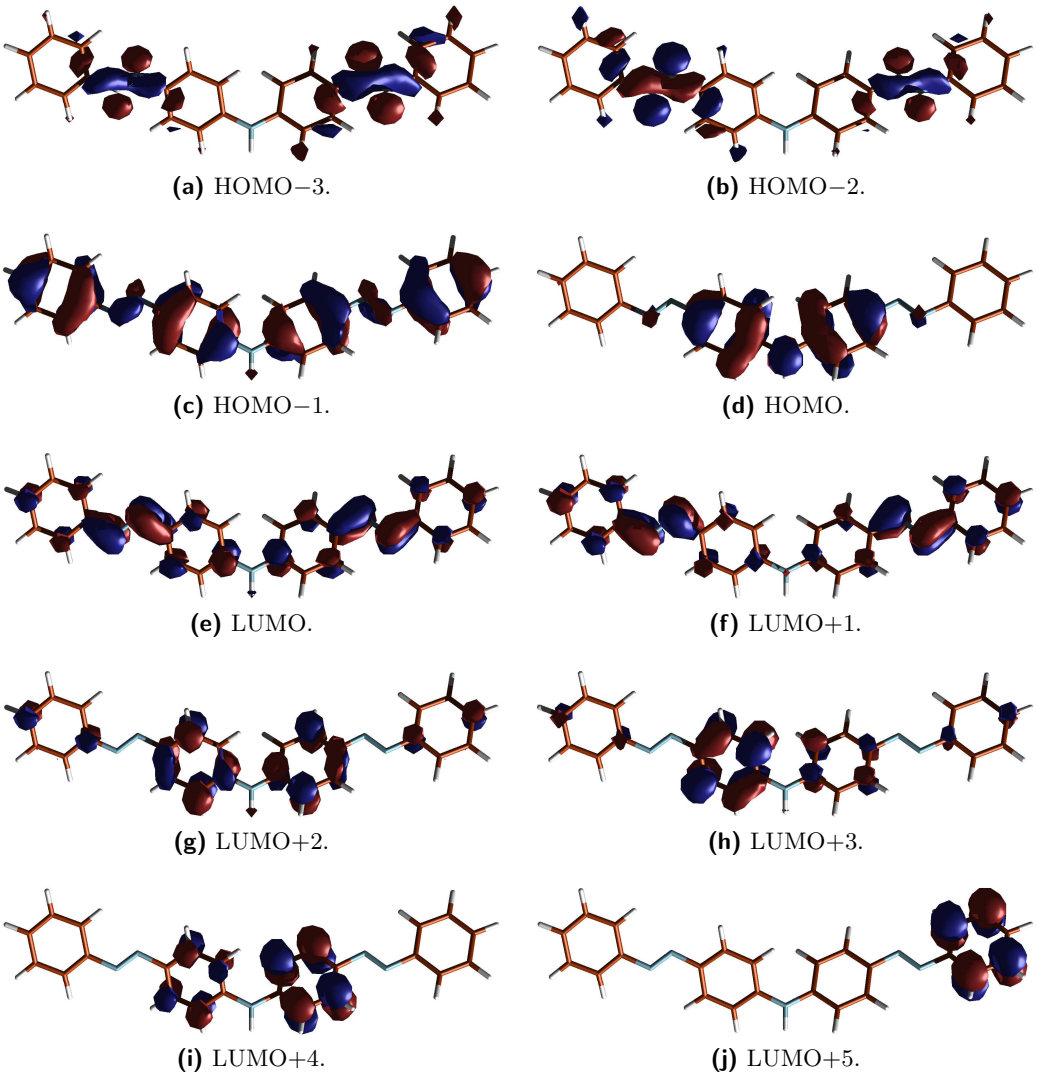

(a) HOMO−3. **(b)** HOMO−2.

(c) HOMO−1. **(d)** HOMO.

(e) LUMO. **(f)** LUMO+1.

(g) LUMO+2. **(h)** LUMO+3.

(i) LUMO+4. **(j)** LUMO+5.

Figure 6.9: Important orbitals for the five lowest-lying excited states for the MRCI-OM2 simulations of EE-bis[4-(phenylazo)phenyl]amine.

as linear combinations of the n-orbitals of two separate 4-amino-azobenzene units (figures 6.10a and 6.11c). For the energetically lowest π^*-orbitals (figures 6.8f, 6.8g for CC2 and 6.9e, 6.9f for MRCI-OM2) that are dominated by π^* character in the N=N double bond, the picture is similar. The orbitals depicted in figures 6.10d and 6.11e act as 'parent' orbitals for the dichromophoric orbitals. Within this picture, the two $n\pi^*$-states S_1 and S_2 of EE-bis[4-(phenylazo)phenyl]amine can be interpreted as linear combinations of excited states of two E-4-amino-azobenzene units. Going beyond a simple linear combination scheme of orbitals, the comparison to the exciton model is the next step. Since the orbitals of the $n\pi^*$-states fit well into a linear combination scheme, a straightforward exciton scheme for a chromophore dimer in the CC2/def2-TZVPP model would predict the S_1-state to consist of a HOMO-8 to LUMO transition. This is the positive linear combination of a $n\pi^*$-electron-hole-pair on each of the subunits, formed by the orbitals in figures 6.10a and 6.10d, which corresponds to the S_1-state of 4-amino-E-azobenzene (see table 6.5). While the first excited state of EE-bis[4-(phenylazo)phenyl]amine consists mostly of the predicted excitation (52%), a sizeable contribution from the HOMO-9 to LUMO+1 excitation (39%) is present. The S_2-state should arise from a HOMO-9 to LUMO+1 transition (the negative linear combination). The S_2-state consists mostly of two excitations of the same weights as before. The differences are the involved occupied orbitals which interchange, so that the state consists of 52% HOMO-9 to LUMO excitation and 39% HOMO-8 to LUMO+1 transition. The described characteristics of the states are not compatible with the exciton model. While the S_1-state contains character from both expected exciton states, in the S_2-state the involved orbitals flip, which can not be rationalised by the exciton approach, which contains the electron hole pair located on every chromophore as one unit, and therefore with the same sign in the total wavefunction. Therefore when the hole (the orbital from which the excitation happens) is a subtractive linear combination, the electron (the final orbital of the excitation) must be too, which is not the case for the S_2-state. In the OM2-MRCI model, the two $n\pi^*$-states are represented by a mixture of the states described for the CC2 model.

For the two energetically highest π-orbitals of EE-bis[4-(phenylazo)phenyl]amine the situation is more complicated. The HOMO of the dichromophore in both wave function models (figures 6.8e and 6.9d) is nearly completely localised on the phenyl rings directly connected to the amino group. The HOMO-1 orbitals (figures 6.8d and 6.9c) on the other hand are nearly symmetrically delocalised over the outer phenyl rings of the azobenzene subunits. When these points are ignored for a moment, the orbitals can be viewed as linear combinations of the HOMO of 4-amino-E-azobenzene (figures 6.10c and 6.11d). The distribution of the electrons over the azobenzene unit in the monochromophore lies in the middle between the distributions for the HOMO and HOMO-1 of the dichromophore. The increase in asymmetry is not huge but can not be interpreted as the result of any linear combination scheme for monomer

Table 6.5: Important excitations (absolute coefficient or amplitude 0.20 and greater) of the three lowest excited states of 4-amino-E-azobenzene, based on CC2/TZVPP and MRCI-OM2 wave function models.

State	CC2/TZVPP			MRCI-OM2		
	from	to	amplitude	from	to	coefficient
S_1	HOMO−4	LUMO	90%	HOMO−1	LUMO	94%
	HOMO−4	LUMO+12	7%(−)			
S_2	HOMO	LUMO	91%	HOMO	LUMO	53%(−)
				HOMO−2	LUMO+3	11%(−)
S_3	HOMO	LUMO+1	57%	HOMO−3	LUMO	30%(−)
	HOMO−3	LUMO	21%(−)	HOMO−2	LUMO+2	21%(−)
	HOMO−3	LUMO+4	6%(−)	HOMO	LUMO+2	15%(−)
	HOMO	LUMO+2	5%(−)	HOMO−3	LUMO+3	14%(−)

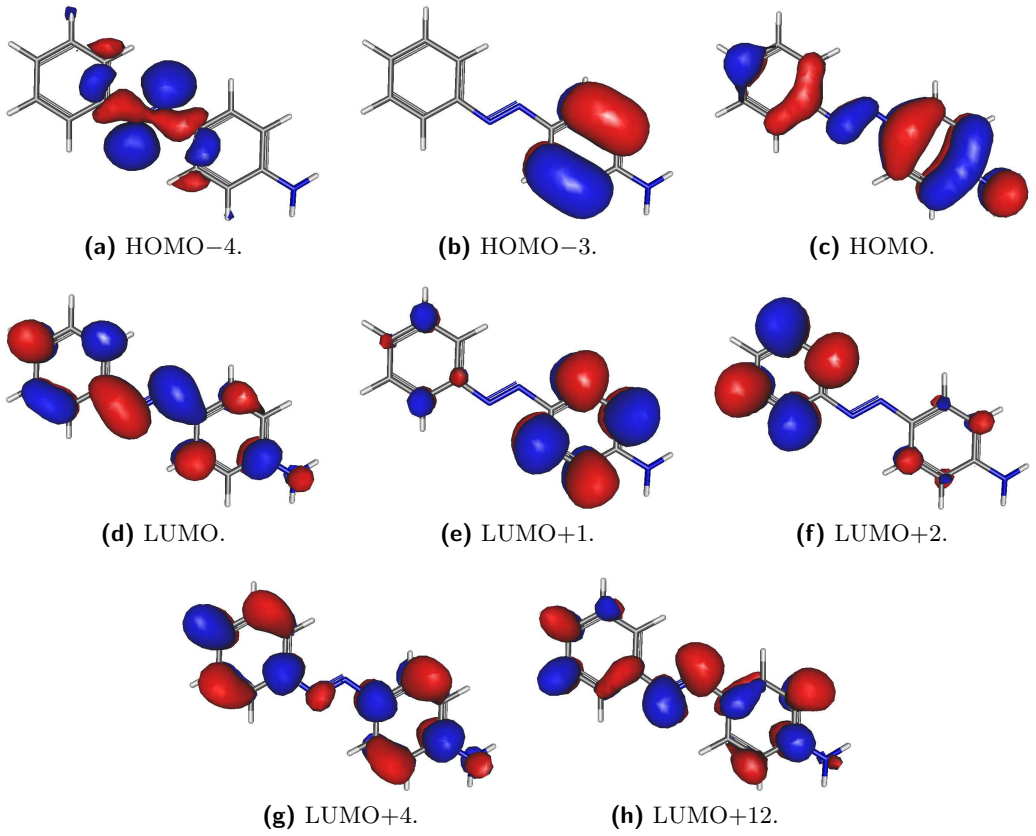

(a) HOMO−4. **(b)** HOMO−3. **(c)** HOMO.

(d) LUMO. **(e)** LUMO+1. **(f)** LUMO+2.

(g) LUMO+4. **(h)** LUMO+12.

Figure 6.10: Important orbitals for the three lowest-lying excited states for the CC2/TZVPP simulations of 4-amino-E-azobenzene.

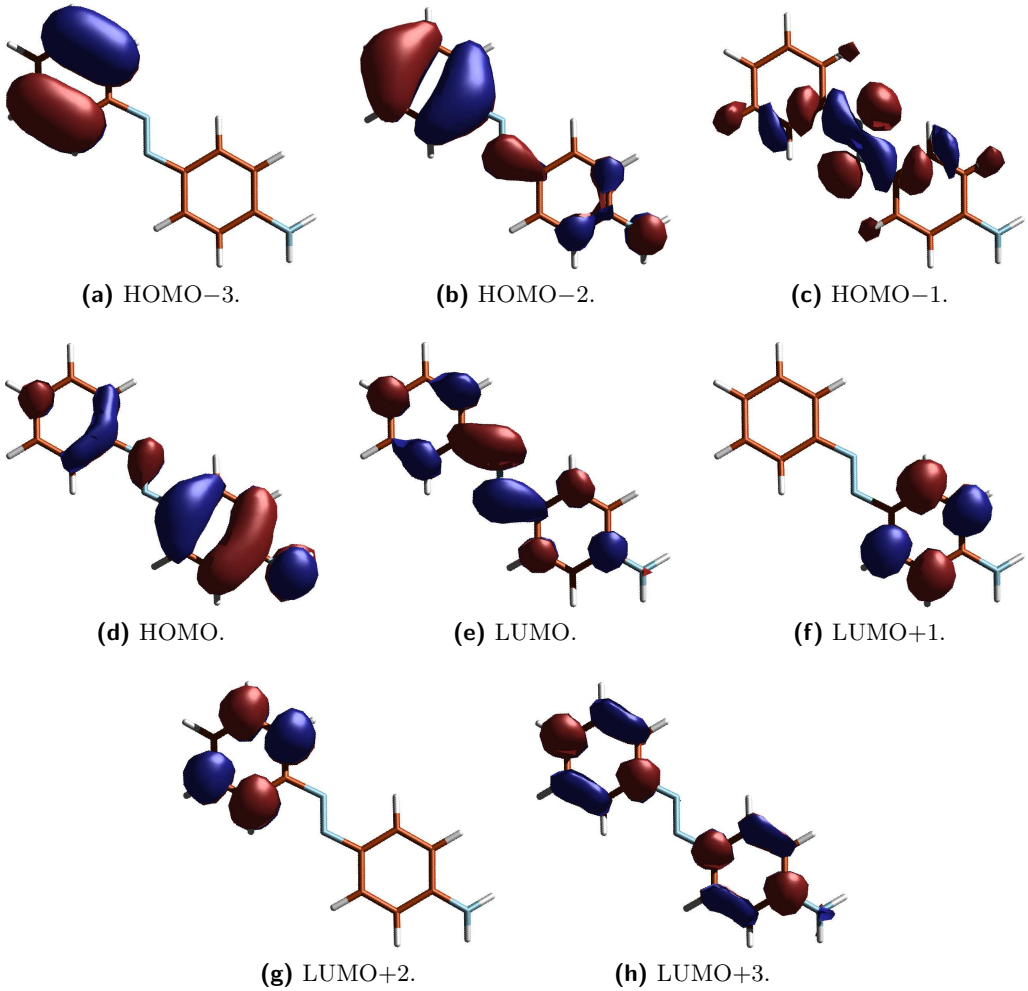

(a) HOMO−3. **(b)** HOMO−2. **(c)** HOMO−1.

(d) HOMO. **(e)** LUMO. **(f)** LUMO+1.

(g) LUMO+2. **(h)** LUMO+3.

Figure 6.11: Important orbitals for the three lowest-lying excited states for the MRCI-OM2 simulations of 4-amino-E-azobenzene.

orbitals. A detailed look into the composition of the excited states S_3 and S_4 shows that, although the CC2 states are more dominantly represented by the respective major excitation, the basic composition of the electronic states is identical in the CC2 and the OM2-MRCI model. Similar to the $n\pi^*$-states in the CC2 model, the $\pi\pi^*$-states contain relevant contributions from two excitations: the HOMO to LUMO and HOMO-1 to LUMO+1 for the S_3-state, and HOMO to LUMO+1 and HOMO-1 to LUMO for the S_4-state. The difference thus is that the $n\pi^*$-states share the most important virtual orbital, while the $\pi\pi^*$-states share the most important occupied orbital. Therefore, an exciton model is not applicable to these states for the same reasons as before, while a linear combination approach for the underlying orbitals might be useful but clearly is deficient. The OM2-MRCI model, on the other hand, compares very well with the CC2 model and thus further supports its applicability in coming photo-de-excitation dynamics simulations.

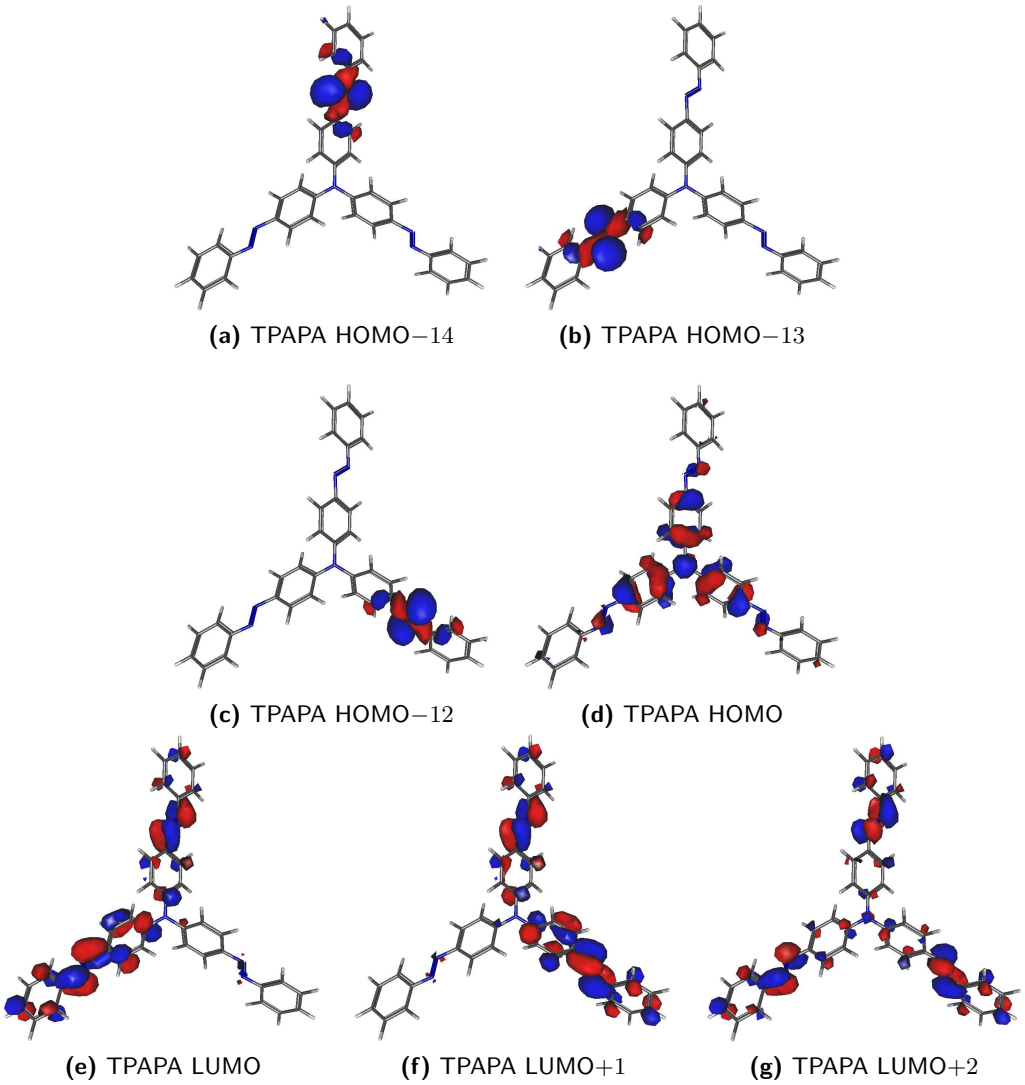

(a) TPAPA HOMO−14 **(b)** TPAPA HOMO−13

(c) TPAPA HOMO−12 **(d)** TPAPA HOMO

(e) TPAPA LUMO **(f)** TPAPA LUMO+1 **(g)** TPAPA LUMO+2

Figure 6.12: Important orbitals for the six lowest-lying excited states for the CC2/def2-SVP simulations of EEE-tris[4-(phenylazo)phenyl]amine.

Further studies of the oligomerisation were carried out by calculating the six energetically lowest electronic states of EEE-tris[4-(phenylazo)phenyl]amine in a CC2/def2-SVP wave function model at the B3LYP/6-31+G(d,p) Franck-Condon point supplied by Dipl. Chem. Julia Bahrenburg [124]. Although the basis set is too small to expect accurate results, the data can be used for a qualitative interpretation. The relevant orbitals for the simulated excited states are depicted in figure 6.12. To achieve the comparability of the calculations in the double zeta basis, EE-bis-[4-(phenylazo)phenyl]amine and 4-amino-E-azobenzene were also simulated in the double-zeta wave function model. The relevant orbitals do not change qualitatively upon reduction of the basis set, which supports the aforementioned qualitative applicability of the simulations. The excitation energies of EE-bis[4-(phenylazo)phenyl]-amine rise in the less flexible model, with the $\pi\pi^*$-states being more sensitive (about 0.2 eV higher in def2-SVP) than the $n\pi^*$-states (about 0.03 eV). In table 6.6, energies, relevant excitations and their weights, and corresponding oscillator strengths of comparable excited states of the molecules under study are given. All results listed were taken from CC2/def2-SVP simulations to retain the comparability. Obviously, the effect of the di- and trimerisation on the $\pi\pi^*$-states is much larger than for the $n\pi^*$-states and the effect of the dimerisation on the $\pi\pi^*$-states is much larger than that of the trimerisation. The average $\pi\pi^*$-excitation energy changes from 4.00 eV to 3.56 eV to 3.30 eV. Although not quantitatively matching experimental excitation energies, both basic trends, differentiating the excitation types and the smaller effect of adding the third chromophore on the electronic spectra, fit the experimental data very well.

Analysis of the orbitals of the trimer reveals the n-orbitals to be localised on the respective azobenzene units while the π-orbitals delocalise over the chromophores to some extent. In a similar fashion to the orbitals of the dimer, two of the π-orbitals of the trimer localise over the arms of the oligomer. In this sense, the HOMOs of the di- and trimer are comparable in their localisation around the bridging nitrogen atom (the trimer to a larger extent than the dimer) and the LUMO+2 of the trimer comparable to the LUMO+1 of the dimer being localised on the outer parts of the system. The latter asymmetry is less pronounced in the trimer, in which the orbital lobes seem rather to localise on the azo nitrogen atoms. The other two relevant virtual π-orbitals (LUMO and LUMO+1) are basically subtractive linear combinations of the LUMOs of two of the chromophoric subunits, with the one appearing in both orbitals being less pronounced. Neglecting the localisation of the LUMO+2 and the uneven weighting of the LUMO and LUMO+1, these orbitals can be expected from a perturbation scheme analogous to the one explained in section 2.4.5, arising from a linear combination of the LUMOs of three monomers only. The characteristics explained for the virtual orbitals also hold for the occupied orbitals, with the HOMO-1 and HOMO-2 corresponding to the LUMO and LUMO+1 (the two occupied orbitals are not depicted because they play no relevant role in the creation

of configurations to represent the excited-state wave functions) and the HOMO to the LUMO+2. Transition to the exciton model leads to the electron and the hole to be interpreted as one entity. This picture is only partly compatible with the findings from the simulations. The n-orbitals are localised and the excitation schemes are at least partially compatible with a localisation of the excited electron to where the excitation happens, which would be necessary in the picture of three uncoupled and thus localised excitons. For the $\pi\pi^*$-states, all orbitals, virtual and occupied, are similarly delocalised, so a simple excitation scheme is expected from exciton theory. Although the simulated excitation scheme is simple, it is completely incompatible with the exciton model in that the three states are all created by excitation from the HOMO and thus the shape of the hole and the excited electron are independent from each other.

Table 6.6: Dominant excitations in the energetically lowest excited states of 4-amino-E-azobenzene (AAB), EE-bis[4-(phenylazo)phenyl]amine (BPAPA) and EEE-tris-[4-(phenylazo)phenyl]amine (TPAPA) calculated on CC2/def2-SVP level.

System	State	excitation from	excitation to	weight	oscillator strength	Excitation energy/eV
AAB	S_1	HOMO−4	LUMO	90%	$4 \cdot 10^{-5}$	2.92
	S_2	HOMO	LUMO	91%	$8 \cdot 10^{-1}$	4.00
BPAPA	S_1	HOMO−8	LUMO	51%	$9 \cdot 10^{-4}$	2.85
		HOMO−9	LUMO+1	40%		
	S_2	HOMO−9	LUMO	51%	$1 \cdot 10^{-5}$	2.85
		HOMO−8	LUMO+1	40%		
	S_3	HOMO	LUMO	85%	$2 \cdot 10^{0}$	3.25
	S_4	HOMO	LUMO+1	83%	$9 \cdot 10^{-2}$	3.87
TPAPA	S_1	HOMO−14	LUMO+1	35%	$1 \cdot 10^{-3}$	2.81
		HOMO−14	LUMO	32%		
		HOMO−14	LUMO+2	21%		
	S_2	HOMO−13	LUMO	60%	$1 \cdot 10^{-4}$	2.81
		HOMO−13	LUMO+2	24%		
	S_3	HOMO−12	LUMO+1	58%	$2 \cdot 10^{-4}$	2.81
		HOMO−12	LUMO+2	26%		
	S_4	HOMO	LUMO	56%	$1 \cdot 10^{0}$	3.07
		HOMO	LUMO+1	28%		
	S_5	HOMO	LUMO+1	57%	$1 \cdot 10^{0}$	3.08
		HOMO	LUMO	27%		
	S_6	HOMO	LUMO+2	83%	$3 \cdot 10^{-3}$	3.74

In summary, a straightforward linear combination approach of excited states of the mono-chromophoric molecule can gather some of the features of the excited states of the di-chromophoric system, but misses some qualitative characteristics, especially for the $\pi\pi^*$-excited states. A more suitable ansatz might be to separate electron and hole and form dimer and trimer orbitals from a linear combination ansatz depending on the angle between the π-systems of the azobenzene units. A proper setup of this

model will need more calculations, in particular scans of the aforementioned angle. For the same reasons, the calculations presented before strictly only apply to the Franck-Condon points and the features of the excited states will change away from these points.

The simulations presented in this section offer a possible explanation for experimental findings for the static spectra [124] that show a huge impact of the dimerisation on these states, when at the same time the $n\pi^*$-excited states are not influenced much, while the trimerisation does not change much in both types of excited states relative to the dimer, with respect to the excitation energies but is predicted to significantly change with respect to the detailed composition of the excited states.

6.7 Electronic character of low-lying states of a azopyridin-functionalised nickel porphyrin

The azopyridin-functionalised nickel porphyrin (in the following text called azo-porphyrin, for short) presented in [125] is the first molecule to show the light-driven coordination-induced spin-state-switching (LD-CISSS) effect. The molecule is a nickel porphyrin functionalised with an azopyridin to act as on- and off-switchable fifth ligand. As depicted in figure 6.13, the E-isomer of the azopyridin cannot coordinate the central nickel atom. This leaves the nickel atom tetra-coordinated and therefore the molecule has a diamagnetic low-spin ground state, as usual for tetra-coordinated Ni^{2+}. Upon irradiation with green light of 500 nm, the molecule can isomerise to the Z-form, in which the azopyridin can act as fifth ligand, transforming the molecule into a paramagnetic high-spin form.

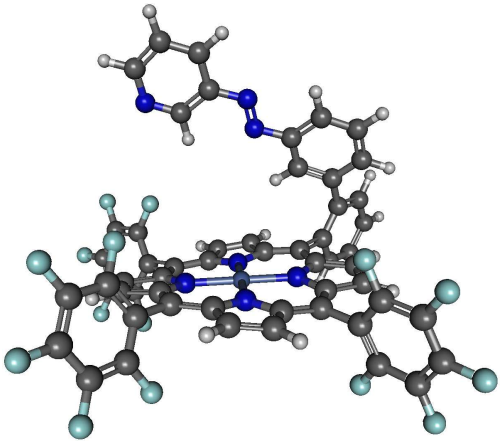

Figure 6.13: E-isomer of azo-porphyrin. The atoms are carbon: silver, hydrogen: white, nitrogen: dark blue, flourine: turquoise, nickel: metallic blue.

The understanding of the underlying processes puts a very difficult task to experiment and theory. In the following chapter, a first step into the theoretical understanding of the electronic states at the Franck-Condon point of the E-isomer

and at a hypothetical conical intersection point based on multireference quantum chemistry will be presented.

6.7.1 MCSCF calculations of the E-isomer of the azopyridin-functionalised nickel porphyrin.

The first step towards the characterisation of the excited states was a series of RASSCF calculations with continuously shrinking active spaces and growing excitations to pinpoint the most important orbitals. All multiconfigurational calculations presented in this section (6.7) were performed using a Cholesky decomposition [101–104] with a cut-off of 10^{-5} to speed up the integral calculations, for this reason the energy-convergence threshold was set to 10^{-5} Hartree. Two different basis sets were used in these calculations, the details of which are given in table 6.7. The steps used while shrinking the active space are listed in tables 6.8 and 6.9. The tables present the final orbitals of the MCSCF optimisations at a geometry optimised on MARIJ-RI-BP86/ECP-10-MDF (Ni) and def-SV(P) (other elements) level, supplied by Prof. Bernd Hartke. The flourine lone pairs did not make it into any of the optimised active space although they were included in the initial guess.

Table 6.7: Basis set specifications for the different MCSCF calculations. The ANO basis sets can be found in [99, 100]

basis set index	1	2
Ni	(8s7p6d1f)/[6s5p3d1f].18e-MDF [126]	
N	ANO-L-MB	ANO-L-VDZP
azo-C	ANO-L-MB	ANO-L-VDZP
porphyrin-C	ANO-L-MB	ANO-S-VDZP
linker-C	ANO-L-MB	ANO-S-VDZP
fluorophenyl-C	ANO-L-MB	ANO-L-MB
fluorophenyl-F	ANO-L-MB	ANO-L-MB
azo-H	ANO-H-MB	ANO-S-VDZP
porphyrin-H	ANO-H-MB	ANO-L-VDZP
linker-H	ANO-H-MB	ANO-S-VDZP

This series of calculations allowed for a reduction of the active space to a set of 12 electrons in 12 orbitals, treating a total of 8 states. The final orbitals are depicted in figures 6.14 and 6.15.

As already shown by TD-DFT simulations of nickel porphyrins [127], the involvement of d-orbitals in the excitation pattern significantly increases the complexity of the excited states compared to more simple metal porphyrins [128]. By analysis of the 8-states state-averaged-CASSCF(12,12) calculation, it is possible to start addressing the character of the low-lying excited singlet states of the studied azoporphyrin. As shown in tables 6.10 and 6.11, the lowest excited state in the 8-states-calculation is a doubly excited one with mixed character, resulting from a d_{z^2}

Table 6.8: Character and size of optimised active spaces from RASSCF calculations of azo-pophyrin. The numbers in parentheses give the total number of electrons in the respective orbital set. First part.

calculation number			1	2	3	4
Basis set			1	1	1	2
orbitals in RAS1			22	22	12	12
orbitals in RAS3			18	18	9	9
allowed holes in RAS1			1	2	3	3
allowed electrons in RAS3			1	2	3	3
number of states			5	5	5	8
orbital	nickel	d	2(2.00)	2(2.00)	2(2.00)	2(2.00)
character	nickel	p	1(2.00)	1(2.00)	0	0
	nickel	f	1(0.00)	0	0	0
	nickel	s	0	1(2.00)	0	0
	azopyridin	π	0	5(9.77)	2(3.93)	2(3.96)
	azopyridin	π^*	3(0.20)	5(0.23)	2(0.08)	2(0.04)
	azopyridin	n	2(3.80)	0	1(2.00)	1(2.00)
	azopyridin	σ	1(2.00)	0	0	0
	porphyrin	π	11(21.60)	8(15.56)	8(15.16)	8(15.08)
	porphyrin	π^*	6(0.40)	7(0.44)	6(0.84)	6(0.94)
	porphyrin	σ	6(12.00)	0	0	0
	porphyrin	σ^*	7(0.00)	0	0	0
	fluoro-phenyl	π	0	3(5.99)	0	0
	fluoro-phenyl	π^*	0	3(0.01)	0	0
	linker-phenyl	π	0	3(5.98)	0	0
	linker-phenyl	π^*	0	2(0,01)	0	0

Table 6.9: Character and size of optimised active spaces from RASSCF calculations of azo-pophyrin. The numbers in parentheses give the total number of electrons in the respective orbital set. Second part.

calculation number			5	6	7	8
Basis set			1	2	2	2
orbitals in RAS1			11	9	9	9
orbitals in RAS3			9	9	9	9
allowed holes in RAS1			4	4	4	4
allowed electrons in RAS3			4	4	4	4
number of states			8	8	10	8
orbital	nickel	d	2(2.00)	2(2.00)	2(2.00)	2(2.00)
character	nickel	p	0	0	0	0
	nickel	f	0	0	0	0
	nickel	s	0	0	0	0
	azopyridin	π	2(3.77)	2(3.77)	2(3.80)	2(3.77)
	azopyridin	π^*	2(0.23)	2(0.23)	2(0.21)	2(0.23)
	azopyridin	n	1(2.00)	1(2.00)	1(2.00)	1(2.00)
	azopyridin	σ	0	0	0	0
	porphyrin	π	8(15.07)	5(9.15)	5(9.07)	5(9.15)
	porphyrin	π^*	6(0.93)	6(0.85)	6(0.93)	6(0.85)
	porphyrin	σ	0	0	0	0
	porphyrin	σ^*	0	0	0	0
	fluoro-phenyl	π	0	0	0	0
	fluoro-phenyl	π^*	0	0	0	0
	linker-phenyl	π	0	0	0	0
	linker-phenyl	π^*	0	0	0	0

Table 6.10: Final states from the 8-state calculation and the respective orbital occupation numbers for the more-than-half-filled orbitals. The orbitals are labeled by their index in figure 6.14.

state	6.14a	6.14b	6.14c	6.14d	6.14e	6.14f
S_0	1.95	1.95	1.88	1.89	1.87	1.86
S_1	1.95	1.92	1.88	1.87	1.04	1.00
S_2	1.95	1.95	1.88	1.89	1.87	1.00
S_3	1.95	1.91	1.88	1.71	1.19	1.00
S_4	1.95	1.89	1.88	1.09	1.83	1.00
S_5	1.88	1.95	1.07	1.89	1.87	1.00
S_6	1.95	1.95	1.88	1.27	1.64	1.00
S_7	1.95	1.88	1.88	1.52	1.36	1.86

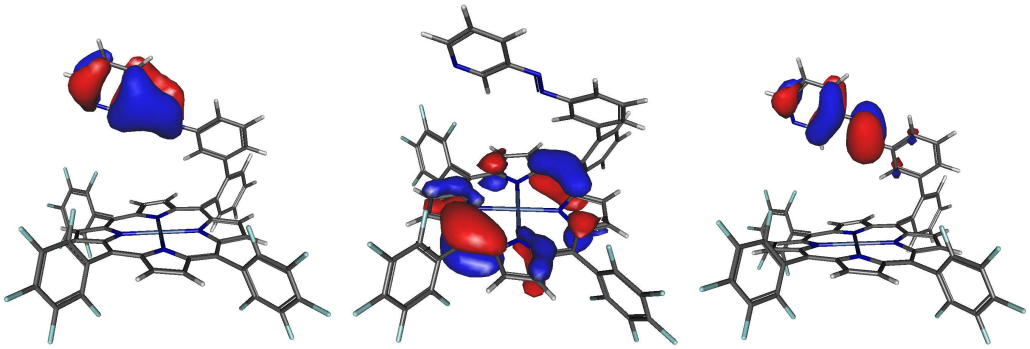

(a) occupation: 1.94 **(b)** occupation: 1.92 **(c)** occupation: 1.78

(d) occupation: 1.65 **(e)** occupation: 1.58 **(f)** occupation: 1.22

Figure 6.14: More-than-half-filled set of the final CASSCF(12,12) orbitals established for the studied azo-porphyrin.

(figure 6.14f) to $d_{x^2-y^2}$ (figure 6.15a) and a $\pi\pi^*$ excitation. The next state is dominated by the d_{z^2} to $d_{x^2-y^2}$ excitation followed by two more $\pi\pi^*$ and d_{z^2} to $d_{x^2-y^2}$ doubly excited states. The fifth excited state consists of doubly excited configurations resulting from excitations from one of the azopyridin π-orbitals (figures 6.14a and 6.14c) to the azo-pyridin π^*-orbitals (figures 6.15d and 6.15f) and the aforementioned excitation within the nickel d-orbitals. The seventh state is a porphyrin $\pi\pi^*$-excited and nickel $d_{z^2}d_{x^2-y^2}$-excited state with double-excitation chracter, while the seventh excited state is dominated by porphyrin-$\pi\pi^*$ excitations.

Table 6.11: Final states from the 8-state calculation and the respective orbital occupation numbers for the less-than-half-filled orbitals. The orbitals a labeled by their index in figure 6.15.

state	6.15a	6.15b	6.15c	6.15d	6.15e	6.15f
S_0	0.14	0.11	0.13	0.12	0.05	0.05
S_1	1.00	0.14	0.96	0.12	0.05	0.05
S_2	1.00	0.11	0.13	0.12	0.05	0.05
S_3	1.00	0.78	0.30	0.12	0.10	0.05
S_4	1.00	0.91	0.17	0.12	0.10	0.05
S_5	1.00	0.11	0.13	0.94	0.05	0.12
S_6	1.00	0.35	0.73	0.13	0.07	0.05
S_7	0.13	0.63	0.49	0.12	0.11	0.05

Starting from the 8-state calculation, a 6-state CASSCF(12,12) calculations was run to make a perturbative dynamic correlation treatment via CASPT2 possible. The final states of the CASSCF simulation with corresponding orbital occupations are given in tables 6.12 and 6.13. Although the orbitals change a bit between the two calculations their basic character stays the same. Therefore the orbitals are not depicted again and tables 6.12 and 6.13 refer to figures 6.14 and 6.15, although the orbitals depicted are not exactly the final orbitals of the 6-state calculation.

Table 6.12: Final states from the 6-state calculation and the respective orbital occupation numbers for the more-than-half-filled orbitals. The orbitals are labeled by their index in the figure 6.14.

state	6.14a	6.14b	6.14c	6.14d	6.14e	6.14f
S_0	1.96	1.96	1.88	1.90	1.88	1.86
S_1	1.96	1.94	1.88	1.88	1.04	1.00
S_2	1.96	1.96	1.88	1.90	1.88	1.00
S_3	1.96	1.96	1.88	1.83	1.09	1.00
S_4	1.96	1.91	1.88	1.08	1.86	1.00
S_5	1.96	1.94	1.88	1.14	1.86	1.00

Inspection of tables 6.12 and 6.13 shows no $\pi\pi^*$-excited state for the azopyridin unit among the first five excited states of the studied porphyrin. Instead, a state showing $\pi\pi^*$ excitation in the porphyrin (in addition to the nickel d excitation) is the

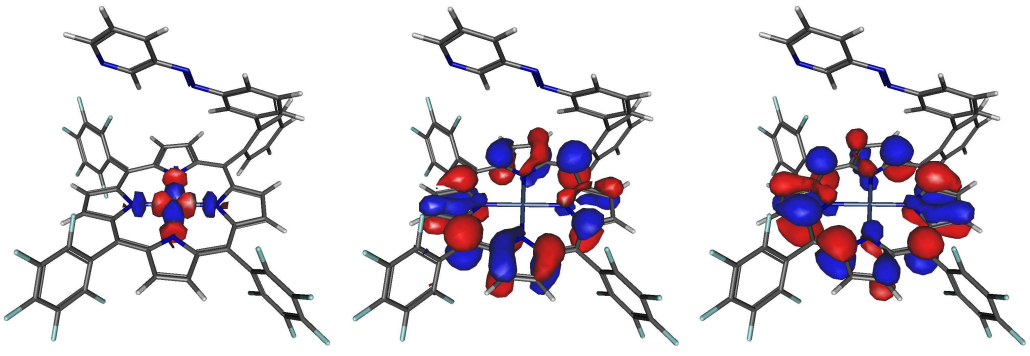

(a) occupation: 0.78 **(b)** occupation: 0.39 **(c)** occupation: 0.38

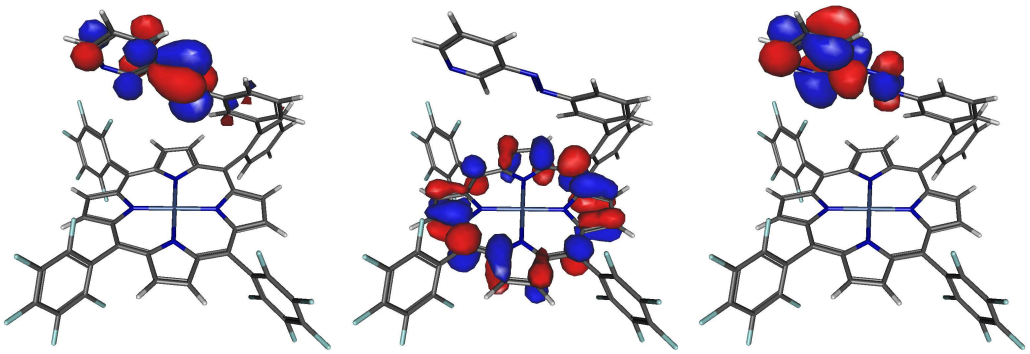

(d) occupation: 0.22 **(e)** occupation: 0.08 **(f)** occupation: 0.06

Figure 6.15: Less-than-half-filled set of the final CASSCF(12,12) orbitals established for the studied azo-porphyrin.

Table 6.13: Final states from the 6 state calculation and the respective orbital occupation numbers for the less-than-half-filled orbitals. The orbitals are labeled by their index in the figures 6.15.

state	6.15a	6.15b	6.15c	6.15d	6.15e	6.15f
S_0	0.14	0.11	0.12	0.12	0.04	0.04
S_1	1.00	0.13	0.96	0.12	0.06	0.04
S_2	1.00	0.11	0.12	0.12	0.04	0.04
S_3	1.00	0.89	0.16	0.12	0.07	0.04
S_4	1.00	0.93	0.14	0.12	0.07	0.04
S_5	1.00	0.21	0.88	0.12	0.05	0.04

S_5-state. This state is similar in character to the S_6 state in the 8-states calculation. This observation is consistent with the RASSCF(RAS1:9,RAS2:0,RAS3:9) calculation with four excitations (number **8** in table 6.9). The S_6-state in that calculation is the azopyridin-excited state, while the S_5-state has the same character as in the CASSCF(12,12) calculation for six states.

To further investigate this, the azopyridin orbitals were substituted by porphyrin π-orbitals in four of the calculations to check the effects of this substitution on the state-averaged energy. The calculations were two RASSCF(RAS1:9,RAS:0,RAS3:9) calculations with four excitations accounting for eight and ten electronic states, and two CASSCF(12,12) calculations accounting for eight and six states, respectively. In these calculations, the total energy is a measure for the quality of the wave function, due to the variational character of the applied methods. The resulting data is given in table 6.14. Here, the Hartree energy-scale is used since then it is simpler to regard the inaccuracy caused by the Cholesky decomposition and the energy-convergence threshold, which is expected to be below the last given digit [102].

Table 6.14: Total state-averaged energies for four different calculations setups, with two different active space characters, one of them containing azopyridine π-orbitals, the other not. The energies are given in Hartree, with a constant 4135 Hartree added.

	calculation type			
active space	RASSCF – 8 states	RASSCF – 10 states	CASSCF(12,12) – 8 states	CASSCF(12,12) – 6 states
azopyridin-π	−0.6178	−0.6048	−0.5748	−0.5888
porphyrin-π	−0.6285	−0.6159	−0.5681	−0.5830

The data shows that the azopyridin-located orbitals contribute to the quality of the wave function to a very low extent. The contribution is unfavourable for the RASSCF simulations and favourable for the CASSCF simulations. What table 6.14 does not show is whether this reduction stems from the energy of special states with a strong contribution from the respective orbitals (basically an effect of static correlation) or whether it is due to a non-discriminating enhancement in the description of all states (an effect of dynamic correlation). For this reason, table 6.15 and 6.16 list the state-resolved energies for the aforementioned calculations.

For the CASSCF calculations, the azopyrin-located orbitals have a small positve effect on the majority of the electronic states. The most preeminent exception, though, is the fifth excited state in the 8-states simulation. This state is dominated by the configuration excited in the azopyridin moiety and is energetically higher than the corresponding state in the calculation without azopyridin-located orbitals. In the RASSCF calculations on the other hand, the incorporation of azopyridin orbitals in in active space leads to worse results for most states. Here the most important change happens in the S_6-state. In the 8-states simulation this is a state with

Table 6.15: Total energies of the electronic states for three different calculation setups, with two different active space characters, one of them containing azopyridin π-orbitals, the other not. The energies are given in Hartree and a constant 4135 Hartree added for CASSCF calculations and 4143 Hartree for CASPT2 calculations. States strongly influenced by the azopyridin moiety are marked with an asterisk.

	CASSCF(12,12) – 8 states		CASSCF(12,12) – 6 states		CASPT2(12,12) – 6 states
	azopy.	no azopy.	azopy.	no azopy.	azopy.
S_0	-0.6322	-0.6210	-0.6313	-0.6209	-0.1326
S_1	-0.6124	-0.5988	-0.6080	-0.5984	-0.0795
S_2	-0.5882	-0.5805	-0.5889	-0.5825	-0.0792
S_3	-0.5833	-0.5770	-0.5861	-0.5784	-0.0788
S_4	-0.5651	-0.5679	-0.5665	-0.5676	-0.0683
S_5	-0.5420*	-0.5500	-0.5516	-0.5500	-0.0656
S_6	-0.5412	-0.5317	—	—	—
S_7	-0.5342	-0.5176	—	—	—

Table 6.16: Total energies of the electronic states for two different calculation setups, with two different active space characters, one of them containing azopyridin π-orbitals, the other not. The energies are given in Hartree with a constant 4135 Hartree added. States strongly influenced by the azopyridin moiety are marked with an asterisk.

	RASSCF – 10 states		RASSCF – 8 states	
	azopy.	no azopy.	azopy.	no azopy.
S_0	-0.6838	-0.6965	−0.6837	−0.6968
S_1	-0.6401	-0.6569	−0.6401	−0.6572
S_2	-0.6302	-0.6377	−0.6303	−0.6381
S_3	-0.6189	-0.6293	−0.6197	−0.6302
S_4	-0.6101	-0.6243	−0.6107	−0.6253
S_5	-0.6048	-0.6108	−0.6041	−0.6099
S_6	-0.5766	-0.6014	−0.5771*	−0.6017
S_7	-0.5730	-0.5690	−0.5765	−0.5689
S_8	-0.5645*	-0.5688	—	—
S_9	-0.5458	-0.5647	—	—

important contributions from a configuration excited in azopyridin-located orbitals. In the RASSCF calculation that include these orbitals an energy gap occurs between S_5 and S_6, while this gap moves to between the S_6- and S_7-state without them. The reason for this is a significant drop in the energy of the S_6-state without the azopyridin orbitals. At this point an important remark for the later discussions (see section 6.7.2.1) shall be highlighted: The observed gap might very well be the gap between Q- and Soret-band in the experimental spectrum. Even if the active space contains azopyridin orbitals the states excited in this moiety will be above this gap.

Dynamic correlation was treated for the CASSCF(12,12) wave function with azopyridin-located orbitals by 6-states MS-CASPT2 calculations with a level shift of 0.2 Hartree. The dynamic correlation treatment was not repeated for the azopyridin-orbital-free active space, since the calculations take major amounts of computation time and resources, and the results in column four and five of table 6.15 indicate that the orbitals contribute only via dynamic correlation effects. Therefore, the results will probably not change significantly. The results are given in the rightmost column of table 6.15. The results for this calculation are qualitatively very similar to the CASSCF(12,12) calculations treating 6 states. Most importantly the excited states shift to higher energies relative to the ground state upon incorporation of dynamic correlation by about 0.04 Hartree. The five excited states are very close to each other in energy, even closer than the ones for the CASSCF wave function. The CASPT2-states span an energy interval of about 0.015 Hartree, compared to about 0.04 Hartree for the CASSCF calculation. This finding further supports the assertion that the gap between Q- and Soret-band appears somewhere above S_6, which is also in agreement with [127].

As a side note it shall be highlighted that there is no excited state that shows $n\pi^*$-charater in the azopyridin moiety, although the calculations of the free azopyridin, carried out for use in section 6.7.2.1, show such a state as first excited state. Therefore, this has to attributed to the nickel porphyrin it is connected to. This is also supported by the observation that the first state that has significant excited character in the azopyridin moiety is doubly excited with contributions from the nickel *d*-orbitals. The two parts of the system are thus significantly coupled.

6.7.2 MCSCF calculations of a azopyridin functionalised nickel porphyrin for an intersection geometry of the azopyridin.

To get a basic idea of whether the excitation energy for a $\pi\pi^*$-state in the azopyridin unit at the Franck-Condon point might be enough to cause E to Z isomerisation in that part of the molecule, a model geometry was set up using the porphyrin structure from before but replacing the E-azopyridin by a structure for which the S_1-state and the S_0-state intersect for the parent azopyridin. The azopyridin ligand was pointed towards the metal center, so that a sucessful isomerisation would allow for coordination. This model was used since an optimisation of the conical intersection in

the full system with sufficient orbital felxibility in the azopyridin moiety is prohibitively time-consuming. Based on the previous calculations, it was possible that the coupling of the azopyridin ligand to the porphyrin is sufficiently low, to make it possible that the conical intersection structure of the ligand alone is close enough to the intersection seam of the full system to allow for qualitative studies of the relative energies.

6.7.2.1 MCSCF calculation of the S_1-S_0-intersection geometry of azopyridin.

For the azopyridin depicted in figure 6.16a, a conical intersetion optimisation was started for the intersection point of the S_1 and S_0 state. A CASSCF(14,12)/6-31g(d,p) wave function simultaneously optimised for the three lowest electronic states was used in the geometry optimisation. The active space consisted of the six highest-energy π-orbitals, a minus linear combination of the lone pairs of the azo moiety and the five lowest-energy π^*-orbitals of the system.

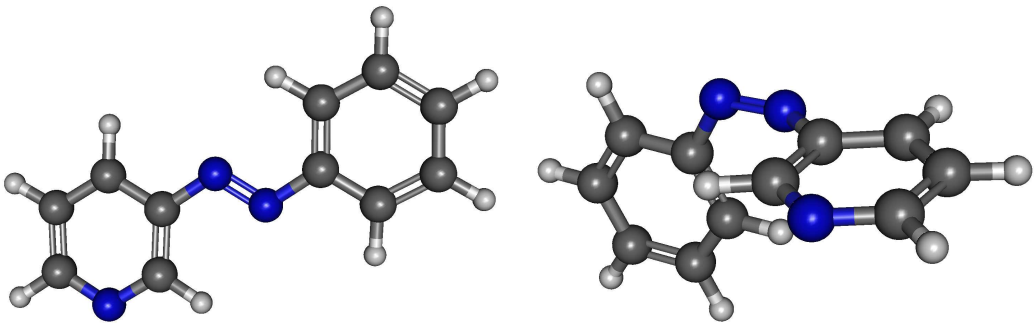

(a) E-isomer.

(b) Structure used as model for intersection geometry.

Figure 6.16: Different geometries of the parent azopyridin used here. The E-isomer (a) for reasons of easier identification and the model geometry (b) used as a hypothetical transient structure in the E/Z-isomerisation.

Full convergence of the conical intersection search was not reached in the calculation. Nonetheless, the calculation broke down in a region with large coupling of S_1 and S_0, very small energy separation between the states (below 1 kJ/mol) and only slight energy changes within the optimisation. Due to the purely qualitative character of the present scheme a full convergence of the geometry was unnecessary, and was therefore not pursued.

6.7.2.2 MCSCF calculation of the electronic-state-characters of the azopyridin functionalised nickel-porphyrin.

The azopyridin geometry depicted in figure 6.16a was connected to the porphyrin base using the bond length, the bond angle and the dihedral angle from the E-isomer (figure 6.13) while keeping the internal degrees of freedom of both parts of the molecule intact. Using this system, various RASSCF and CASSCF calculations

Table 6.17: Total energies of the electronic states for CASSCF(12,12) calculations for a singlet and a triplet wave function at the E/Z-isomerisation model geometry, with two different active space characters, one of them containing azopyridin π-orbitals, the other not. The energies are given in Hartree with a constant 4135 Hartree added. States strongly influenced by the azopyridin moiety are marked with an asterisk.

state	6 states-triplet		6 states-singlet	
index	azopy.	no azopy.	azo-py.	no azopy.
0	-0.5973	-0.5768	-0.5703∗	-0.5303
1	-0.5391	-0.5101	-0.5329	-0.5077
2	-0.5023	-0.4922	-0.5133	-0.4918
3	-0.5002	-0.4874	-0.5071∗	-0.4878
4	-0.4925	-0.4764	-0.5059∗	-0.4767
5	-0.4809	-0.4638	-0.4944	-0.4588

were carried out in a similar —though not that thorough— fashion as in section 6.7.1, for a singlet and a triplet wave function. By this approach, states with $\pi\pi^*$- or $n\pi^*$-excited character in the azopyridin unit and lower in energy than excited states at the Franck-Condon point, which might facilitate the E to Z isomerisation, were to be identified. Depending on the relative energies of the various states, an estimation can be made on whether the isomerisation is caused by a direct excitation of the azopyridin part of the molecule or an excitation in the porphyrin part and following redistribution of the electronic energy to the azopyridin that might then undergo the isomerisation. Resulting total energies of the electronic states of the transient model are listed in tables 6.18 and 6.17 which should be compared to tables 6.16 and 6.15. Triplet state energies were calculated to check whether a possible spin-flip occuring before the full isomerisation might be a driving force in the reaction.

The most important result that can be deduced is that the CASSCF and the RASSCF model exhibit states with significant excited character in the azopyridin at the model geometry for the singlet wave functions, while they lack that in the triplet wave functions. In the CASSCF model, the states with character of an excitation in the azopyridin moiety are S_0 and the nearly degenerate states S_3 and S_4. While the states S_3 and S_4 are comparatively high in energy (see also table 6.15), the S_0-state at this geometry is low enough to be reached with the energy put into the system by excitation into the higher Q-bands. The lack of a state degenerate to the S_0 is not unexpected due to the simplicity of the model but does not allow for an easy explanation for the isomerisation process, since the simulations do not contain information on whether there is a suitable region for radiationless decay that might facilitate the E to Z isomerisation. In the RASSCF simulation, in contrast to the CASSCF simulation, the singlet wave function shows nearly degenerate S_0 and S_1-states, with the S_1-state exhibiting important contributions from excited character in the azo moiety. Energetically, the two states are in the region of the S_5-state at

Table 6.18: Total energies of the electronic states for RASSCF(RAS1:9,RAS:0,RAS3:9) calculations for a singlet and a triplet wave function at the E/Z-isomerisation model geometry, with two different active space characters, one of them containing azo-pyridin π-orbitals, the other not. The energies are given in Hartree with a constant 4135 Hartree added. States strongly influenced by the azopyridin moiety are marked with an asterisk.

state	8 states-triplet		8 states-singlet	
index	azo-py.	no azo-py.	azo-py.	no azo-py.
0	-0.6326	-0.6262	-0.6069	-0.5982
1	-0.5675	-0.5597	-0.6040∗	-0.5539
2	-0.5567	-0.5527	-0.5595	-0.5436
3	-0.5384	-0.5317	-0.5512	-0.5335
4	-0.5378	-0.5288	-0.5405	-0.5257
5	-0.5273	-0.5271	-0.5396∗	-0.5203
6	-0.5251	-0.5256	-0.5318	-0.4967
7	-0.5225	-0.5185	-0.5199	-0.4826

the E-isomers geometry at the same level of calculation (see table 6.16). As in the CASSCF calculation, the triplet ground state is energetically lowest at the model geometry on RASSCF level. It is evident that, no matter what method is used, the presence of azopyridin-localised orbitals is essential for the description of the system, as can be seen in the total energies of calculations only differing in the character of the active space. Since the results strongly differ between the two models, an evaluation of the reliability of the two models is necessary. The most reliable source for this is probably the total energy: Since both models are variational, the lower the total energy the more reliable the wave function model is. At both simulated geometries, the RASSCF energy is much lower than the CASSCF energy, thus the RASSCF model is deemed to convey the more reliable picture. Judging from the RASSCF data, the isomerisation of the azopyridin moiety is energetically feasible, especially since an optimised conical intersection is expected to be lower in energy than the energy calculated for the model geometry.

Summing up the data, some interpretations are possible regarding the E to Z photo-isomerisation process observed in [125], although the level of calculation and the restrictions in the model do not allow for a definite answer. Judging from the comparably large gap between S_5 and S_6 (table 6.16), the excitation on the blue side of the Q-bands presumably happens into a state below localised excitation in the azopyridin moiety. Since none of the states show any electronically excited character in the azopyridin moiety, no large gradients within the atoms of this moiety are expected. Thus, to facilitate the isomerisation, other influences, most likely accidental vibrational excitations of the substituent, are probably necessary. In that case, the molecule can evolve to the azopyridin-excited state, which allows for the isomerisation. This has to happen quickly, before too much of the energy put into

the molecule dissipates to the surroundings, otherwise the energy would not be sufficient to reach the conical intersection seam that governs the isomerisation. The sketched mechanism is only a qualitative picture which depends on strong simplifications but is not unlikely. In particular, it offers a straightforward explanation for the low isomerisation quantum yield observed experimentally [129]. Basically, the E to Z isomerisation might very well be just a freak accident during the de-excitation after absorption in the Q-band region.

Since the calculations predict a state primarily excited in the azopyridin ligand in the region of the Soret-band, a very different de-excitation pathway can be expected in the case of excitation with wavelengths corresponding to this region.

6.8 Project Summary

Within the project, various azobenzene-based molecules, from the internally restrained diazocine to a spin-switchable azopyridin-functionalised nickel porphyrin, were studied by various approaches and computational methods specifically chosen for the problem and system at hand.

Multireferential *ab-initio* calculations were performed and used to support dynamical interpretations from simulation [110] and experiment [109] for the dynamics of the studied diazocine.

Through detailed semiempirical dynamics, and semiempirical and CC2 static studies of oligomerised aminoazobenzenes it was possible to set up a useful semiempirical model for the dimer that can be put to future use for studies of photo-excitation dynamics. Expansion of the *ab-initio* simulations to the trimeric system allowed for a detailed analysis of the comparability of the excited-state character from monomer over dimer to trimer. The comparison was especially focused on the applicability of the exciton model. The exciton model seems to be most applicable in case of the $n\pi^*$-states of the trimer where the close-to-orthogonal conformation of the chromophores leads to a localisation of the states and a very weak coupling of the states. All other states differ more or less significantly from the situation expected from an exciton model.

Using various multiconfigurational calculations it was possible to approach the photo-isomerisation from E- to Z-form of an azopyridin-functionalised nickel porphyrin, a promising system as a proof of principle of a class of photo-switchable contrast agents for magnetic resonance imaging. The simulations imply the energetic accessibility of an isomerisation-facilitating part of the conical intersection seam of the electronic ground state and the first excited state but also show that the initial excitation very likely does not cause excitation of the electronic wave function in the azopyridin moiety. Thus, an efficient isomerisation process facilitated by steep gradients directly after the excitation can not be expected, and this picture is

in agreement with the rather poor photo-isomerisation quantum yields observed in experiment.

7

Summary and outlook

The scope of this thesis is the detailed theoretical analysis of various photochemical switches. Two important basic types of molecular switches are addressed. The chapters 3, 4 and 5 deal with electrocyclic ring-closure and -opening switches, which are the major focus of the thesis. The extended chapter 6 treats various kinds of azobenzene-based molecules that show reversible E/Z-photo-isomerisation.

Fundamental studies of the isomerisation processes are not only necessary for understanding the specific system at hand but also for deducing common features and trends, and thus laying the basis for a rationally driven design process of systems with tailor-made properties. As a result from trying to reach the goal of this design process, a broad field of theoretical and experimental studies already exists, from static *ab-initio* studies [85] to time-resolved spectroscopy [78]. Building on and challenging the available data and models, the thesis presents studies on systems thus far not completely understood or on completely new systems, employing well-established models, and models thus far not sufficiently established for the problems at hand, to gain insights into the underlying processes happening during photo-isomerisation.

The most basic of the electrocyclic switches, the 1,3-cyclohexadiene and 1,3,6-hexatriene system, is the topic of chapter 3. The chapter presents a two-dimensional quantum-dynamical study of the ring-opening reaction of cyclohexadiene. The unique feature of this study is that it is based on a fully relaxed potential energy surface of the first excited state, in contrast to reaction-path-based approaches used in previous studies of other groups [64], while the coordinates themselves were taken from these previous studies. This approach for the first time reaches reasonable agreement with the frequency of the depopulation-events of the S_1 state observed in experiment [63]. Supported by the good agreement of the simulations with the experimental data, the applicability of the cyclohexadiene/hexatriene-system as a model system for the more complicated furylfulgides is challenged. Furthermore, the simulations are used to highlight a fundamental inaccuracy in reaction-path-based interpretations. The inherent funneling present in the paths in the case of

cyclohexadiene causes the de-excitation events to occur on too short timescales [64]. The results from cyclohexadiene indicated the necessity of full-dimensional models in simulations of photo-de-excitations dynamics, which are applied in the following chapters.

Leaving cyclohexadiene as unsuitable model system, the furylfulgides themselves are in the focus of chapter 4. Full-dimensional direct dynamics simulations using a semiempirical wave function model are presented for the ring-closure reaction of two different furylfulgide derivatives. The accuracy of the semiempirical model and therefore its applicability is evaluated by a detailed comparison with experiment and with accurate multireferential *ab-initio* results. The simulations offer a straightforward explanation for the experimental findings that the seemingly minor change from a peripheral isopropyl group to a methyl group imposes significant changes regarding the isomerisation properties. The involvement of important kinematic processes highlights the need for dynamic treatments, since although the most important conical intersections have already been known for related compounds [84,85], their interplay cannot be represented in a purely static treatment. The need for independence from previous assumptions of important points of the electronic surface and of important coordinates becomes obvious in the very different structures encountered during de-excitation events for the methyl- and the isopropyl-derivative, which, especially in the case of the isopropyl-derivative, often occur far away from minimum-energy paths connecting the respective conical intersections and the Franck-Condon point. The applicability of Thiel's MR-CI-OM3 method to furylfulgide systems, as proven in this part of the thesis, opens up possibilities for further studies of the furylfulgides, regarding the other directions of the and reactions the effect of other substitutions, in order to tune these molecules for specific applications.

In further studies of methylfurylfulgide, the involvement of partial $n\pi^*$-excitation character in the Z to E isomerisation is studied by accurate CASPT2 simulations revealing this major difference to the E to Z isomerisation and thus offering a possible explanation for the rather complicated appearance of the experimental transient spectra [78].

Section 4.8.3 deals with the details of the first absorption band in the electronic spectra of cyclic furylfulgides. The basic question is what the reason for the shoulder within the very broad absorption band might be. Different possible explanations, from a second low-lying electronic state to explicit effects of the Franck-Condon factor of only one excited state, are studied by static CC2 excitation-energy simulations, semi-empirical direct dynamics and a nuclear quantum-mechanical model calculation of Franck-Condon factors. The gathered data favours the explanation based on the Franck-Condon factors. The finding that the nuclear wave function of the excited state and not just a ground state sampling is needed for a qualitatively correct representation of a spectral band is an unusual feature in molecules of the size of furylfulgides in solvent and is directly traceable to the geometrical proximity

of Franck-Condon point, S_1-minimum, and S_1-S_0 conical intersection. In the future, accurate *ab-initio* calculations that identify the important coordinate can be used to move from a proof of principle, which was presented here, to evidential data from a real system, maybe even via explicitly coupled nuclear quantum dynamics.

In the last chapter (5) dealing with electrocyclic ring-closure and -opening switches, the development of a new type of electrocyclic switches is presented. The design process is guided by the information gained in the previous chapters and leads to the suggestion of a framework for photochromic switches thus far unstudied. Two molecules, a dilactame and a dilactone based on this framework, are studied intensely, using static CC2 and CASPT2 simulations and semiempirical direct dynamics. The static simulations treat the Franck-Condon points and intermediate structures on the photo-de-excitation paths, while semiempirical photo-de-excitation dynamics were started from the cyclic and the open form. The simulations show promising results for ring-closure quantum yields, and spectral features at wavelengths in spectral ranges suitable for excitation. For both systems, the simulations indicate an insufficient splitting of spectral bands to predict selective excitation of the closed isomer, but the spectral features together with the expected inaccuracies of the methods do not indicate an impossiblity of selective excitation for real systems. More limiting for the specific molecules at hand, but not for the basic systems, are degradation reactions appearing in the photo-de-excitation dynamics of the cyclic forms, and insufficient ring-opening quantum yields. The limitations are addressed, and possible modifications of the basic frameworks are suggested that might solve the problems and should be studied in future investigations.

Studies of various azo-moiety-containing molecules are presented in chapter 6. Static CASPT2 studies of a diazocine are presented, verifying the applicability of the FOCI-AM1 [21] method in section 6.2 and supporting experimental interpretations in section 6.4.

The azobenzene-related studies are expanded to mono-, di-, and trimers of azobenzene moieties linked in para-position via an amino linker. A suitable semiempirical setup for upcoming isomerisation dynamics studies of the dimer is identified and tested against CC2 simulations and experiment. After expansion of the CC2 simulations to the trimeric system, a detailed analysis of the excited-state characters is presented, treating one $n\pi^*$- and one $\pi\pi^*$-state for each chromophoric unit. The analysis focuses on the question in how far the states can be interpreted on the basis of the exciton model.

The final part of chapter 6 is devoted to a multiconfigurational study of an azopyridin-functionalised nickel porphyrin. The molecule is the first one to show a LD-CISSS process, from a tetra-coordinated singlet to a penta-coordinated triplet system. The spin-switching is made possible by the fact that the ligand is tetradentate in its E- and penta-dentate in its Z-form. The molecule shows E to Z isomerisation upon irradiation into its Q-band. In extended RASSCF and CASSCF

calculations, it is shown that the isomerisation pathway is probably a very unlikely de-excitation pathway after excitation into the states in the Q-band. The calculations imply that there is no azopyridin-excitation-character created directly by the excitation but that the energy in principle is enough for the molecule to reach an intersection seam caused by geometrical changes in the azopyridin moiety. The theoretical data implies that nothing drives the de-excitation towards the isomerisation pathway but that enough energy is present in the system to, so to speak, accidentally cause the isomerisation, which is consistent with the low quantum yields observed experimentally. Based on the presented data, future studies can address further intermediate structures that might be encountered during the E to Z isomerisation, for example created via an interpolation scheme, and start to investigate the Z to E isomerisation.

In summary, both the methods used as well as the systems under study cover a wide range. Hence, the thesis offers a broad insight into the properties of various molecular photo-switches. The data gathered is used to explain experimental findings and support experimental explanations, to challenge established theoretical approaches, and to put forth others.

Bibliography

[1] P. Atkins and J. de Paula, *Atkins' Physical Chemistry* (Oxford University Press, Oxford, 2002).

[2] M. A. Robb, M. Olivucci, and F. Bernardi, Photochemistry, in *Encyclopedia of Computational Chemistry*, p. 2056, John Wiley & Sons, 1998.

[3] G. Herzberg *Molecular Spectra and Molecular Structure* Vol. I (D. Van Nostrand, New York, 1950).

[4] T. Helgaker, P. Jørgensen, and J. Olsen, *Molecular Electronic-Structure Theory* (John Wiley & Sons, Ltd., 2000).

[5] F. Jensen, *Introduction to Computational Chemisty* (John Wiley and Sons Ltd, Chichester, 2007).

[6] I. N. Levine, *Quantum Chemistry* (Prentice-Hall International Inc., Englewood Cliffs (NJ), 2000).

[7] I. Shavitt, *In Mathematical Frontiers in Computational Chemical Physics* (Springer, 1989).

[8] I. M. Gelfand and M. L. Tsetlin, Dokl. Akad. Nauk SSSR **71**, 825 (1950).

[9] I. M. Gelfand and M. L. Tsetlin, Dokl. Akad. Nauk SSSR **71**, 1017 (1950).

[10] W. Thiel, 2007, MNDO program, version 6.1. Max-Planck-Institut für Kohlenforschung, Mülheim an der Ruhr, Germany.

[11] A. Koslowski, M. E. Beck, and W. Thiel, J. Comput. Chem. **24**, 714 (2003).

[12] H. Koch and P. Jørgensen, J. Chem. Phys. **93**, 3333 (1990).

[13] O. Christiansen, H. Koch, and P. Jørgensen, Chem. Phys. Letters **243**, 409 (1995).

[14] A. D. McLean and G. S. Chandler, J. Chem. Phys. **72**, 5639 (1980).

[15] H.-J. Werner, P. J. Knowles, R. Lindh, F. R. Manby, M. Schütz, P. Celani, T. Korona, A. Mitrushenkov, G. Rauhut, T. B. Adler, R. D. Amos, A. Bernhardsson, A. Berning, D. L. Cooper, M. J. O. Deegan, A. J. Dobbyn, F. Eckert, E. Goll, C. Hampel, G. Hetzer, T. Hrenar, G. Knizia, C. Köppl, Y. Liu, A. W.

Lloyd, R. A. Mata, A. J. May, S. J. McNicholas, W. Meyer, M. E. Mura, A. Nicklass, P. Palmieri, K. Pflüger, R. Pitzer, M. Reiher, U. Schumann, H. Stoll, A. J. Stone, R. Tarroni, T. Thorsteinsson, M. Wang, and A. Wolf, Molpro, version 2008.1, a package of ab initio programs, 2008.

[16] M. J. S. Dewar and W. Thiel, J. Am. Chem. Soc. **99**, 4899 (1977).

[17] M. J. S. Dewar, E. G. Zoebisch, E. F. Healy, and J. J. P. J. Stewart, J. Am. Chem. Soc. **107**, 3902 (1985).

[18] J. J. P. Stewart, J. Comput. Chem. **10**, 209 (1989).

[19] W. Weber and W. Thiel, Theor. Chem. Acc. **103**, 495 (2000).

[20] O. Weingart, Z. Lan, A. Koslowski, and W. Thiel, J. Phys. Chem. Lett. **2**, 1506 (2011).

[21] G. Granucci and A. Toniolo, Chem. Phys. Lett. **325**, 79 (2000).

[22] K. Andersson, P. A. Malmqvist, B. O. Roos, A. J. Sadlej, and K. Wolinski, J. Phys. Chem. **94**, 5483 (1990).

[23] K. Andersson, P. A. Malmqvist, and B. O. Roos, J. Chem. Phys. **96**, 1218 (1992).

[24] J. J. W. McDuall, K. Peasley, and M. A. Robb, Chem. Phys. Lett. **148**, 183 (1988).

[25] B. O. Roos and K. Andersson, Chem. Phys. Lett. **245**, 215 (1995).

[26] B. O. Roos, K. Andersson, M. P. Fülscher, L. Serrano-Andrés, K. Pierloot, M. Merchán, and V. Molina, J. Mol. Struct. THEOCHEM **388**, 257 (1996).

[27] E. K. U. Gross and W. Kohn, Adv. Comput. Chem. **21**, 255 (1990).

[28] T. Schwab and S. Grimme, Phys. Chem. Chem. Phys. **9**, 3397 (2007).

[29] T. Yanai, D. P. Tew, and N. C. Handy, Chem. Phys. Lett. **393**, 51 (2004).

[30] B. G. Levine, C. Ko, J. Quenneville, and T. J. Martinez, Mol. Phys. **104**, 1039 (2006).

[31] Z. Li and W. Liu, J. Chem. Phys. **136**, 24107 (2012).

[32] J. A. Pople, D. P. Santry, and G. A. Segal, J. Chem. Phys. **43**, S129 (1965).

[33] J. A. Pople and G. A. Segal, J. Chem. Phys. **43**, S136 (1965).

[34] J. A. Pople and G. A. Segal, J. Chem. Phys. **44**, 3289 (1966).

[35] D. P. Santry and G. A. Segal, J. Chem. Phys. **47**, 158 (1967).

[36] J. A. Pople, D. L. Beveridg, and P. A. Dobosh, J. Chem. Phys. **47**, 2026 (1967).

[37] W. Weber, PhD thesis, Universiät Zürich, Switzerland, 1996.

[38] E. Fabiano, T. W. Keal, and W. Thiel, Chem. Phys. **349**, 334 (2008).

[39] T. W. Keal, M. Wanko, and W. Thiel, Theor. Chem. Acc. **123**, 145 (2009).

[40] J. A. Gámez, O. Weingart, A. Koslowski, and W. Thiel, J. Chem. Theory Comput. **8**, 2352 (2012).

[41] G. Granucci, M. Persico, and A. Toniolo, J. Chem. Phys. **114**, 10608 (2001).

[42] C. Ciminelli, G. Granucci, and M. Persico, Chem. Eur. J. **10**, 2327 (2004).

[43] C. Ciminelli, G. Granucci, and M. Persico, J. Chem. Phys. **123**, 174317 (2005).

[44] C. Ciminelli, G. Granucci, and M. Persico, Chem. Phys. **349**, 325 (2008).

[45] M. Kolb and W. Thiel, J. Comput. Chem. **14**, 775 (1993).

[46] A. S. Davydov, *Theory of molecular excitons (translated by M. Kasha and M. Oppenheimer, Jr.* (McGraw-Hill, 1992).

[47] E. G. McRae and M. Kasha, J. Chem. Phys. **28**, 721 (1958).

[48] M. Kasha, H. R. Rawls, and M. Ashraf El-Bayoumi, Pure and Applied Chem. **11**, 371 (1965).

[49] E. G. McRae and M. Kasha, *Physical Processes in Radiation Biology* (Academic Press, 1964).

[50] D. J. Tannor, *Introduction to Quantum Mechanics: A Time-Dependent Perspective* (University Science Books, Sausalito (CA), 2007).

[51] F. Gatti and G. A. Worth, *Multidimensional Quantum Dynamics* (Wiley–VCH, 2009).

[52] D. Frenkel and B. Smit, *Understanding Molecular Simulation* (Academic Press, San Diego (CA), 2002).

[53] H.-D. Meyer and W. H. Miller, J. Chem. Phys. **72**, 2272 (1980).

[54] J. C. Tully, J. Chem. Phys. **93**, 1061 (1990).

[55] P. Celani, S. Ottani, M. Olivucci, F. Bernardi, and M. A. Robb, J. Am. Chem. Soc. **116**, 10141 (1994).

[56] P. Celani, F. Bernardi, M. A. Robb, and M. Olivucci, J. Phys. Chem. **100**, 19364 (1996).

[57] S. Lochbrunner, W. Fuss, W. Schmid, and K.-L. Kompa, J. Phys. Chem. A **102**, 9334 (1998).

[58] H. A. and R. de Vivie-Riedle, J. Chem. Phys. **112**, 5054 (2000).

[59] W. Fuß, W. E. Schmid, and S. A. Trushin, J. Chem. Phys. **112**, 8347 (2000).

[60] M. Garavelli, C. S. Page, P. Celani, M. Olivucci, W. E. Schmid, S. A. Trushin, and W. Fuss, J. Phys. Chem. A **105**, 4458 (2001).

[61] A. Hofmann and R. de Vivie-Riedle, Chem. Phys. Lett. **346**, 299 (2001).

[62] D. Geppert, L. Seyfarth, and R. de Vivie-Riedle, Appl. Phys. B Lasers O. **79**, 987 (2004).

[63] K. Kosma, S. A. Trushin, W. Fuss, and W. E. Schmid, Phys. Chem. Chem. Phys. **11**, 172 (2009).

[64] D. Geppert, *Molekulare Schalter mit Cyclohexadien als photoaktivem Zentrum: Struktur, Dynamik und Kontrolle*, PhD thesis, LMU München, 2006.

[65] J. Voll, T. Kerscher, D. Geppert, and R. de Vivie-Riedle, J. Photochem. Photobiol. A **190**, 352 (2007).

[66] A. Nenov, P. Kölle, M. A. Robb, and R. de Vivie-Riedle, J. Org. Chem. **75**, 123 (2010).

[67] B. Hartke and J. Manz, J. Am. Chem. Soc. **110**, 3063 (1988).

[68] F. A. Schäfer, C. Huber, and R. Ahlrichs, J. Chem. Phys. **100**, 5829 (1994).

[69] G. Karlström, R. Lindh, P.-Å. Malmqvist, B. O. Roos, U. Ryde, V. Veryazov, P.-O. Widmark, M. Cossi, B. Schimmelpfennig, P. Neogrady, and L. Seijo, Comput. Mat. Sci. **28**, 222 (2003).

[70] Y. Yokoyama, Chem. Rev. **100**, 1717 (2000).

[71] A. S. Dvornikov, Y. Liang, C. S. Cruse, and P. M. Rentzepis, J. Phys. Chem. B **108**, 8652 (2004).

[72] R. Matsushima, T. Hayashi, and M. Nishiyama, Mol. Cryst. Liq. Cryst. **344**, 241 (2000).

[73] L. Khedhiri, A. Corval, R. Casalegno, and M. Rzaigui, J. Phys. Chem. A **108**, 7473 (2004).

[74] J. Harada, R. Nakajima, and K. Ogawa, J. Am. Chem. Soc. **130**, 7085 (2008).

[75] F. Renth, M. Foca, A. Petter, and F. Temps, Chem. Phys. Lett. **428**, 62 (2006).

[76] L. Khedhiri, A. Corval, R. Casalegno, and M. Rzaigui, J. Phys. Chem. A **108**, 7473 (2004).

[77] R. Siewertsen, F. Renth, F. Temps, and F. Sönnichsen, Phys. Chem. Chem. Phys. **11**, 5952 (2009).

[78] R. Siewertsen, F. Strübe, J. Mattay, F. Renth, and F. Temps, Phys. Chem. Chem. Phys. **13**, 3800 (2011).

[79] F. O. Koller, W. J. Schreier, T. E. Schrader, S. Malkmus, C. Schulz, S. Dietrich, K. Rück-Braun, and M. Braun, J. Phys. Chem. A **112**, 210 (2008).

[80] T. Cordes, T. T. Herzog, S. Malkmus, T. Brust, J. A. DiGirolamo, W. J. Lees, and M. Braun, Photochem. Photobiol. Sci. **8**, 528 (2009).

[81] B. Heinz, S. Malkmus, S. Laimgruber, S. Dietrich, C. Schulz, K. Ruck-Braun, M. Braun, W. Zinth, and P. Gilch, J. Am. Chem. Soc. **129**, 8577 (2007).

[82] S. Draxler, T. Brust, S. Malkmus, J. A. DiGirolamo, W. J. Lees, W. Zinth, and M. Braun, Phys. Chem. Chem. Phys. **11**, 5019 (2009).

[83] F. Strübe, R. Siewertsen, F. D. Sönnichsen, F. Renth, F. Temps, and J. Mattay, Eur. J. Org. Chem. **2011**, 1947 (2011).

[84] A. Nenov and R. de Vivie-Riedle, J. Chem. Phys. **135**, 034304 (2011).

[85] G. Tomasello, M. J. Bearpark, M. A. Robb, G. Orlandi, and M. Garavelli, Angew. Chem. Int. Ed. **49**, 2913 (2010).

[86] R. Ahlrichs, M. Bär, M. Häser, H. Horn, and C. Kölmel, Chem. Phys. Lett. **162**, 165 (1989).

[87] A. Schäfer, H. Horn, and R. Ahlrichs, J. Chem. Phys. **97**, 2571 (1992).

[88] F. Weigend, M. Häser, H. Patzelt, and R. Ahlrichs, Chem. Phys. Lett. **294**, 143 (1998).

[89] Y. Yoshioka, M. Usami, M. Watanabe, and K. Yamaguchi, J. Mol. Struct. THEOCHEM **623**, 167 (2003).

[90] M. J. Frisch, G. W. Trucks, H. B. Schlegel, G. E. Scuseria, M. A. Robb, J. R. Cheeseman, G. Scalmani, V. Barone, B. Mennucci, G. A. Petersson, H. Nakatsuji, M. Caricato, X. Li, H. P. Hratchian, A. F. Izmaylov, J. Bloino, G. Zheng, J. L. Sonnenberg, M. Hada, M. Ehara, K. Toyota, R. Fukuda, J. Hasegawa, M. Ishida, T. Nakajima, Y. Honda, O. Kitao, H. Nakai, T. Vreven, J. A. Montgomery, Jr., J. E. Peralta, F. Ogliaro, M. Bearpark, J. J. Heyd, E. Brothers, K. N. Kudin, V. N. Staroverov, R. Kobayashi, J. Normand, K. Raghavachari, A. Rendell, J. C. Burant, S. S. Iyengar, J. Tomasi, M. Cossi, N. Rega, J. M. Millam, M. Klene, J. E. Knox, J. B. Cross, V. Bakken, C. Adamo, J. Jaramillo, R. Gomperts, R. E. Stratmann, O. Yazyev, A. J. Austin, R. Cammi, C. Pomelli, J. W. Ochterski, R. L. Martin, K. Morokuma, V. G. Zakrzewski, G. A. Voth, P. Salvador, J. J. Dannenberg, S. Dapprich, A. D. Daniels, . Farkas, J. B. Foresman, J. V. Ortiz, J. Cioslowski, and D. J. Fox, Gaussian 09 Revision A.1, Gaussian Inc. Wallingford CT 2009.

[91] T. H. Dunning, Jr., J. Chem. Phys. **90**, 1007 (1989).

[92] R. Siewertsen, *Ultrafast photochromic reactions of structurally modified furylfulgides and a bridged azobenzene*, PhD thesis, University of Kiel, 2011.

[93] A. Perrier, F. Maurel, and D. Jacquemin, Acc. Chem. Res. **45**, 1173 (2012).

[94] S. Pu, R. Wang, G. Liu, W. Liu, S. Cui, and P. Yan, Dyes and Pigments **94**, 195 (2012).

[95] S. Kuehn, S. Friede, M. Zastrow, C. Gahl, K. Rueck-Braun, and T. Elsaesser, Chem. Phys. Lett. **542**, 94 (2012).

[96] S. Draxler, T. Brust, S. Malkmus, F. O. Koller, B. Heinz, S. Laimgruber, C. Schulz, S. Dietrich, K. Rück-Braun, W. Zinth, and M. Braun, J. Mol. Liq. **141**, 130 (2008).

[97] T. Brust, S. Malkmus, S. Draxler, S. A. Ahmed, K. Rück-Braun, W. Zinth, and M. Braun, J. Photochem. and Photobiol. A **207**, 209 (2009).

[98] W. J. Hehre, R. F. Stewart, and J. A. Pople, J. Chem. Phys. **51**, 2657 (1969).

[99] P. O. Widmark, P. A. Malmqvist, and B. O. Roos, Theor. Chem. Acc. **77**, 291 (1990).

[100] K. Pierloot, B. Dumez, P. O. Widmark, and B. O. Roos, Theor. Chem. Acc. **90**, 87 (1995).

[101] N. H. F. Beebe and J. Linderberg, Int. J. Quantum Chem. **12**, 683 (1977).

[102] H. Koch, A. Sánchez de Merás, and T. B. Pedersen, J. Chem. Phys. **118**, 9481 (2003).

[103] F. Aquilante, P.-A. Malmqvist, T. B. Pedersen, A. Ghosh, and B. O. Roos, J. Chem. Theory Comput. **4**, 694 (2008).

[104] F. Aquilante, T. K. Todorova, L. Gagliardi, T. B. Pedersen, and B. O. Roos, J. Chem. Phys. **131**, 034113 (2009).

[105] Z. F. Liu, K. Hashimoto, and A. Fujishima, Nature **347**, 658 (1990).

[106] T. Ikeda and O. Tsutsumi, Science **268**, 1873 (1995).

[107] J. Iwicki, E. Ludwig, M. Kallane, J. Buck, F. Kohler, R. Herges, L. Kipp, and K. Rossnagel, Appl. Phys. Lett. **97**, 063112 (2010).

[108] B. Baisch, D. Raffa, U. Jung, O. M. Magnussen, C. Nicolas, J. Lacour, J. Kubitschke, and R. Herges, J. Am. Chem. Soc. **131**, 442 (2009).

[109] R. Siewertsen, J. B. Schönborn, B. Hartke, F. Renth, and F. Temps, Phys. Chem. Chem. Phys. **13**, 1054 (2011).

[110] O. Carstensen, J. Sielk, J. B. Schönborn, G. Granucci, and B. Hartke, J. Chem. Phys. **133**, 124305 (2010).

[111] J. Wachtveitl, T. Nagele, B. Puell, W. Zinth, M. Kruger, S. RudolphBohner, D. Oesterhelt, and L. Moroder, J. Photochem. Photobiol. A **105**, 283 (1997).

[112] T. Nagele, R. Hoche, W. Zinth, and J. Wachtveitl, Chem. Phys. Lett. **272**, 489 (1997).

[113] I. Lednev, T. Ye, L. Abbott, R. Hester, and J. Moore, J. Phys. Chem. A **102**, 9161 (1998).

[114] T. Fujino, S. Arzhantsev, and T. Tahara, Bull. Chem. Soc. Jpn. **75**, 1031 (2002).

[115] H. Satzger, C. Root, and M. Braun, J. Phys. Chem. A **108**, 6265 (2004).

[116] T. Pancur, F. Renth, F. Temps, B. Harbaum, A. Kruger, R. Herges, and C. Nather, Phys. Chem. Chem. Phys. **7**, 1985 (2005).

[117] L. Wang and X. Wang, J. Mol. Struct. THEOCHEM **847**, 1 (2007).

[118] R. Siewertsen, H. Neumann, B. Buchheim-Stehn, R. Herges, C. Näther, F. Renth, and F. Temps, J. Am. Chem. Soc. **131**, 15594 (2009).

[119] J. Bahrenburg, K. Roettger, R. Siewertsen, F. Renth, and F. Temps, Photochem. Photobiol. Sci. **11**, 1210 (2012).

[120] H. Fliegl, A. Köhn, C. Hättig, and R. Ahlrichs, J. Am. Chem. Soc. **125**, 9821 (2003).

[121] A. Cembran, F. Bernardi, M. Garavelli, L. Gagliardi, and G. Orlandi, J. Am. Chem. Soc. **126**, 3234 (2004).

[122] C. R. Crecca and A. E. Roitberg, J. Phys. Chem. A **110**, 8188 (2006).

[123] T. Cusati, G. Granucci, M. Persico, and G. Spighi, J. Chem. Phys. **128**, 194312 (2008).

[124] J. Bahrenburg, C. Sievers, J. B. Schönborn, B. Hartke, F. Renth, F. Temps, C. Näther, and F. D. Sönnichsen, Photochem. Photobiol. Sci. – under revision

.

[125] S. Venkataramani, U. Jana, M. Dommaschk, F. D. Sönnichsen, F. Tuczek, and R. Herges, Science **331**, 445 (2011).

[126] M. Dolg, U. Wedig, H. Stoll, and H. Preuss, J. Chem. Phys. **86**, 2123 (1987).

[127] S. Patchkovskii, P. M. Kozlowski, and M. Z. Zgierski, J. Chem. Phys. **121**, 1317 (2004).

[128] M. Rubio, B. O. Roos, L. Serrano-Andres, and M. Merchan, J. Chem. Phys. **110**, 7202 (1999).

[129] R. Siewertsen and F. Temps, private communication of unpublished data.

[130] E. Fabiano, T. W. Keal, and W. Thiel, Chem. Phys. **349**, 334 (2008).

Curriculum Vitae

Personal Data

◇	Name:	Jan Boyke Schönborn
◇	Nationality:	german
◇	Date of birth:	11/12/1983
◇	Place of birth:	Eckernförde
◇	Address:	Lutherstraße 24, 24114 Kiel

Education:

◇	since 05/2008	Doctoral candiate on the topic *Dynamics of Photoinduced Switching Processes* in the group of Prof. Bernd Hartke, Theoretical Chemistry, Univ. Kiel
◇	03/2008–04/2008	Internship in the group of Prof. T. Düren, Univ. Edinburgh, Grand Canonical Monte-Carlo simulations of sorption processes
◇	09/2007–02/2008	Diploma thesis *Design molekularer Rotoren mit Quantenchemie und Molekül̈dynamik* with Prof. Bernd Hartke, Theoretical Chemistry, Univ. Kiel
◇	10/2003–02/2008	University studies (Chemistry: Diploma), Univ. Kiel
◇	08/1994–05/2003	School education at "Domschule Schleswig – Gymnasium mit altsprachlichem Zweig", Abitur majoring in Mathematics and Chemistry, additional qualification: Latinum

Teaching experience and qualifications:

◇	2011–2012	3 advanced practical courses in theoretical chemistry with Julian Müller, BSc, Uta Corinna Stange, BSc and Tim Raeker, BSc
◇	10/2011	University Didactics Advanced course "Munterrichtsmethoden"
◇	02/2011	University Didactics Basic course
◇	10/2010–07/2012	Teaching assistant in "Mathematics for chemists I & II"
◇	04/2009–07/2010	Teaching assistant in Basic and advanced practical course in Physical Chemistry
◇	05/2008–02/2009	Teaching assistant in "Mathematics for chemists I & II"
◇	10/2007–02/2008	Student assistant in Exercises "Mathematics for chemists I"
◇	10/2006–04/2007	Student assistant in Exercises "Physical Chemistry V (Electro Chemistry and statistical Thermodynamics)"
◇	04/2006–07/2006	Student worker in the "Basics Practical Course in Inorganic Chemistry"

Talks, Posters and other Conference Contributions:

◇	05/2011	Talk at the 2011 SFB 677 international meeting: "Molecular Switches: Elementary Processes and Applications", Plön
◇	09/2010	Contributed talk at the "Symposium für Theoretische Chemie 2010", Münster
◇	03/2010	Invited topical talk at the "DPG Spring meeting 2010 – Condensed phase", Regensburg
◇	09/2009	Awarded poster at the "Symposium für Theoretische Chemie 2009", Neuss
◇	08/2009	Poster at and organisation (in collaboration with Dr. Antje Modrow) of the second annual meeting of the graduate students and post-docs of SFB677, Sehlendorf
◇	05/2009	Poster at the 2009 SFB 677 international meeting: "Molecular Switches: Elementary Processes and Applications", Salzau
◇	04/2009	Visit and student talk at the "Frontiers in Computational Chemistry" summer school, Svendborg, DK
◇	10/2008	Talk at and Organisation (in collaboration with Dr. Antje Modrow) of the first annual meeting of the graduate students and post-docs of SFB677, Sehlendorf
◇	05/2008	Visit and poster at the 2008 SFB 677 summerschool, Salzau

Awards and fellowships:

◇	07/2009	Sponsored admission to the 2009 Lindau Nobel Laureate Meeting
◇	12/2008	BASF young scientists award for the best Diploma in chemistry at CAU in the year 2008
◇	03/2006	Diploma fellowship by the "Studienstiftung des Deutschen Volkes"
◇	01/2006	Best "Vordiplom" in chemistry at CAU in the year 2005

Publications

Related to the Thesis

- J. Bahrenburg, C. Sievers, J.B. Schönborn, B. Hartke, F. Renth, F. Temps, C. Näther and F.D. Sönnichsen, *Photochemical properties of multi-azobenzene compounds*, Manuscript published online, Photochem. Photobiol. Sci., **2013**
- J.B. Schönborn and B.Hartke, *Importance of a low-lying $n\pi^*$-state in the photo-isomerisation reaction of Z-methylfurylfulgide*, Manuscript submitted to J. Phot. Chem. Phot. Biol. A **2012**
- J.B. Schönborn, A. Koslowski, W. Thiel and B.Hartke, *Photochemical Dynamics of E-iPr-Furylfulgide*, Phys. Chem. Chem. Phys. **2012**, *14* , 12193
- R. Siewertsen, J.B. Schönborn, B. Hartke, F. Renth, F. Temps, *Superior $Z \rightarrow E$ and $E \rightarrow Z$ photoswitching dynamics of dihydrodibenzodiazocine, a bridged azobenzene, by S1($n\pi^*$) excitation at $\lambda = 387$ and $490nm$*, Phys. Chem. Chem. Phys. **2010**, *13*, 1054
- O. Carstensen, J. Sielk, J.B. Schönborn, G. Granucci and B. Hartke, *Unusual photochemical dynamics of a bridged azobenzene derivative*, J. Chem. Phys. **2010**, *133*, 124305
- J.B. Schönborn, J. Sielk and B. Hartke, *Photochemical Ring Opening of Cyclohexadiene yielding Hexatriene: Quantum Wavepacket Dynamics on a Global ab initio Potential Energy Surface*, J. Phys. Chem. A **2010**, *114*, 4036

Unrelated to the Thesis

- S. Buller, C. Koch, W. Bensch, P. Zalden, R. Sittner, S. Kremers, M. Wuttig, U. Schürmann, L. Kienle, T. Leichtweiss, J. Janek, B. Schönborn, *Influence of partial substitution of Te by Se and Ge by Sn on the properties of the Blu-ray phase-change material Ge8Sb2Te11*, under minor revision at Chem. Mater. **2012**
- E.-K. Mucke, J.B. Schönborn, F. Köhler, R. Herges, *Stability and Aromaticity of Charged Mobius[4n]Annulenes*, J. Org. Chem. **2011**, *76*, 35
- J.B. Schönborn, R. Herges and B.Hartke, *Brownian molecular rotors: Theoretical design principles and predicted realizations*, J. Chem. Phys. **2009**, *130*, 234906
- G. Friedrichs, E. Goos, J. Gripp, H. Nicken, J.B. Schönborn, H. Vogel, F. Temps, *The Products of the Reactions of o-Benzyne with Ethene, Propene, and Acetylene: A Combined Mass Spectrometric and Quantum Chemical Study*, Z. Chem. **2009**, *223*, 387

Declaration

Hereby, I declare that the work presented in thesis was done by me, under the supervision of Prof. Bernd Hartke with no other help than the referenced sources in the text.

This is my first dissertation and the work has never been used in any other dissertation attempts.

The dissertation complies to the good scienticfic practice rules as proposed by the Germand Resarch Foundation (DFG).

Kiel, 26/10/2012

Jan Boyke Schönborn

Acknowledgements

First I would like to thank the person without whom even thinking about this would have been close to an impossibility, my supervisor Prof. Bernd Hartke. I owe him my utmost thanks, for the possibility to work on this project, the ever-supportive discussions at virtually any time of the day and helping me on my first steps on the unclimbable mountain called science. Thanks!

I am grateful for the fruitful collaborations in and out of the SFB677. Thanks to Prof. Temps and the members and former members of his Group Dr. Ron Siewertsen, Dr. Falk Renth and Dipl. Chem. Julia Bahrenburg, for fruitful discussions and access to unpublished data. I also would like to thank Prof. Thiel and his group members Dr. Axel Koslowski and Dr. Oliver Weingart, for allowing me to use the MNDO program and the support in the use of it and beyond. Gratidute to the DFG, which payed my position and sponsored various conference visits via the SFB677.

To all members of the Hartke group, Sushi (mach mal youtube), Ole Carstensen (die Wathose stinkt), Yan Li (now I know some chinese), Julian Müller (lies mal deine Mails) and the former members Florian Koskowski (LoSo oder was), Jan Sielk (du tanzt da in meinen Handschuhen, danke für die Layouts), Frank von Horsten (schmeckt irgendwie salzig) and Mats Eriksson (Skö): "Thank you, it was great times."

Thanks to all my friends here in Kiel. Especially To the sweden crew (1000 weiße lilien), Saskia (Apfelzähne sind besser als...), Heiko (Nee, das klappt um), Stolti (Einreiben oder Scheit?) and Eckli (da muss Struktur rein) but also to the lunch people Johnny (du schuldest mir noch was Kampftänzer) and Nils (sofern du nicht gerade was besseres zu tun hast) and all the others.

Thanks to the guys from Schleswig. To Christian (Gnhä, gnhä, gnhä), Alex (da gehen die...), Jan-Markus (dem Schönbornfreund), Stephan (wie geil ein Cyberman) and Lutz (nein er liegt nicht bei mir).

To the guys at sports to Torge, Claudia, Anna, Gabriele, Ruben and so many. Nothing helps in frustration like sports and I was lucky enough to do that with people I gladly talk to. You all know I need it.

Thanks to you all!

To my family, thank you! For major contributions in making me the person I am today and for your support.

Finally, thank you Freddy, for so much.